INVESTIGATION OF CRYSTALLIZATION OF POLY(3-HYDROXYBUTYRATE-*CO*-3-HYDROXYVALERATES) AND THEIR BAMBOO FIBER REINFORCED COMPOSITES

By

JUN QIAN

A thesis submitted in partial fulfillment of

The requirements for the degree of

MASTER OF SCIENCE IN CIVIL ENGINEERING

WASHINGTON STATE UNIVERSITY

Department of Civil and Environmental Engineering

December 2006

To the Faculty of Washington State University:

The members of the Committee appointed to examine the thesis of JUN QIAN find it satisfactory and recommend that it be accepted.

_____
Chair

_____

_____

ACKNOWLEDGMENT

First of all, I would like to thank my advisor Jinwen Zhang for his generous help in my thesis research. I am benefited from his wide professional knowledge and exact research philosophy.

Second, I would like to thank all faculty members and students in Wood Material and Engineering Lab. They gave me many suggestions to my experiments and thesis writing.

Finally I would like to mention Liying Zheng and my parents, who give me emotional and financial support. They are my solid bases in the future of my life.

INVESTIGATION OF CRYSTALLIZATION OF POLY(3-HYDROXYBUTYRATE-*CO*-3-HYDROXYVALERATES) AND THEIR BAMBOO FIBER REINFORCED COMPOSITES

ABSTRACT

by Jun Qian, M.S.
Washington State University
December 2006

Chair: Jinwen Zhang

Based on renewable resources and with good mechanical properties, bamboo pulp fiber (BPF) reinforced poly(3-hydroxybutyrate-*co*-3-hydroxyvalerates) (PHBVs) composites have the potential to replace petrochemical polymer based composites in many applications. In this study, nucleation and crystallization of PHBVs in neat forms and in composites and its effects on properties, and the effects of coupling agent or compatibilizer on physical properties and mechanical properties, were investigated. Crystallization kinetics of PHBVs (containing 8, 12 and 21 mol% 3-hydroxyvalerate), nucleated with boron nitride, thymine and melamine, were studied. The results indicate that all three nucleating agents increased the overall crystallization rate of PHBVs, with boron nitride and thymine being superior to melamine. Adding nucleating agent also improved the mechanical properties of the composites. BPF demonstrated excellent reinforcing effects, and it improved not only tensile and flexural properties but also impact strength. Addition of polydiphenylmrthane diisocyanate and maleic anhydride grafted PHBV greatly improved the interfacial adhesion in the composites, as seen in the increases in mechanical and dynamic mechanical properties and fewer fiber pullouts at the fracture surfaces.

TABLE OF CONTENTS

LIST OF TABLES

LIST OF FIGURES

LIST OF ABBREVIATIONS

BN: boron nitride

BPF: bamboo pulp fiber

DSC: differential scanning calorimetry

EPA: Environmental Protection Agency

pMDI: polymeric methylene diphenyl diisocyanate

MA-PHBV8: maleic anhydride grafted PHBV8

NA: nucleating agent

NCC: nano-sized calcium carbonate

PBS: poly(butylene succinate)

PHA: polyhydroxyalkanoate

PHB: poly(3-hydroxybutyrate)

PHBV: poly(3-hydroxybutyrate-co-3-hydroxyvalerate)

PHBV8: poly(3-hydroxybutyrate-co-3-hydroxyvalerate) containing 8 mol% poly(3-hydroxyvalerate)

POM: polarized optical microscopy

SEM: scanning electron microscopy

TCL: transcrystalline layer

CHAPTER 1 INTRODUCTION

1.1 Background

In 2000, annual worldwide fossil fuel use for all thermoplastics was ca. 270 million tons of oil and gas (Gerngross and Slater 2000). Approximately 151 million tons of fossil fuel were used as feedstock for the thermoplastics, while the remainder were utilized as the required energy for performing various steps in the manufacturing process (Gerngross 1999). According to a study by the U.S. Environmental Protection Agency (EPA), plastics alone account for roughly 21% (by volume) of the nearly 200 million tons of municipal waste generated each year in the USA. As concern mounts about the effects of petrochemical plastics on the environment and the increased dependence on oil and gas imports, using polymeric materials from renewable resources could become an important part of the solution. Over the last century, petrochemical plastics have replaced many products that were once made from agricultural or forestry products. As technology advances reduce the production cost of biobased resins, the tide may again turn.

Bioplastics have raised great hopes but have also met enormous challenges. Bioplastics can be loosely defined as man-made plastics that can be processed by established plastics processing technology, and that are based on renewable raw materials and/or are biodegradable. Although niche applications of bioplastics, such as utensils, food packaging, grocery bags, and mulch films, are emerging, bioplastics have only an insignificant share in the current marketplace dominated by petrochemical plastics.

Typically, bioplastics are made of resins either derived biologically and/or chemically from renewable resources, or resins incorporated directly with natural polymeric materials. The former includes Polylactic acid, Polyhydroxyalkanoates (**PHAs**) and vegetable oil-based polyurethane, etc. The latter includes plastics using soy protein, starch, cellulose, and some other natural polymers as one of the major ingredients.

Bacteria in the fermentation process, using sugars or enzyme-thinned starch, directly produce pHAs. Poly (3-hydroxybutyrate) (**PHB**) and poly(3-hydroxybutyrate-co-3-hydroxyvalerate) (**PHBV**) are the most common members in the PHA family. Depending on the monomer units, PHAs can be homopolymers or copolymers, and exhibit behavior varying from rubbery to rigid plastic. PHB and some PHBVs demonstrate high tensile strength and modulus comparable to many fossil oil based plastics, for example, polypropylene (Howells 1982). When discarded or composted, bacteria that naturally occur in the soil grow on PHA and turn it into water and carbon dioxide (Jenkins 2004). PHAs have been studied extensively as replacements or substitutes for current mainstream petrochemical plastics. PHBVs can be used to produce a wide range of products from grocery bags and soda bottles to disposable razors and flatware *(*Jenkins 2004). Since the costs of PHAs are still higher than those of most petrochemical plastics, the long-term outlook for marketing these products is likely to depend on global regulatory developments and continued improvements in cost-reducing technologies. In addition, the brittleness of some PHAs remains the major problem in applications.

Manufacturing cost effective and performance enhanced PHA products is critical to the promotion of bioproduct applications in the conventional plastics marketplace, and contributes to the transition of our economy to one built on sustainable and renewable materials and energy resources rather than on fossil oil.

1.2 Problem statement

In fact, PHB and some PHBVs demonstrate high tensile strength and Young's modulus, which are comparable to that of many petrochemical plastics. As new polymer materials, however, PHAs encounter several barriers in competing with petrochemical plastics. In general, those obstacles include:

I. Processing

- Narrow processing window
- Slow crystallization
- Low melt strength
- Thermal and hydrolytic (moisture) degradations

II. Performance

- Brittleness
- Low impact strength

III. Production cost

- High resin prices

1.3 Approach

Traditionally, blending and filling are the most often used measures for improving material properties, broadening processing window, and reducing cost of polymer products. A variety of natural polymers and synthetic thermoplastic polymers have been blended with PHA for different purposes. The former include starch (Yasin *et al* 1989, Ke and Sun 2001, Wang *et al* 2001), soy protein (Zhang *et al* 2006) and natural rubber (Yoona *et al* 1999, Parulekar and Mohanty 2006) etc; the latter include poly(vinyl acetate) (Gajria *et al* 1996), poly(ethylene oxide) (Na *et al* 2002) and poly(ε-caprolactone) (Maglio *et al* 1999, Meredith and Amis 2000) etc. Different inorganic fillers (Urayama *et al* 2003) including nanoparticles (Wang *et al* 2005) have also been used to fill PHA.

In recent years, research has shown growing interest in using natural fibers as reinforcement for thermoplastics including biopolymers (Herrmann *et al* 1998, Riedel and Nickel 1999, Wong *et al* 2002, Shanks *et al* 2004). In comparison with glass fiber reinforcement, natural fiber reinforced polymeric composites have the advantages of low density, high strength or stiffness to weight ratio, low cost, good thermal and acoustic insulation, and ease of processing (Wong *et al* 2002). PHA biocomposites with wood fiber (Reinsch and Kelley 1997, Fernandes *et al* 2004), flax (Wong *et al* 2002, Shanks *et al* 2004, Van De Velde and Kiekens 2002), recycled cellulose fiber (Bhardwaj *et al* 2006) and other natural fibers (Herrmann *et al* 1998, Riedel and Nickel 1999) have been

reported. However, it is often noted that short fiber reinforced plastics may show little or even detrimental effects on toughness and impact strength.

In this study, crystallization of PHBV8 (containing 8 mol% HV) and reinforcement with bamboo pulp fiber (BPF) were investigated. Compared with PHB, PHBV copolymer yields lower melting point and higher ductility but also slower crystallization and lower crystallinity, and these characteristics become serious problems with increasing 3-HV comonomer content. It is well known that the crystalline structure and crystallinity of a polymer have significant effects on its mechanical and physical properties. Adding nucleating agent in a semicrystalline polymer often result in fine and homogeneous crystalline structure and is desirable for high performance and quality. Two new chemicals were introduced as nucleating agents, and their effects on nucleation and crystallization of were studied and compared with that of the conventional boron nitride.

Bamboo has received considerable attention as a substitute for wood in recent years (Lee and Wang 2006). Bamboo is an abundant natural resource in Asia and other regions around the world. Bamboo can be renewed much more rapidly than wood since the time required for bamboo to reach its mature size is only six to eight months, less than 5% of the time required for most woods. Its overall mechanical properties are comparable to those of wood. In addition, the average length of bamboo pulp fiber is only second to that of softwood. Bamboo fiber reinforced other polymer composites have been studied elsewhere, and a general improvement of mechanical properties was reported (Chen *et al*

1998). The crystallization of PHBV became more complicated in presence of BPF because of the fiber-induced crystallization. It is common to observe the fiber-induced crystallization in fiber reinforced composite system if the polyer is semicrystalline. In its extreme case, this induced crystallization manifests as tightly aligned spherulites growing outward from the fiber, called transcrystalline layer (TCL). The BPF induced crystallization of PHBV8 was studied in this research. The effects of adding nucleatin agent on the fiber induced crystallization and mechanical properties of the composites were investigated. In order to improve the interfacial adhesion, methylene diphenyl diisocyanate (MDI) and maleic anhydride grafted PHBV8 were employed.

1.4 General Objectives

The ultimate goal of this research is to contribute the development of economically viable and environmentally sound technologies for biopolyester plastics products. However, this research does aim to provide solutions for all above-mentioned problems. The research was focused on crystallization kinetics of PHBV8 using alternative nucleating agents to boron nitride, crystallization of PHBV8 in the composites and what the effects of adding nucleating agent, coupling agent and compatibilizer on crystallization and mechanical properties. Specifically, the following objectives are expected through this study:

1. The effect of alternative nucleating agents (NAs) to boron nitride (BN) on Crystallization for PHB and PHBVs;

2. Effects of crystallization and adding nucleating agent on the properties of BPF reinforced PHBV8 composite;

3. Effects of coupling agent and compatibilizer on physical properties of bamboo pulp fiber reinforced PHBV8 composite.

1.5 Reference

- Bhardwaj, R.; Mohanty, A.; Drzal, L.T., Pourboghrat, F.; Misra, M. Renewable resource-based green composites from recycled cellulose fiber and poly(3-hydroxybutyrate-co-3-hydroxyvalerate) bioplastic, *Biomacromolecules* 2006, 7, online.

- Chen, X.; Guo, Q.; Mi, Y. Bamboo Fiber-Reinforced Polypropylene Composites: A Study of the Mechanical Properties, *J. Appl. Polym. Sci.* 1998, 69, 1891-1899.

- Fernandes, E.G.; Pietrini, M.; Chiellini, E. Biobased polymeric composites comprising wood flour as filler, *Biomacromolecules* 2004, 5, 1200 – 1205.

- Gajria, A.; Dave, V.; Gross, R.; McCarthy, S. Miscibility and biodegradability of blends of poly(lactic acid) and poly(vinyl acetate), *Polymer* 1996, 37, 437-44.

- Gerngross, T. Can biotechnology move us toward a sustainable society? *Nature Biotechnol.* 1999, 17, 541-544.

- Gerngross, T.; Slater, S. How green are green plastics? *Scientific American* 2000 283, 36-41.

- Herrmann, A.; Nickel, J.; Riedel, U. Construction materials based upon biologically renewable resource- from components to finished parts, *Polym. Degrad. Stabil.* 1998, 59, 251-261.

- Howells, E.R. Single-cell protein and related techniligy, Chem. Ind. 1982, 15, 508-511.
- Jenkins, D. Desorption as a rate limiting step for gas permeation through a polymer membrane, *Journal of Physical Chemistry B* 2004, 108, 19325-19329.
- Ke, T.; Sun, X. Effects of moisture content and heat treatment on the physical properties of starch and poly(lactic acid) blends, *J. Appl. Polym. Sci.* 2001, 81, 3069-3082.
- Lee, S.; Wang, S. Biodegradable polymers/bamboo fiber biocomposite with bio-based coupling agent, Composites: Part A 2006, 37, 80-91.
- Maglio, G.; Migliozzi, A.; Palumbo, R.; Immirzi, B.; Volpe, M.G. Compatibilized poly(β-caprolactone)/poly(L-lactide) blends for biomedical uses, *Macromol. Rapid Commun.* 1999, 20, 236-238.
- Meredith, J.C.; Amis, E.J. LCST phase separation in biodegradable polymer blends: poly(D,L-lactide) and poly(β-caprolactone), *Macromol. Chem. Phy.* 2000, 201, 733-739.
- Na, Y.; He, Y.; Asakawa, N.; Yoshie, N.; Inoue, Y. Miscibility and phase structure of blends of poly (ethylene oxide) with poly (3-hydroxybutyrate), poly (3-hydroxypropionate), and their copolymers, *Macromolecule*s 2002, *35,* 727-735.

- Parulekar, Y.; Mohanty, A. Biodegradable toughened polymers from renewable resources: blends of polyhydroxybutyrate and maleated polybutadiene, *Green Chemistry* 2006, 8, 206-213.
- Reinsch, V.; Kelley, S. Crystallization of poly(hydroxybutyrate-co-hydroxyvalerate) in wood fiber-reinforced composites, *J. Appl. Polym. Sci.* 1997, 64, 1785-1796.
- Riedel, U.; Nickel, J. Natural fibre-reinforced biopolymers as construction materials new discoveries, *Die Angewandte Makromolekulare Chemie* 1999, 272, 34-40.
- Shanks, R.; Hodzic, A.; Wong, S. Thermoplastic Biopolyester Natural Fiber Composites, *J. Appl. Polym. Sci.* 2004, 91, 2114-2121.
- Urayama, H.; Ma, C.; Kimura, Y. Mechanical and thermal properties of poly (l-lactide) incorporating various inorganic fillers with particle and whisker shapes. *Macromol. Mater. Eng.* 2003, 288, 562-568.
- Van De Velde, K.; Kiekens, P. Biopolymers: overview of several properties and consequences on their applications, *Polym. Test.* 2002, 21, 433-442.
- Wang, H.; Sun, X.; Seib, P. Strengthening blends of poly (lactic acid) and starch with methylenediphenyl diisocyanate, *J. Appl. Polym. Sci.* 2001, 82, 1761-1767.
- Wang, S.; Song, C.; Chen, G.; Guo, T.; Liu, J.; Zhang, B.; Takeuchi, S. Characterization and biodegradation properties of poly (3-hydroxybutyrate-co-3-

hydroxyvalerate) / organophilic montmorillonite (PHBV/OMMT) nanocomposites, *Polym. Degrad. Stab.* 2005, 87, 69-76.

- Wong, S.; Shanks, R.; Hodzic, A. Properties of poly (3-hydroxybutyric acid) composites with flax fibres modified by plasticizer Absorption, *Macromol. Mater. Eng.* 2002, 287, 647-655.

- Yasin, M.; Holland, S. J.; Jolly, A.M.; Tighe, B. J. Polymers for biodegradable medical devices. VI. Hydroxybutyrate-hydroxyvalerate copolymers: accelerated degradation of blends with polysaccharides, *Biomaterials* 1989, 10, 400-412.

- Yoona, J.; Leea, W.; Jin, H.; China, I.; Kimb, M.; Goa, J. Toughening of poly (3-hydroxybutyrate) with poly (*cis*-1,4-isoprene), *Eur. Polym. J.* 1999, 35, 781-788.

- Zhang, J.; Jiang, L.; Zhu, L.; Jane, J.; Mungara, P. Morphology and properties of soy protein and polylactide blends, *Biomacromolecules* 2006 7, 1551-1561.

CHAPTER 2 EFFECT OF ALTERNATIVE NUCLEATING AGENTS TO BN ON CRYSTALLIZATION FOR PHB AND PHBV

2.1 Abstract

In this study, thymine and melamine were introduced as nucleating agents (NAs) for poly(3-hydroxybutyrate-co-3-hydroxyvalerates) (PHBVs) and poly(3-hydroxybutyrate) (PHB), and their effects were compared with that of boron nitride (BN). The study focused on the crystallization of PHBVs, because the overall crystallization rate of PHBVs decreases drastically with the increase in the 3-hydroxyvalerate (3-HV) comonomer content. Isothermal crystallization kinetics of neat PHBVs and nucleated PHBVs was studied by differential scanning calorimetry (DSC), and Avrami equation and parameters were derived and assessed. The nucleation and crystal growth were examined using polarized optical microscopy (POM). All NAs had similar particle sizes and showed good dispersion in the polymer matrix as demonstrated by scanning electron microscopy (SEM). The results indicated BN and thymine greatly increased the overall crystallization rate for all PHBVs studied and demonstrated very similar effects.

2.2 Introduction

Since poly(3-hydroxybutyrate) (PHB) was first produced in pilot scale in the early 1980s (Barham *et al* 1984), bacterial polyhydroxyalkanoates (PHAs) have received extensive studies. PHAs are produced from renewable feedstock such as sugars or enzyme-thinned starch, and are thermoplastic polymers and fully biodegradable. PHB has received the most study in the PHA family, and possesses many similar mechanical and physical properties to that of polypropylene (Barham *et al* 1984). However, PHB is susceptible to thermal degradation and shows severe post-process embrittlement, which prevents them from broad applications (de Koning and Lemstra 1993). The brittleness of PHB is attributed to the large spherulites and the secondary crystallization. Although PHB is easy to crystallize and gives high crystallinity, it yields low nucleation density and consequently forms large-sized spherulites commonly known to impair the mechanical properties of the materials (El-Hadi and Schnabel 2002). Embrittlement from the post-process secondary crystallization further deteriorates this brittleness problem. In addition, the poor thermal stability of PHAs, particularly PHB, often presents a problem for processes such as molding, sheet and film extrusion. The thermal degradation also contributes to the poor performance of the materials. It is believed that the thermal degradation of PHB is dominated by a random *cis*-elimination reaction. Because of the activated C-H bond neighboring the carbonyl involving a six-member ring transition state, PHB and other PHAs, are less thermally stable than those polymers from other hydroxyl

carboxylic acids, e.g., PLA and PCL (Aoyagi *et al* 2002, Grassie *et al* 1984, Morikawa and Marchessault 1981).

Many efforts have been used to battle the brittleness of PHB. These include blending with other polymers (Saito *et al* 2001, Cavallaro 1994, Zhang *et al* 1996 and Avella and Martuscelli 1988), using reverse temperature processing (Zhang *et al* 2004), annealing of the molded articles (de Koning and Lemstra 1993) and copolymerization of 3-hydroxybutyrate (3-HB) with other monomers (Homes 1985 and Doi *et al* 1988). Copolymers of 3-HB and 3-hydroxyvalerate (3-HV), poly (3-hydroxybutyrate-*co*-3-hydroxyvalerates) (PHBVs) generally give higher ductility than PHB and require lower processing temperatures that ease the problem of thermal degradation. However, PHBV yields slow crystallization rate and low crystallinity, and these properties became serious with increasing 3-HV comonomer content. The low crystallization rate of PHBVs introduces some serious problems during processing. In injection molding the part is soft and may not be properly ejected unless a long cooling time allowed; in extrusion it is tacky and tends to stick onto itself. In addition, a large fraction of the copolymer remains amorphous and slowly undergoes crystallization during storage. Therefore, it is very important to accelerate the crystallization rate of these copolymers by adding nucleating agents (NAs). Even for PHB that crystallizes fast, adding a NA will produce small and more homogeheous spherulite sizes and enhance its mechanical properties.

A number of chemicals has been studied as NAs for PHB and PHBVs including boron nitride (BN) (Liu *et al* 2002 and Kai *et al* 2005), talc (Liu *et al* 2002 and Kai *et al* 2005), saccharin (Black *et al* 1990), lignin (Kai *et al* 2004), terbium oxide (Tb_2O_3), lanthanum oxide (La_2O_3) (Liu 2002), α-cyclodextrin (He and Inoue 2003) and organophosphorous compounds (Asrar 1999) etc. In general, adding NAs results in an increase in melt crystallization temperature and narrowing of the crystallization peak during nonisothermal melt crystallization; in other words, less degree of supercooling and shorter crystallization time are needed. Results indicated that BN was a more effective NA than most others on increasing the melt crystallization temperature and accelerating the crystallization rate.

In this study, we introduced thymine and melamine as two potential candidate NAs for PHAs in comparison with the traditional BN. The major objective of this research was to compare the effects of thymine, melamine and boron nitride as NAs on nucleation and crystallization rate of PHBVs. For the purpose of comparison, the effect of these NAs on the nonisothermal crystallization of PHB was also studied. Thymine, isolated from natural resources, is environmentally friendly. Melamine is a stable, non-hazardous and inexpensive chemical, and is widely used in thermoset resins and other applications. Thymine and melamine have been reported as NAs for isotactic polystyrene in literature (Beck 1978), but have not yet been studied as NAs for PHAs. PHBVs with different 3-HV contents and PHB were used in this study.

2.3 Experimental

2.3.1 Materials

PHBVs containing 8, 12 and 21 mol% 3-HV in fine powder form were provided by Metabolix Inc. (Cambridge, MA). PHB in fine powder form was provided from Tianan Biological Material Co. (Ningbo, China). Table 2.1 gives the weight-average molecular weight and polydispersity index of each PHA polymer measured by gel permeation chromatography (GPC). BN in fine powder was obtained from Advanced Ceramics Corporation (Cleveland, OH) and used as received. Thymine and melamine in powder form were obtained from Aldrich Chemicals and were further ground with a mortar before using.

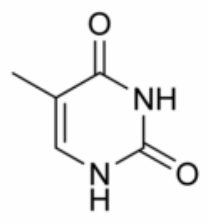

Thymine

Melamine

2.3.2 Sample preparation

PHBV compounds containing different NAs were prepared by melt mixing in a twin screw extruder. The polymers were first dried in an oven at 80ºC for 8-hrs. The polymer and 1 phr (per hundred resin) NA was premixed by manually tumbling in a plastic bag, and subsequently fed into the extruder using a volumetric feeder. A co-rotating twin

screw extruder (Leistritz ZSE-18) equipped with a volumetric feeder and a strand pellet cutter was employed. The screw diameter was 17.8 mm and the L/D ratio was 40. Extrusion temperature was independently controlled on eight zones along the extruder barrel. In order to reduce the thermal degradation, a reverse temperature process was used (Zhang *et al* 2004) and the temperature profile from zone 1 (next to the feeding throat) to zone 8 (die adapter) was 175°C, 175°C, 165°C, 160°C, 155°C, 150°C, 145°C, and 145°C for PHB. For PHBVs, and each zone temperature was set to be 5, 10 and 15°C lower for PHBV8, PHBV 12 and PHBV21, respectively. The screw speed was maintained at 80-rpm for all runs. After exiting the die, the extrudate was cooled in a water bath and then pelletized.

2.3.3 Crystallization

Isothermal and non-isothermal crystallization were studied using a differential scanning calorimeter (Mettler Toledo, DSC 822e). The sample sizes were ca. 5 - 7 mg, and the samples were crimp sealed in 40-ul aluminum crucibles. Each sample was analyzed in duplicates. A non-isothermal melt crystallization test was first performed on each sample. The sample was heated to 185^{o}C at 25^{o}C/min for PHB and PHBV8, to175^{o}C for PHBV12, and to 165^{o}C for PHBV21, and kept isothermally for 2 minutes to erase previous thermal history. It was then cooled at 10ºC/min to -25^{o}C. Finally, a second heat scan was performed at 10^{o}C/min. The enthalpy change and melting temperature were examined. Thereafter non-isothermal tests were performed at different pre-selected

cooling rates, in a similar procedure. For isothermal crystallization, the sample was first heated to melt as in the nonisothermal crystallization process, and kept isothermally for 2 minutes. The sample was then cooled to the pre-determined crystallization temperature at 25°C/min and kept isothermally for sufficient time to allow completion of the crystallization. Finally it was cooled to -25ºC at 25ºC/min, kept isothermally for 1 minute and followed by a second heat scan at 10°C/min to examine the melting temperature and crystallinity. Cystallization kinetics parameters were calculated for both non-isothermal and isothermal crystallization process.

Avrami equation was adopted to describe the isothermal crystallization of PHBVs:

$$1 - X_{rel} = \exp(-Kt^n) \tag{1}$$

Equation (1) can be rearranged as:

$$\mathrm{Log}(-\mathrm{Ln}(1 - X_{rel})) = n\mathrm{Log}(t) + \mathrm{Log}(K) \tag{2}$$

where K is the Avrami crystallization rate constant containing the contributions from both nucleating and growth, n iss the Avrami exponent determined by the mode of nucleation and the crystal geometry, and X_{rel} is the relative crystallinity at time t during the crystallization process and is given as:

$$X_{rel} = \frac{X_c(t)}{X_c(\infty)} = \int_0^t \frac{dH(t)}{dt} dt \Big/ \int_0^\infty \frac{dH(t)}{dt} dt \tag{3}$$

where $X_c(t)$ and $X_c(\infty)$ are the degrees of crystallinity at time t and at the end of crystallization process, respectively. Plot of Log(-Ln(1-X_{rel})) vs. Log(t) gives a straight

line, whose slope is n and the intercept on the coordinate is Log(K). The half time $t_{0.5}$, which is the time when half of the volume of the polymer is filled with crystals, that is to say $X_{rel} = 0.5$, is given as:

$$t_{0.5} = (\frac{Ln2}{K})^{\frac{1}{n}} \tag{4}$$

Modified Avrami equation (5) was adopted to describe the non-isothermal crystallization of PHBVs.

$$1 - X_{rel} = \exp(-Z_t t^n) \tag{5}$$

Similarly it can be rearranged as:

$$Log(-Ln(1 - X_{rel})) = nLog(t) + Log(Z_t) \tag{6}$$

The difference is in non-isothermal crystallization, the effect of cooling rate need to be considered, so the Avrami parameter Z_t is revised as

$$Log(Z_c) = \frac{Log(Z_t)}{\Phi} \tag{7}$$

where Z_c and n in equation (6) and (7) have the same meaning as K and n in equation (2). X_{rel} is the relative crystallinity at temperature T during the crystallization process and is given as:

$$X_{rel} = \int_{T0}^{T} \frac{dH(T)}{dT} dT / \int_{T0}^{T\infty} \frac{dH(T)}{dT} dT \tag{8}$$

where T_0 and T_∞ represent the onset and end set temperature of crystallization process respectively. The relation between crystallization time t and temperature T is given by

$$t = \frac{T_0 - T}{\Phi} \tag{9}$$

where Φ is the cooling rate of the non-isothermal crystallization process. Finally the half time in non-isothermal crystallization can be computed as

$$t_{0.5} = \left(\frac{Ln2}{Z_t}\right)^{\frac{1}{n}} \tag{10}$$

2.3.4 Nucleating agent particle sizes and dispersion

Scanning electron microscopy (SEM, Hitachi S-570) was used to examine the particle sizes of NAs and their dispersion in the polymers. The extrudates from the above extrusion mixing were cryo-fractured and sputter coated with gold prior to examination.

2.3.5 Polarized optical microscopy (POM)

Nucleation and spherulite growth were observed using a polarized optical microscope (Olympus BX51) equipped with a hot stage (Linklam TMS 94). Thin film samples were prepared by melting the materials between microscope cover slips. Samples were heated at 40°C/min from room temperature to the same designated melt temperatures as that in the DSC experiment, isothermally melted for 4 minutes and then cooled at 40°C/min to the selected isothermal crystallization temperatures.

2.4 Results and discussion

2.4.1 Effect of NAs on crystallization

Figure 2.1- 2.4 give the DSC thermograms of melt nonisothermal crystallizations of PHB and PHBVs using different NAs at the cooling rate of 10^{o}C/min. Melt crystallization temperatures and enthalpy of crystallization are summarized in Table 2.2. It is a common practice to evaluate the effect of a NA on crystallization by the change of melts nonisothermal or cold crystallization temperature as well as the increase in crystallinity. Usually, a high melt crystallization temperature or a low cold crystallization temperature is taken as an indirect indicator for fast crystallization. The results showed that without a NA, only PHB could crystallize to a significant degree (high crystallization enthalpy) and had a moderately high crystallization temperature (Figure 2.1 & Table 2.2); the crystallization ability of neat PHBVs decreased rapidly with increase in the 3-HV content. With 21 mol% of 3-HV, neat PHBV21 did not show any melt crystallization at the cooling rate of 10^{o}C/min. In general, all three NAs resulted in certain enhancements of the crystallization ability of the PHBVs as seen in the increases in melt crystallization temperatures (T_cs) and enthalpy of crystallization (ΔH_c). BN and thymine showed very similar effects in nucleating and crystallizing PHB and PHBVs and behaved to be effective nucleating agents. Since PHB itself is easy to crystallize, addition of a NA did not significantly increase its crystallinity. Nevertheless, adding NA still greatly increased its T_c, with 1% BN and thymine resulting in an increase of ca. 28 and 32^{o}C in the T_c of

PHB, respectively. On the other hand, addition of BN and thymine both resulted in large increases in crystallinity (ΔH_c) and T_c of PHBV8 and PHBV12, respectively. Melamine also demonstrated the ability to increase T_c and ΔH_c of PHB and PHBVs, but appeared to be less effective when compared to BN and thymine. Melamine only showed a slight effect on the crystallization of PHBV12 and could not crystallize PHBV21at all, In contrast, both BN and thymine nucleated PHBV21 and yielded substantial degrees of crystallinity.

2.4.2 Polarized Optical Microscope (POM)

The melt crystallizations of PHBV8 and PHBV12 were further investigated using a polarized optical microscope. PHBV8 were heated to 185ºC and PHBV12 to175 ºC at 40ºC/min, isothermally melted for 3 minutes, then cooled to 76ºC and 70 ºC at 40ºC/min, respectively. Figure 2.5- 2.12 show the photomicrographs of spherulites of PHBV8 and PHBV12 within 60s time frame. Comparing neat PHBV8 with neat PHBV12, it is clear to note that the homogeneous nucleation of PHBV8 was much faster than that of PHBV12 (Figures 2.5 & 2.9). While the spherulites of PHBV8 had grown to impinge each other; the spherulites of PHBV12 were only observed sporadically within a similar time frame. This result indicates PHBV8 has stronger crystallization ability than PHBV12, which was consistent with the DSC analysis. Nucleation density was greatly increased with the addition of NAs, consequently, the average size of the spherulites appeared to decrease. A good NA can decrease the activation energy that is needed for

the polymer to create a critical surface of nucleation; in other words, improve the density of nuclei as well as increase the growth rate (Beck 1975).

2.4.3 NA particle sizes and dispersion

NA particle size and its dispersion in the polymer matrix also affect the nucleation density and spherulite sizes and distribution. A NA with fine particle sizes has a high tendency to form more nuclei. It is understood that a good NA can form a fine dispersion of small crystals or a thin crystalline layer absorbed on another substance (Hoffman and Weeks 1962). The BN used is a commercial products of nucleating agent grade and has an average particle size of ca. 2μm. The thymine and melamine was further ground in an effort to achieve comparable sizes to that of BN. SEM micrographs for PHBV8 with different NAs are shown in Figures 2.13-2.16. It appeared that all NAs had very similar and uniform particle sizes, within the 1 - 2 μm range. The NAs also dispersed fairly well in the polymers, and only small agglomerates were observed.

2.4.4 Isothermal crystallization kinetics

The isothermal Avrami plots of PHAs with NAs are given in Figures 2.17-2.26. The enthalpy of isothermal crystallization (ΔH_{ic}) and Avrami parameters, n, K and $t_{0.5}$, are listed in Tables 2.3-2.5. Since the basic Avrami equation 1 is based on many assumptions such as linear crystal growth, primary nucleation, constant volume, etc., it is usually valid at low conversion as long as the impingement is not serious (Wunderlich 1976).

Therefore, the n and K were usually calculated from the early linear segment of the Avrami plot as reported in many other studies (Liu *et al* 2002, Kai *et al* 2004, Kai *et al* 2005). For different PHBV/NA pairs, the isothermal crystallization temperatures (T_{ic}) were selected to be mainly in the vicinity of the peak melt crystallization temperatures as listed in Table 2.2. For comparison purposes, the isothermal crystallization temperatures for neat PHBV8 and PHBV12 were set to be in the same range as that for the respective PHBV/melamine.

Compared with PHBV/NA, neat PHBV yielded Avrami plots and parameters showing different trends with the change of T_{ic}. With the crystallization progress, the Avrami plots of neat PHBV8 and PHBV12 at low T_{ic}s showed clear inflexions that separated the curves into two approximately linear regions corresponding to early and late crystallization stages, respectively. This inflexion faded out with increasing T_{ic} and the plot became a straight line at high T_{ic}. The slope (n) in the first region was smaller than that in the second region, which was close to the slope of the plot for the same sample isothermally crystallized at high temperatures. The n value is dependent on crystal geometry, nucleation mode (athermal or thermal) and rate determination (contact or diffusion control). For the neat PHBV8 and PHBV12, the values of n in Tables 2.3 and 2.4 were determined from the first linear region. It was small (<2) at low T_{ic}s but continuously increased with T_{ic} and eventually leveled off and became similar to that of those NA-containing PHBVs. It appeared that with a large supercoooling ($\Delta T \approx 85°C$, or

$T_{ic} \leq 78°C$ for PHBV8 and $T_{ic} \leq 70°C$ for PHBV12), neat PHBVs showed a crystallization mechanism of spherical growth on diffusion from athermal (simultaneous) nucleation. In an ideal situation, the theoretical n value would be 1.5 for such case. The crystallization mechanism of neat PHBVs was clearly different when the degree of supercooling was reduced, (T_{ic} increasing) as seen in the steady increase of n value. This increase in n value was likely due to the transition of crystal growth mode from diffusion to contact. The slope increase at late crystallization stage (second linear segment) was probably a result of branching crystals (Morgan 1954), particularly at lower T_{ic} (large supercooling) where spherical crystal growth was slow. Macromolecular crystals are known frequently to have an inherent or supercooling caused branching mechanism (Wunderlich 1976). On the other hand, the Avrami plots of all NA-containing PHBVs showed a good linearity throughout most of the crystallization course and were almost parallel to each other. The n value varied in a narrow range, from 2.31 to 2.41 for PHBV8, 2.28 to 2.43 for PHBV12, and 2.24 to 2.36 for PHBV21, respectively. Since these samples contained NAs, their n values suggested a likely crystallization mechanism of spherical growth on contact from athermal nucleation (Wunderlich 1976, Hiemenz 1984). Since the derivation of Avrami equation contains a number of simplifications which do not necessarily apply to the crystallization of macromalecules(Wunderlich 1976), it is common to note the deviation of the n value from the theoretical value (= 3) (Liu *et al* 2002, Kai *et al* 2004, Kai *et al* 2005).

The change of K with T_{ic} was just the opposite for neat PHBV and PHBV/NA. The value of K for PHBV/NA increased continuously with T_{ic}, while the value of K for neat PHBV decreased monotonously with T_{ic}. The K value for the PHBV/NA was also much higher than that of the respective neat PHBV. Figures 2.17-2.24 also indicated that at a given time the crystallinity of neat PHBV8 and PHBV12 was higher at lower temperatures, but the crystallinity of NA-containing PHBVs was lower. In other words, neat PHBV8 and PHBV12 crystallized faster at lower temperatures, while NA-containing PHBVs crystallized faster at higher temperatures. This result suggested that the crystallization of neat PHBV was more nucleation-determined, while the crystallization of PHBVs containing NAs was more growth-determined.

Unlike neat PHBVs whose n value increased with T_{ic}, the n values for NA-containing PHBVs almost showed no change with T_{ic}. The addition of NA also greatly reduced the half crystallization time, particularly for BN and thymine. Furthermore, PHBV/BN and PHBV/thymine were isothermally crystallized in similar temperature ranges and demonstrated very similar n, K, and $t_{0.5}$. In contrast, PHBV/melamine yielded smaller k values than respective PHBV/BN and PHBV/thymine, but larger values than the respective neat PHBVs. The enthalpy of crystallization also decreased slightly with an increase in temperature.

2.4.5 Melting behaviors and equilibrium melting temperature of PHBVs

Figure 2.27-2.29 show the effects of NAs on the melting behavior of those isothermally crystallized PHBVs. The bimodal melting endotherm was characteristic of PHBVs. It is reasoned that the peak with the lower melting temperature (T_{m1}) is attributed to the melting of crystals formed during the isothermal crystallization process; and some of these crystals during DSC heat scan experience melting-recrystallization or crystal rearrangement and then melt at a higher melting temperature (T_{m2}) (Zhang *et al* 2004, Homes 1985, Doi *et al* 1988 and Liu *et al* 2002). It was noted that T_{m1} and T_{m2} of the neat PHBV were lower than that of the corresponding PHBV/NA, suggesting less crystal perfection (lower lamellar thickness) in the former case. The area ratio of peak T_{m1} to peak T_{m2} appeared to increase greatly with the addition of NAs for PHBV8 and PHBV12, with BN and thymine demonstrating the most obvious effects. All these results indicate that the addition of a NA increases not only the crystallization rate but also crystal perfection. The area ratio of peak T_{m1} to peak T_{m2} also appeared to decrease in the order from PHBV8 to PHBV12 to PHBV21, meaning more crystals experienced the recrystallization during the heat scan in the same order. In other words, higher 3-HV content in the PHBV copolymer resulted in more imperfection of the crystals.

Since T_{m2} was the melting of those recrystallized crystals that had thick lamellas, it was independent of the T_{ic} and was almost constant. On the other hand, T_{m1}represented the melting of the crystals formed during melt isothermal crystallization and increased

with T_{ic}. This result suggested that higher T_{ic} led to the formation of more perfect crystals. It also suggested that the addition of a NA resulted in crystals with better perfection. Figure 2.30-2.32 showed that the relationship between T_{m1} and T_{ic} can be described by the Hoffman and Weeks equation (Hoffman and Weeks 1962):

$$T_m = T_m^0[1 - \frac{1}{\gamma}] + \frac{T_{ic}}{\gamma} \qquad (5)$$

where, T_m^0 is the theoretical melting temperature of crystals with infinite lamellar thickness, and γ is the ratio of final to initial lamellar thickness. The approximate value for T_m^0 is obtained by extrapolating T_m vs. T_{ic} curve to the point where $T_m = T_{ic}$ (Hoffman and Weeks 1962). A good linear relation between T_{m1} and T_{ic} was established. This result was in agreement with other studies (Liu *et al* 2002 and Organ *et al* 1991). For each PHBV, Figures 2.30 - 2.32 also showed that the curve of T_{m1} vs. T_{ic} for every NA fell on almost identical lines and tended to yield the same T_m^0, indicating similar crystal perfection resulted in those cases. In this study, the T_m^0s were found to be 166, 160 and 154 ^oC for PHBV8, PHBV12 and PHBV21, respectively.

2.4.6 Non-isothermal crystallization kinetics

The non-isothermal Avrami plots of PHAs with NAs are given in Figures 2.37-2.42. The non-isothermal melt crystallization temperature (T_{nc}), enthalpy of crystallization (ΔH_{nc}) and Avrami parameters, n, Z_{nc} and $t_{0.5}$, are listed in Tables 2.6-2.8. For PHBV8 and PHBV12, the non-isothermal crystallization cooling rates were selected to be

5°C/min, 10°C/min, 20°C/min and 40°C/min. For PHBV21, the non-isothermal crystallization cooling rates were selected to be 2.5°C/min, 5°C/min, 10°C/min and 20°C/min. The DSC thermograms of second heating at 10°C/min after non-isothermal crystallization are given in Figure 2.43 - 2.45.

In Figure 2.33 - 2.42, all non-isothermal Avrami plots were parallel lines for neat PHBVs and PHBVs/NAs as cooling rates increased. It indicated that all blends had the similar crystallization mechanism at different cooling rates. Furthermore, Table 2.6-2.8 showed that PHBV/BN and PHBV/thymine had a higher n value than the corresponding neat PHBV and PHBV/melamine at the same cooling rate. Also from the DSC thermogram of the second heating after the non-isothermal crystallization (Figure 2.43-2.45), the first peak value of melting temperature was higher for the PHBV/NA than for the corresponding neat PHBV. As discussed in isothermal crystallization process, the higher the first peak value of melting temperature was, the more perfect crystals the materials had. All results proved that the nucleating agent helped material yield more homogeneous and perfect crystals than it originally did.

The overall crystallization rate Z_c increased with the addition of NAs, as seen at each cooling rate in Table 2.6-2.8. The value of Z_c of PHBV/BN and PHBV/thymine was higher than that of PHBV/melamine. This observation suggests that BN and thymine accelerated the crystallization process faster than melamine.

By looking at the crystallization temperature and enthalpy of melt crystallization with BN and thymine, it was found that PHBV8 and PHBV12 had comparable

crystallinity. Melamine was less effective in improving the crystallization ability than BN and thymine. Neat PHBV didn't crystallize at the cooling rate of 20^{o}C/min or higher. PHBV8/melamine and PHBV12/melamine could not crystallize at 40^{o}C/min. PHBV8 and PHBV12 with BN and thymine showed no cold crystallization in the second heating process after the non-isothermal crystallization process at the cooling rate of 10^{o}C/min, while the neat PHBV8 and PHBV12 did show in the second heating process at the same cooling rate. For PHBV21, only BN and thymine showed the crystallization process, although the cold crystallization still occurred in the second heating. The neat PHBV21 and PHBV21/melamine could not crystallize at all cooling rates. All of above results supported that BN and thymine had comparable effects on crystallization for PHBVs, and the melamine was less effective than them.

2.5 Conclusion

Both boron nitride (BN) and thymine greatly increased the crystallization ability of PHBVs, and showed very similar nucleating ability on PHBVs. Melamine also improved the crystallization ability of PHBV8 and PHBV12, but was less effective than thymine and BN. Furthermore, melamine could not nucleate PHBV21 at all. POM revealed that all NAs increased nucleation density and appeared to yield simultaneous nucleation of the PHBVs. Isothermal crystallization indicated that the crystallization of neat PHBVs was more nucleation-determined and slower, while the crystallization of PHBVs containing NAs was more growth-determined and much faster. Neat PHBVs required a large

supercooling for the optimal crystallization and showed spherical growth on diffusion from athermal (simultaneous) nucleation, while nucleated PHBVs required a much smaller supercooling for the optimal crystallization and demonstrated spherical growth on contact from athermal nucleation. All NAs resulted in crystalline structures with similar perfection, and the nucleated PHBVs showed higher melting temperatures than neat PHBVs. Melamine as NA resulted in severe thermal degradation and reacted with the carboxylic end groups of PHBVs, hence was not an effective NA for PHBVs. Thymine did not react with PHBVs but showed a slight catalytic effect on the thermal degradation. BN, on the hand, did not react nor catalyze the thermal degradation of PHBVs, and showed the highest nucleating effect.

2.6 References

- Aoyagi, Y.; Yamashita, C.; Doi, Y. Thermal degradation of poly [(R)-3-hydroxybutyrate], poly [ε-caprolactone], and poly [(S)-lactide], *Polym. Degrad. Stab.* 2002, 76, 53-59.
- Asrar, J.; Pierre, J. R. Nucleating agents for polyhydroxyalkanoates and other thermoplastic polyesters and methods for their production and use U.S. Pat No. 5, 973, 100, 1999.
- Avella, M.; Martuscelli, E. Poly-D- (-)(3-hydroxybutyrate)/poly (ethylene oxide) blends: Phase diagram, thermal and crystallization behavior, *Polymer*1988, 29, 1731-1737.
- Beck, H. N. Nucleation of isotactic polystyrene, US Pat No. 4,076, 910, 1978.
- Black, S. N.; Dobbs, B.; Dempsey, P.S.; Davey, R.J. Crystal chemistry and nucleating agents; saccharin and poly-3-hydroxybutyrate, *J. Matr. Sci. Lett.* 1990, 9, 51-52.
- Cavallaro, P.; Immirzi, B.; Malinconico, M.; Martuscelli, E.; Volpe, M. Thermal and structural analysis and crystallization behavior of new poly (ether-alkyl) oxadiazoles *Macromol. Rapid. Commun.* 1994, 15, 103-111.
- de Koning, G. J. M.; Lemstra, P. J. Crystallization phenomena in bacterial poly[(R)-3-hydroxybutyrate]: 2. Embrittlement and rejuvenation, *Polymer* 1993, 34, 4089-4094.

- El-Hadi, A.; Schnabel, R. Correlation between degree of crystallinity, morphology, glass temperature, mechanical properties and biodegradation of poly (3-hydroxyalkanoate) PHAs and their blends, *Polym Test* 2002, 21, 665-674.
- Esposito, F. Synthesis of polymer-embedded metal clusters by thermolysis of mercaptides - Polymer blends, *Plastics News*, Nov. 9 –10, 296-300.
- Grassie, N, Murray, E.J., Holmes, P.A. Thermal degradation of poly (β-(d)-beta-hydroxybutyric acid): Part 1- Identification and quantitative analysis of products, *Polym Degrad. Stab.* 1984, 6, 47-61.
- Grassie, N.; Murray, E. J.; Holmes, P.A. Thermal degradation of poly (β- (d)-beta-hydroxybutyric acid): Part 2-Changes in molecular weight, *Polym Degrad. Stab.* 1984, 6, 95-103.
- Grassie, N.; Murray, E. J.; Holmes, P.A. Thermal degradation of poly (β- (d)-beta-hydroxybutyric acid): Part 3-The reaction of mechanism, *Polym Degrad. Stab.* 1984, 6, 127-134.
- He, Y.; Inoue, Y. α-Cyclodextrin-enhanced crystallization of poly (3-ydroxybutyrate), *Biomacromolecules* 2003, 4, 1865-1867.
- Hoffman, J.D.; Lauritzen, J. I.; J. R.; Passaglia, E.; Ross, G.S. Frolen, L.J.; Weeks, J. J. Kinetics of polymer crystallization from solution and the melt, *Kolloid-Zeit & Zeit fuer Polymere* 1969, 231, 564-592.

- Homes, P. A. Polymerization of macromonomers IV: Monomer reactivity ratios in radical copolymerization of methyl methacrylate with (p-vinylbenzyl) polystyrene macromonomer, *Phys. Technol.* 1985, 16, 32-36.

- Howells, E.R. Single-cell protein and related techniligy, Chem. Ind. 1982, 15, 508-511.

- Kai, W.; He, Y.; Asakawa, N.; Inoue, Y. Effect of lignin particles as a nucleating agent on crystallization of poly (3-hydroxybutyrate), *J. Appl. Polym. Sci.* 2004, 94, 2466-2474.

- Kai, W.; He, Y.; Inoue, Y. Fast crystallization of poly (3-hydroxybutyrate) and poly(3-hydroxybutyrae-*co*-3-hydroxyvalerate) with talc and boron nitride as nucleating agents, *Polym. Intl.* 2005, 54, 780-78.

- Kunioka, M.; Tamaki, A.; Doi, Y. Crystalline and thermal properties of bacterial copolyesters: Poly (3-hydroxybutyrate-co-3-hydroxyvalerate) and poly (3-hydroxybutyrate-co-4-hydroxybutyrate), *Macromolecules* 1989, 22, 694-697.

- Liu, W. J.; Yang, H.L.; Wang, Z.; Dong, L.S.; Liu, J.J. Effect of nucleating agents on the crystallization of poly (3-hydroxybutyrate-*co*-3-hydroxyvalerate), *J. of Appl. Polym. Sci.* 2002, 86, 2145-2152.

- Ogawa, Y.; Akagi, N., Polyester resin composition, U.S. Pat No. 4, 536, 531, 1985.

- Organ, S. J.; Barham, P. J. Nucleation, growth and morphology of poly (hydroxybutyrate) and its copolymers, *J. of Mater. Sci.* 1991, 26, 1368-1374.
- Saito, M.; Inoue, Y.; Yoshie, N. Cocrystallization and phase segregation of blends of poly (3-hydroxybutyrate) and poly (3-hydroxybutyrate-co-3-hydroxyvalerate), *Polymer* 2001, 42, 5573-5580.
- Wunderlich, B. Polymer crystal nucleation and growth from the monomer *Applied Polymer Symposia* 1975, 26, 281-289.
- Zhang, J.; McCarthy, S.; Whitehouse, R. J. Reverse temperature injection molding of Biopol and effect on its properties, *Appl. Polym. Sci*. 2004, 94, 483-491.
- Zhang, L.; Xiong, C.; Deng, X. Miscibility, crystallization and morphology of poly (β-hydroxybutyrate)/poly (d, l-lactide) blends, Polymer 1996, 37, 235-241.

2.7 Figures

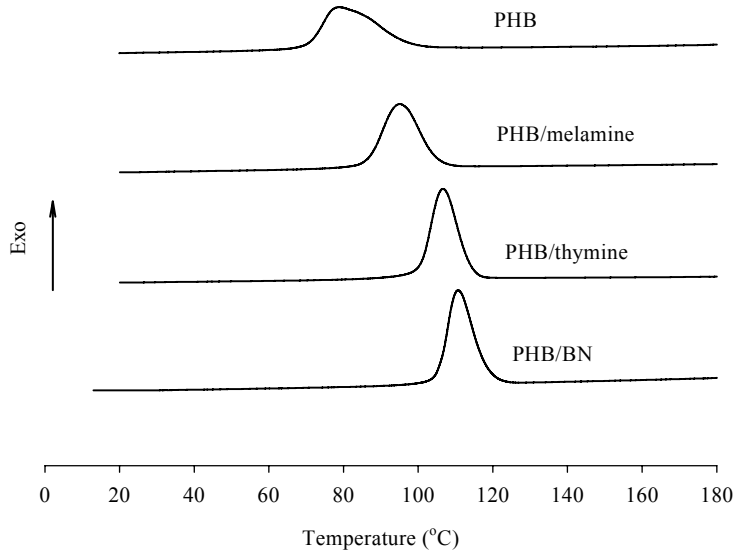

Figure 2.1. DSC thermograms of nonisothermal melt crystallizations for PHB/NA blends at the cooling rate of 10°C/min

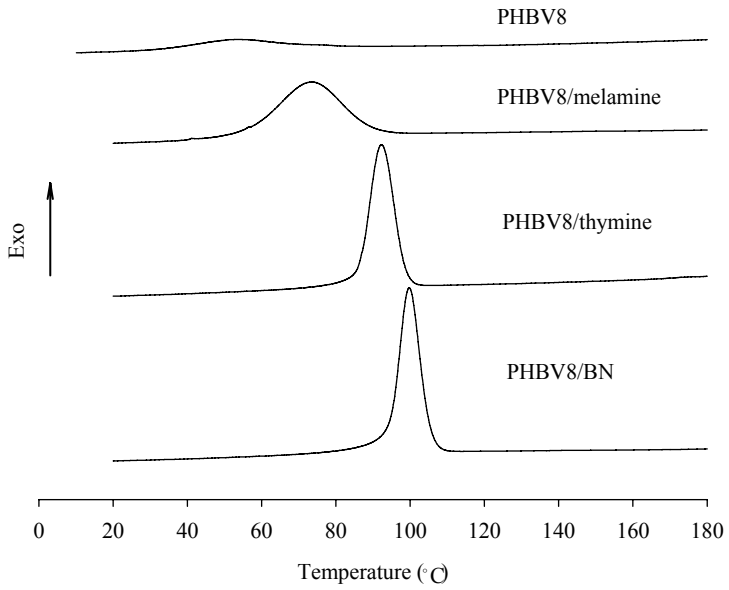

Figure 2.2. DSC thermograms of nonisothermal melt crystallizations for PHBV8/NA blends at the cooling rate of 10°C/min

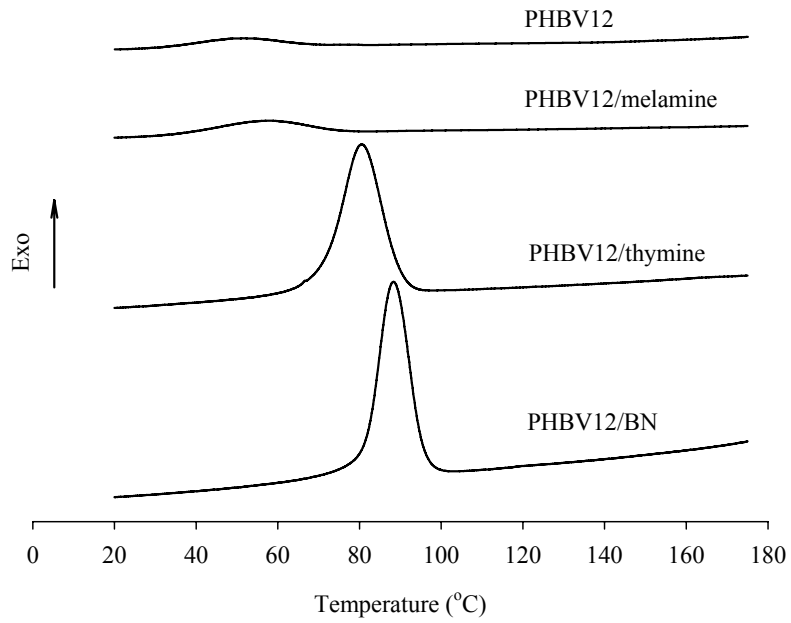

Figure 2.3. DSC thermograms of nonisothermal melt crystallizations for PHBV12/NA blends at the cooling rate of 10°C/min

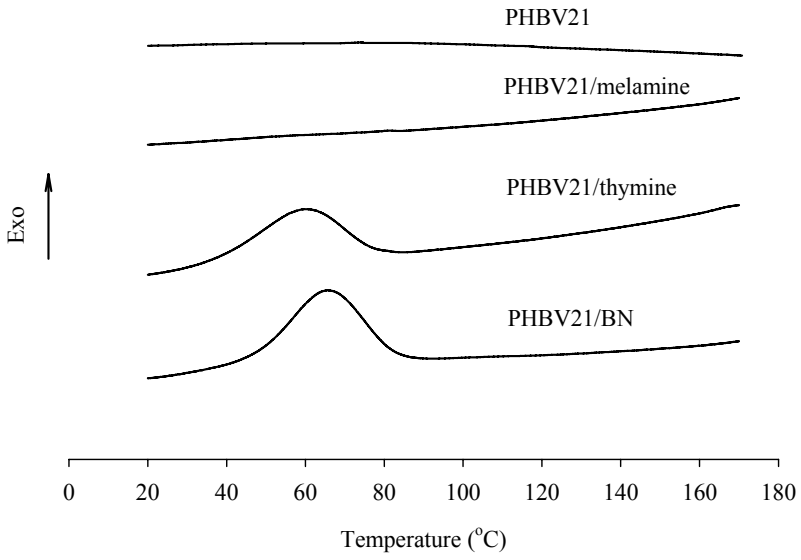

Figure 2.4. DSC thermograms of nonisothermal melt crystallizations for PHBV21/NA blends at the cooling rate of 10°C/min

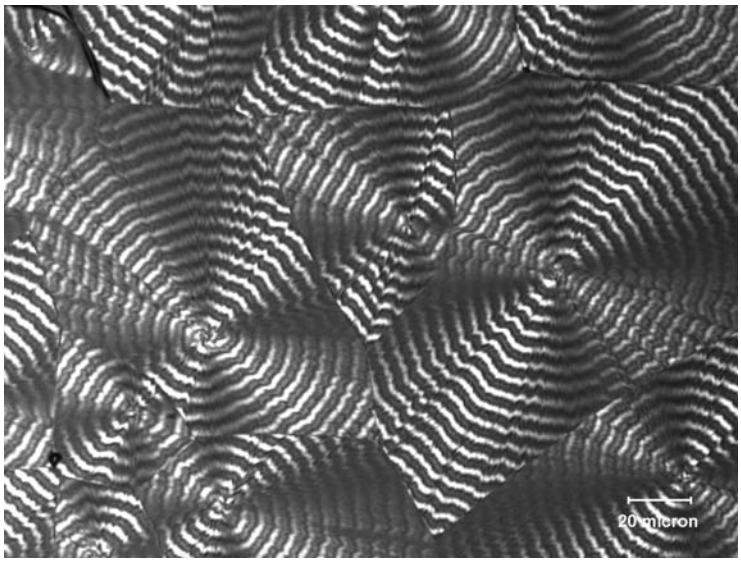

Figure 2.5. POM micrograph of neat PHBV8 (T_c=76^{o}C, t_c=60s)

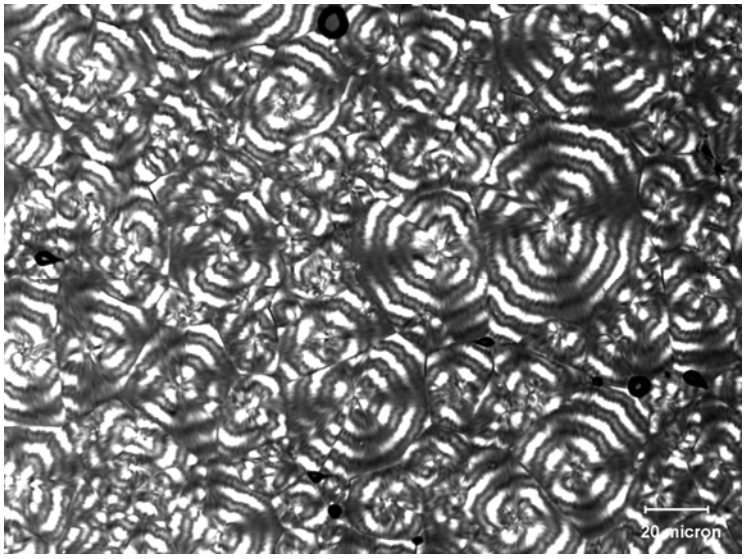

Figure 2.6. POM micrograph of PHBV8/BN (T_c=76^{o}C, t_c=60s)

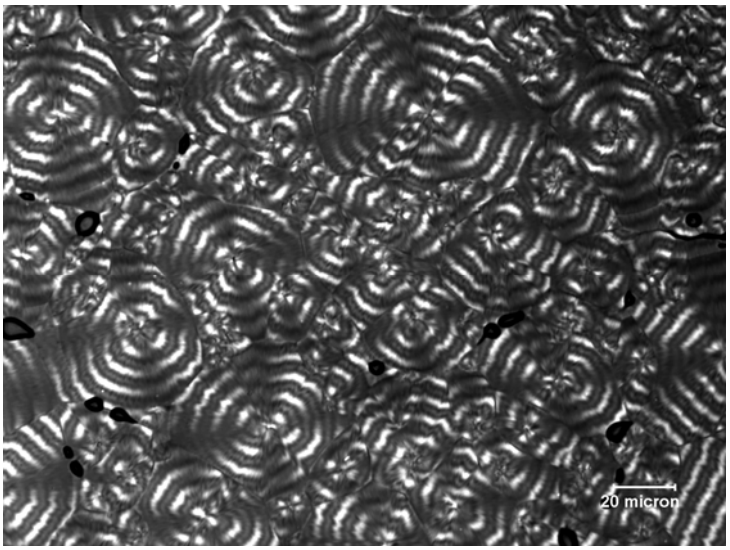

Figure 2.7. POM micrograph of PHBV8/thymine (T_c=76^{o}C, t_c=60s)

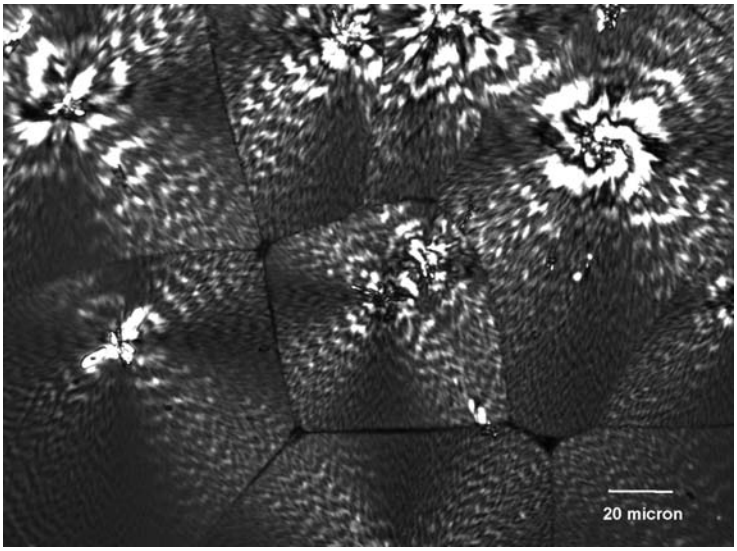

Figure 2.8. POM micrograph of PHBV8/melamine (T_c=76^{o}C, t_c=60s)

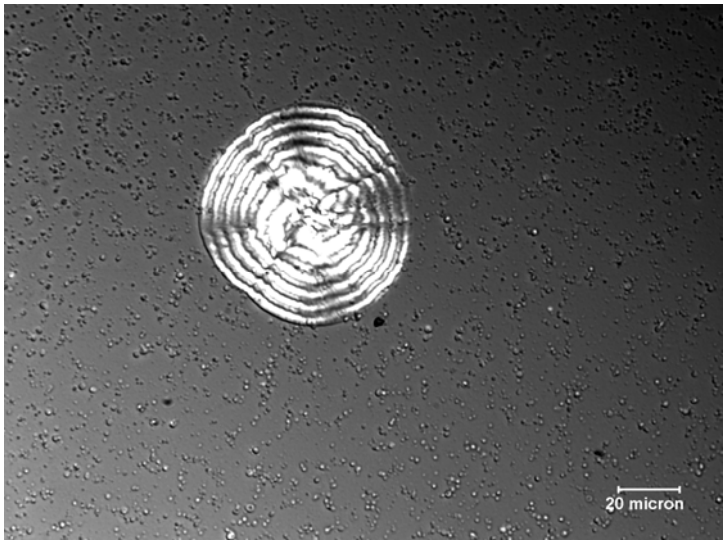

Figure 2.9. POM micrograph of PHBV12 (T_c=70^{o}C, t_c=65s)

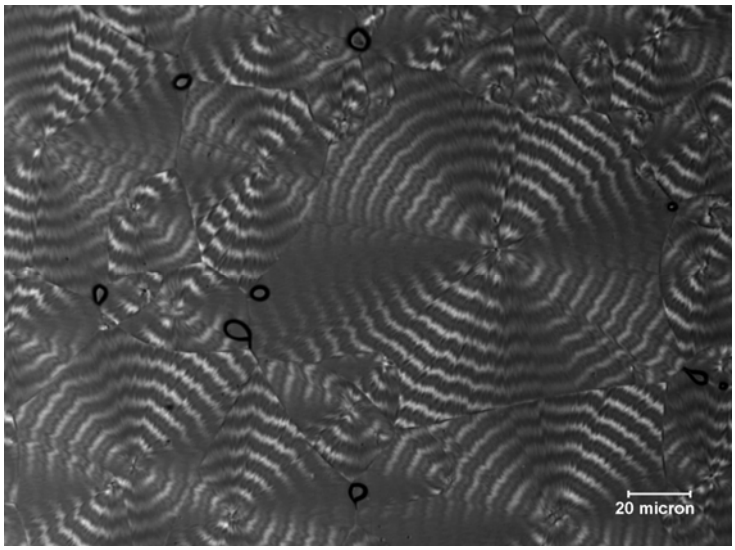

Figure 2.10. POM micrograph of PHBV12/BN (T_c=70^{o}C, t_c=65s)

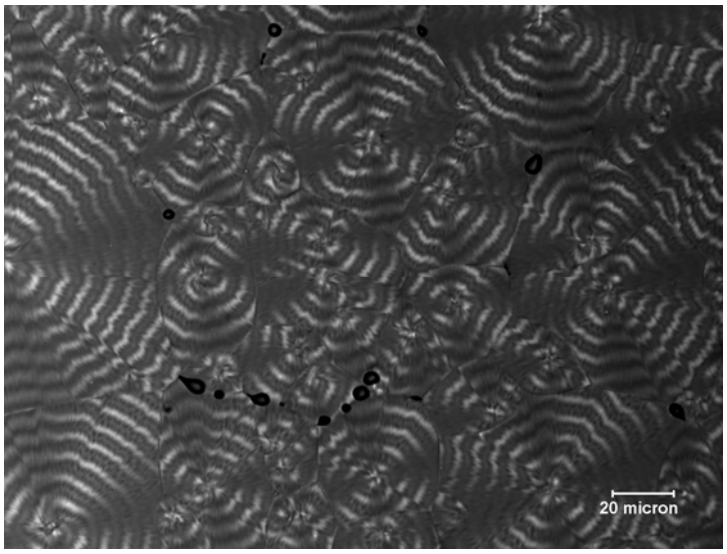

Figure 2.11. POM micrograph of PHBV12/thymine (T_c=70^{o}C, t_c=65s)

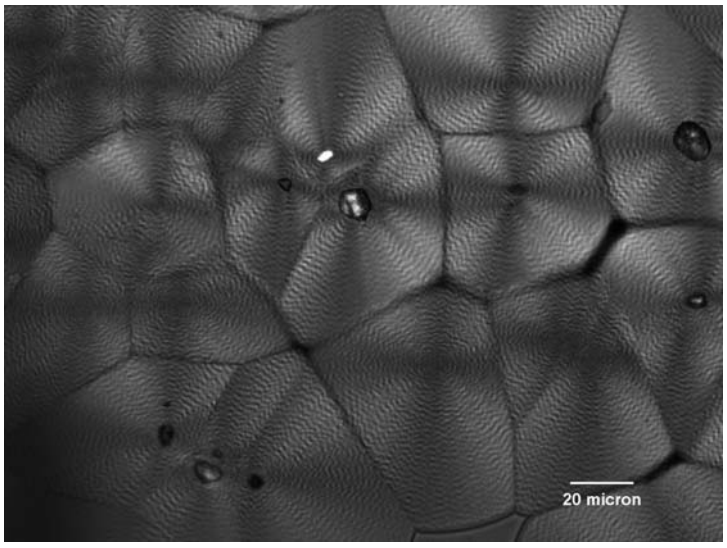

Figure 2.12. POM micrograph of PHBV12/melamine (T_c=70^{o}C, t_c=65s)

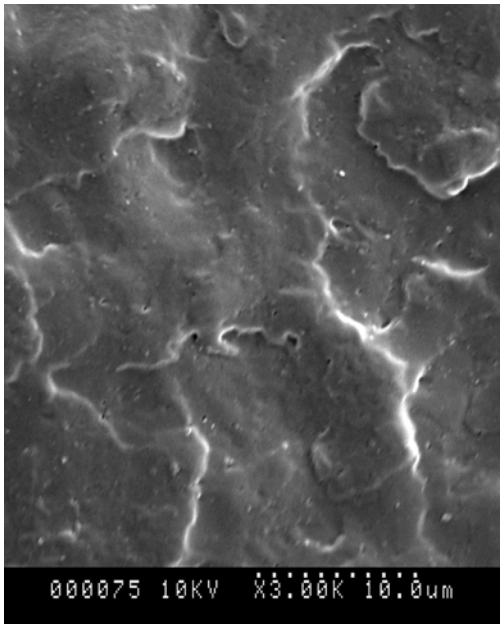

Figure 2.13. SEM micrograph of cryo-fractured PHBV8

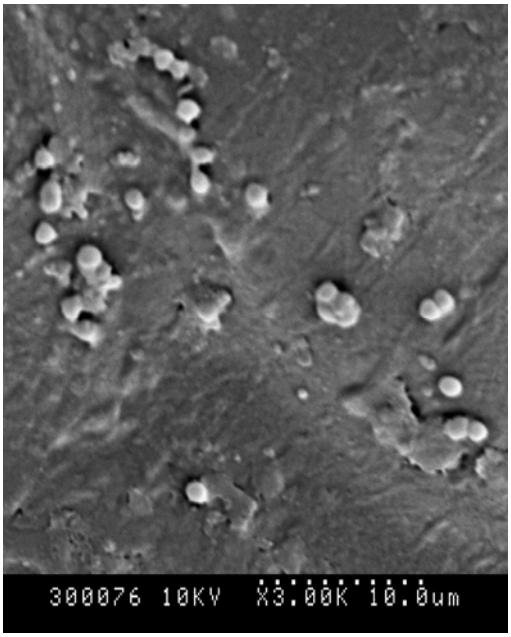

Figure 2.14. SEM micrograph of cryo-fractured PHBV8/BN

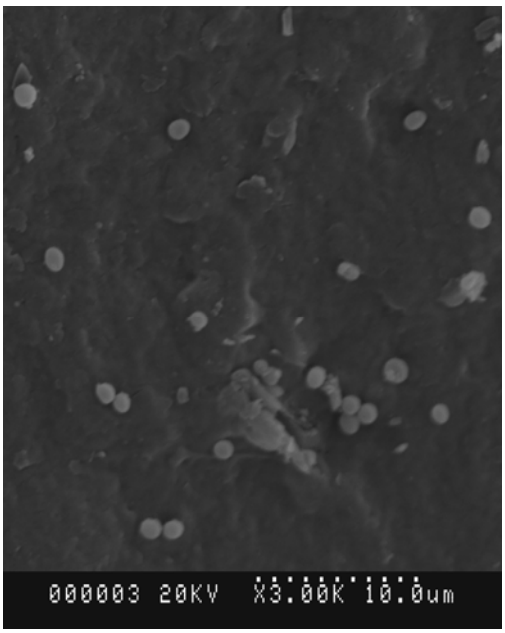

Figure 2.15. SEM micrograph of cryo-fractured PHBV8/thymine

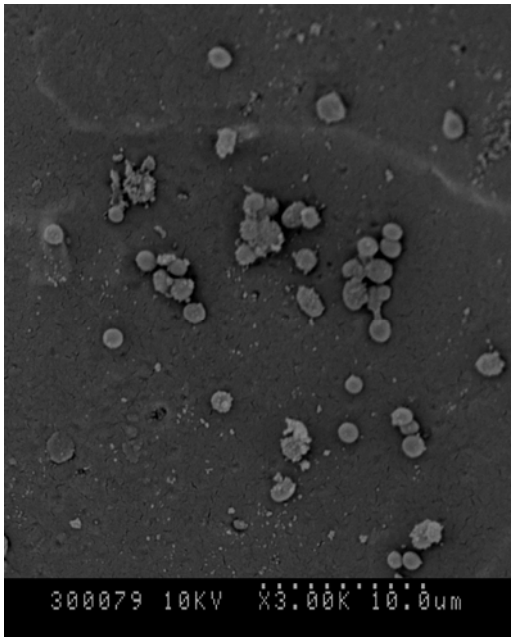

Figure 2.16. SEM micrograph of cryo-fractured PHBV8/melamine

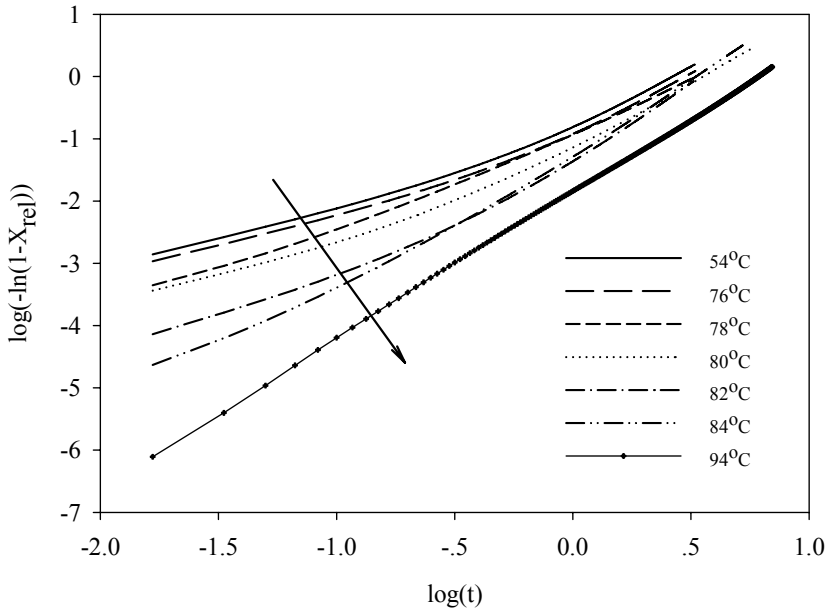

Figure 2.17. Isothermal Avrami plots of PHBV8

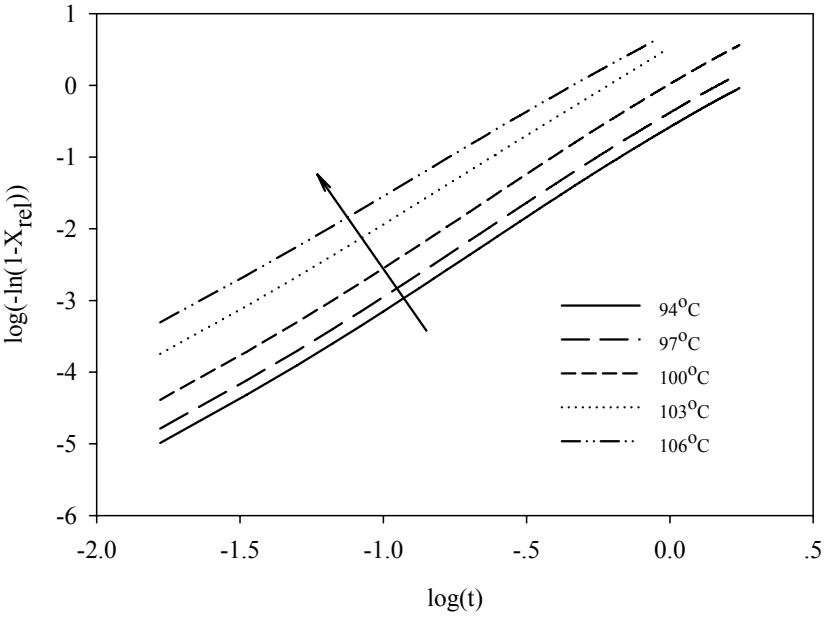

Figure 2.18. Isothermal Avrami plots of PHBV8/BN

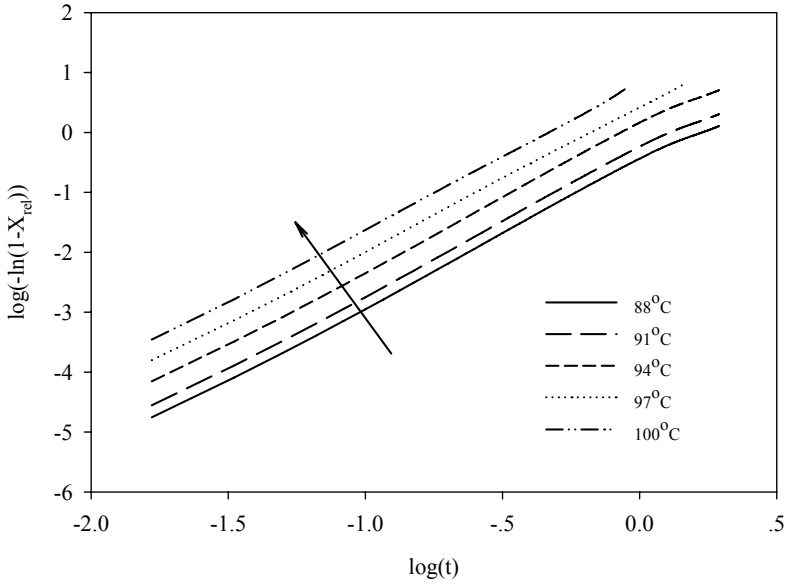

Figure 2.19. Isothermal Avrami plots of PHBV8/thymine

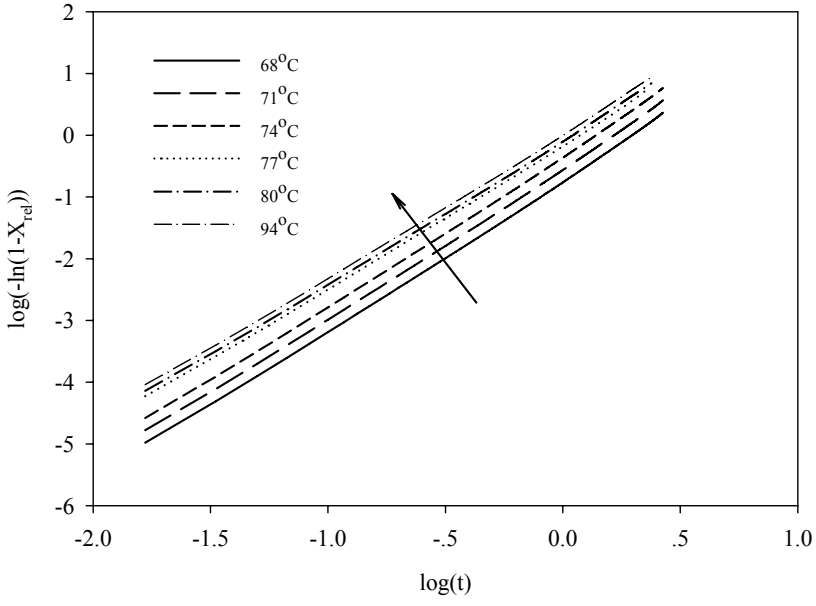

Figure 2.20. Isothermal Avrami plots of PHBV8/melamine

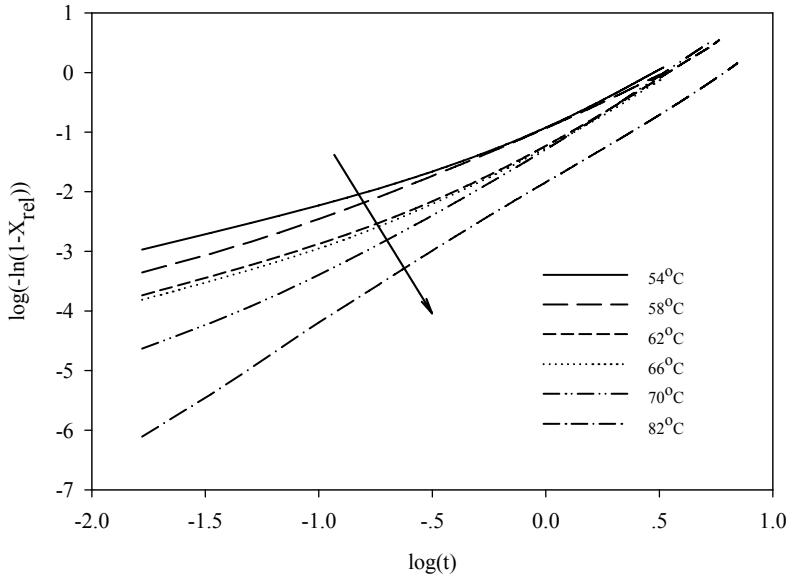

Figure 2.21. Isothermal Avrami plots of PHBV12

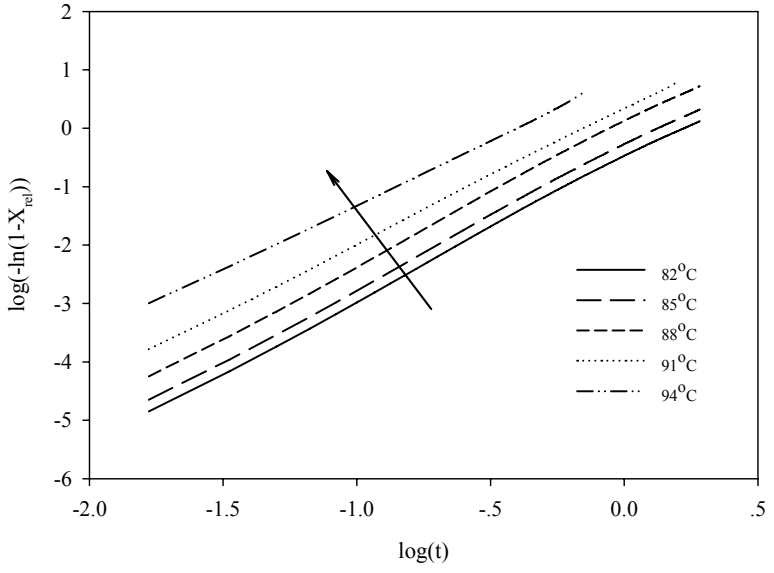

Figure 2.22. Isothermal Avrami plots of PHBV12/BN

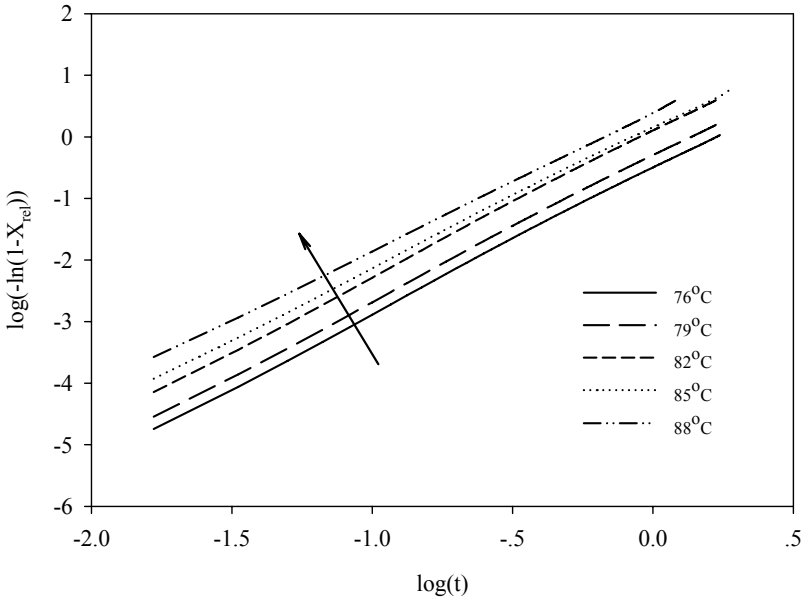

Figure 2.23. Isothermal Avrami plots of PHBV12/thymine

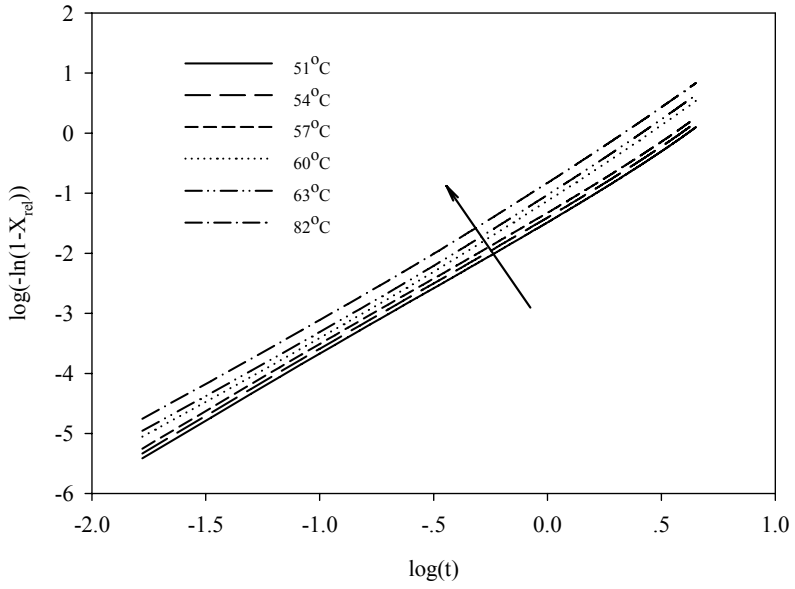

Figure 2.24. Isothermal Avrami plots of PHBV12/melamine

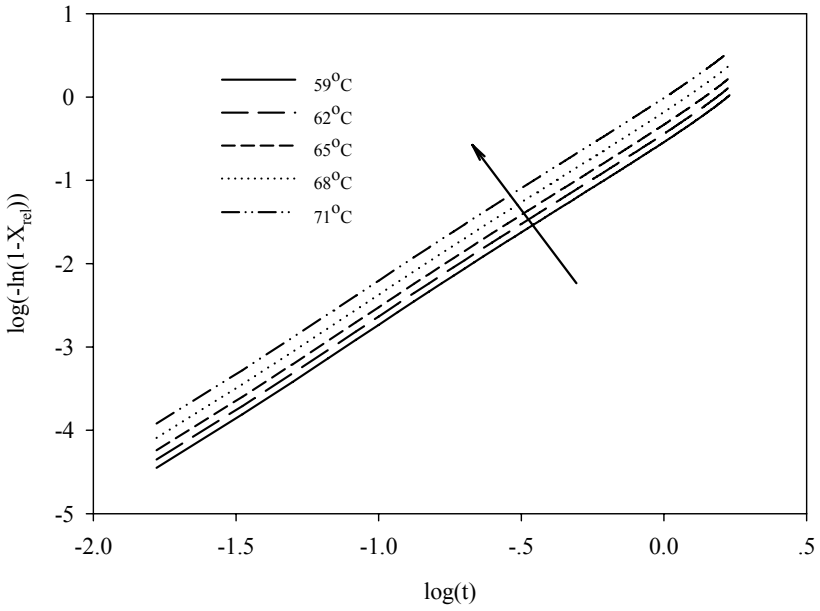

Figure 2.25. Isothermal Avrami plots of PHBV21/BN

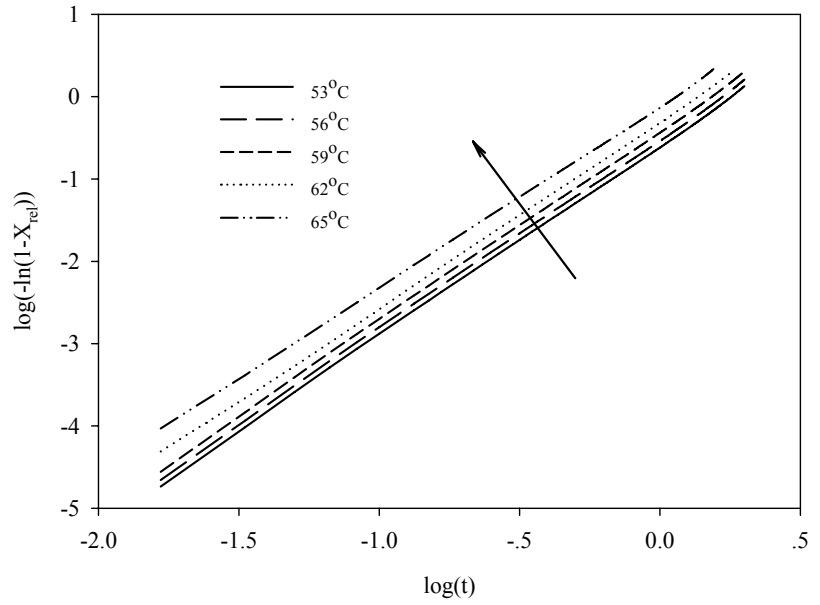

Figure 2.26. Isothermal Avrami plots of PHBV21/thymine

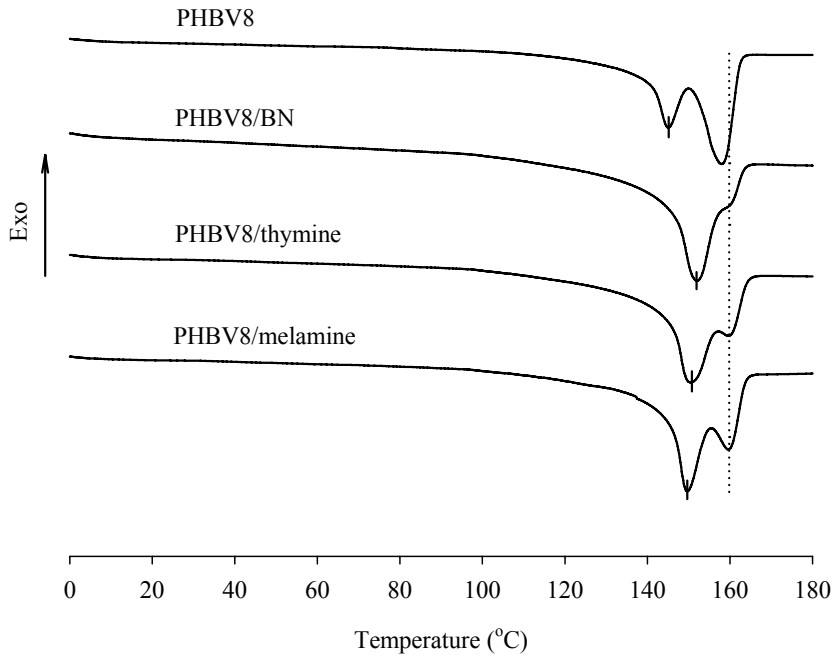

Figure 2.27. DSC thermograms of second heating after isothermal crystallization for PHBV8/NAs at the heating rate of 10°C/min

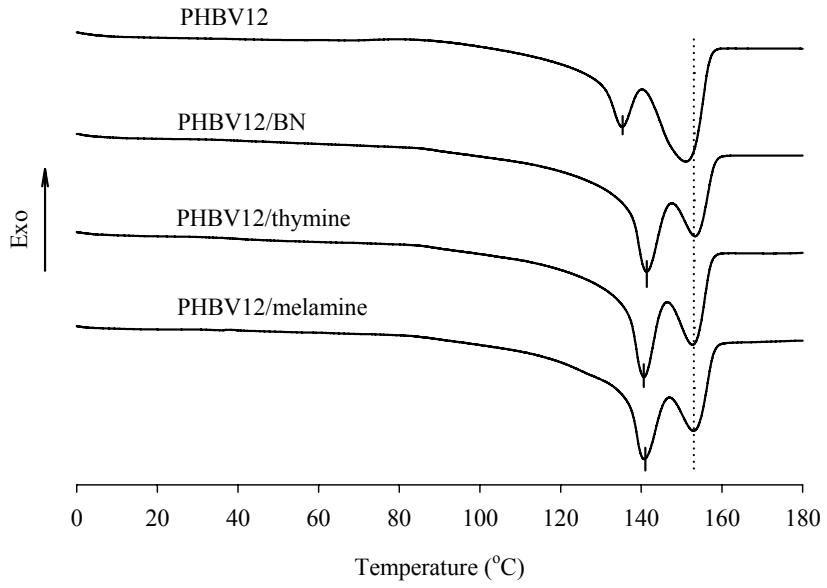

Figure 2.28. DSC thermograms of second heating after isothermal crystallization for PHBV12/NAs at the heating rate of 10°C/min

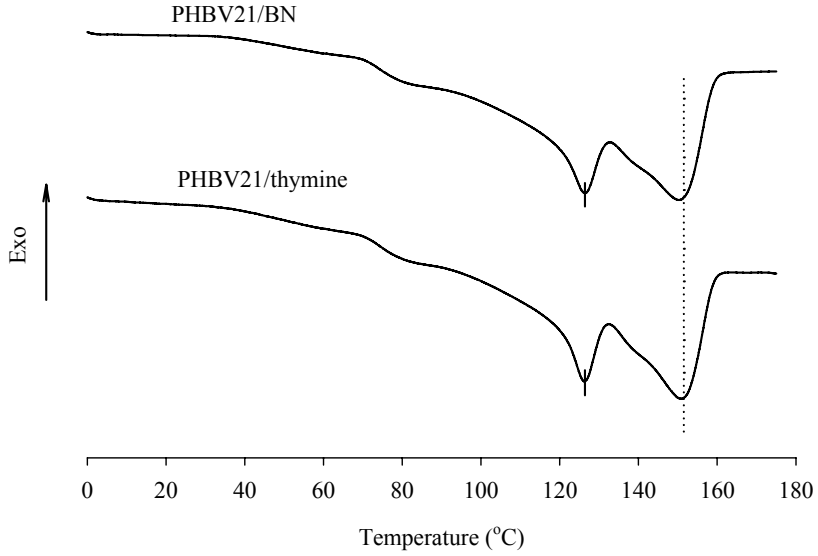

Figure 2.29. DSC thermograms of second heating after isothermal crystallization for PHBV21/NAs at the heating rate of 10°C/min

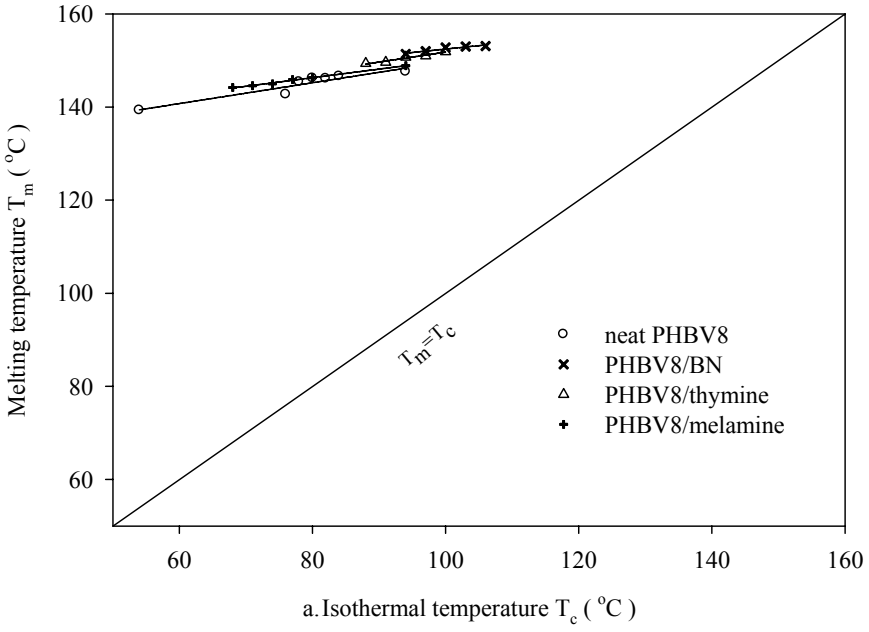

Figure 2.30. Relationship between isothermal crystallization temperature and melting temperature for PHBV8/NAs

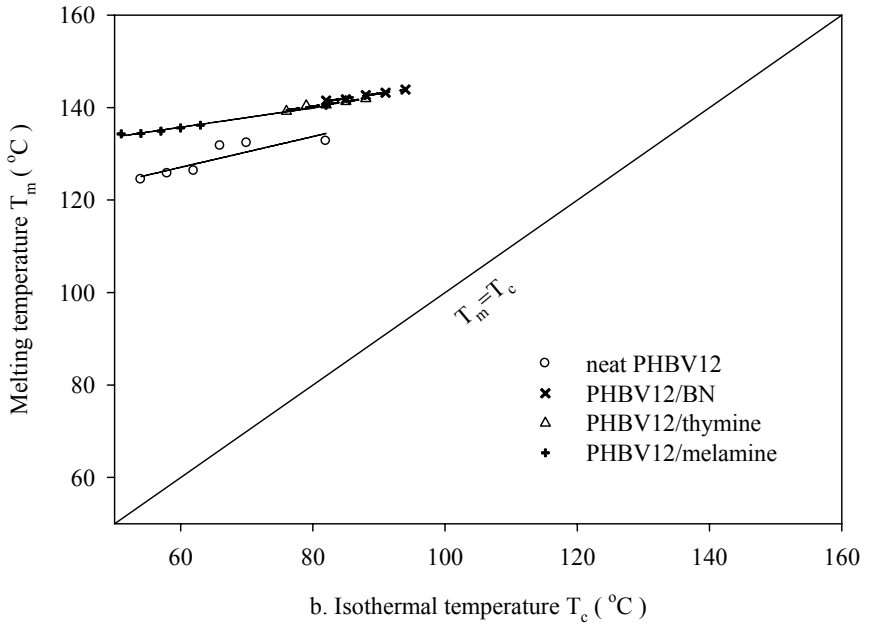

Figure 2.31. Relationship between isothermal crystallization temperature and melting temperature for PHBV12/NAs

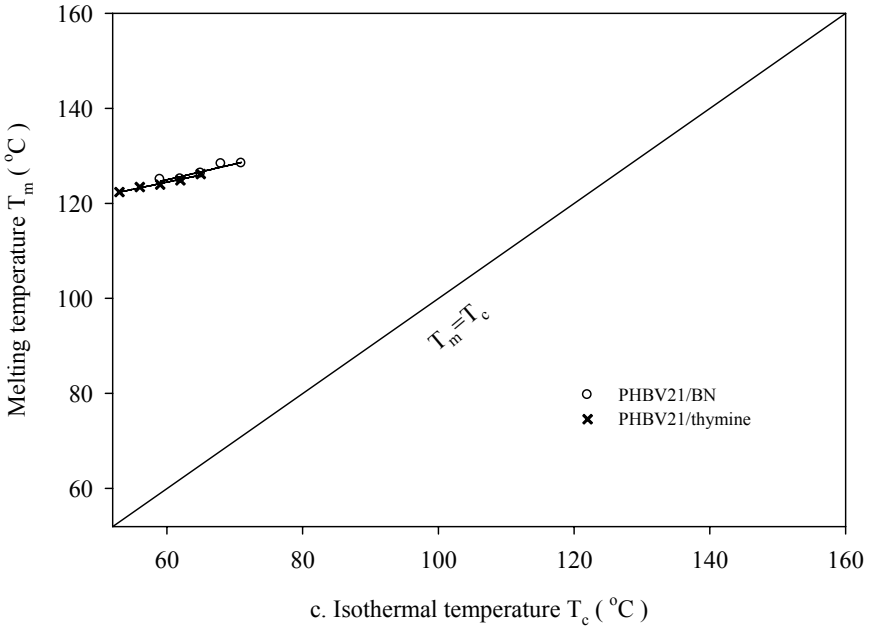

Figure 2.32. Relationship between isothermal crystallization temperature and melting temperature for PHBV21/NAs

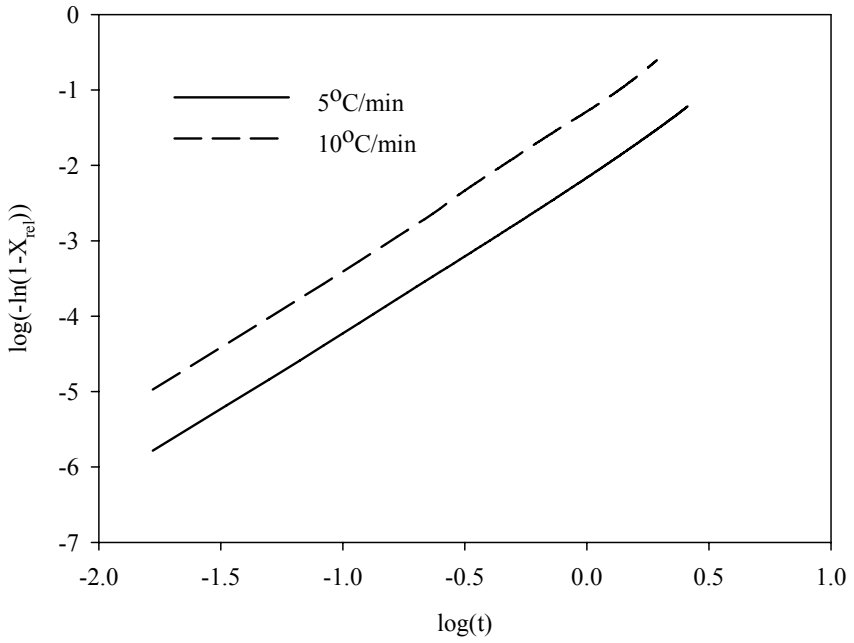

Figure 2.33. Non-isothermal Avrami plots of PHBV8

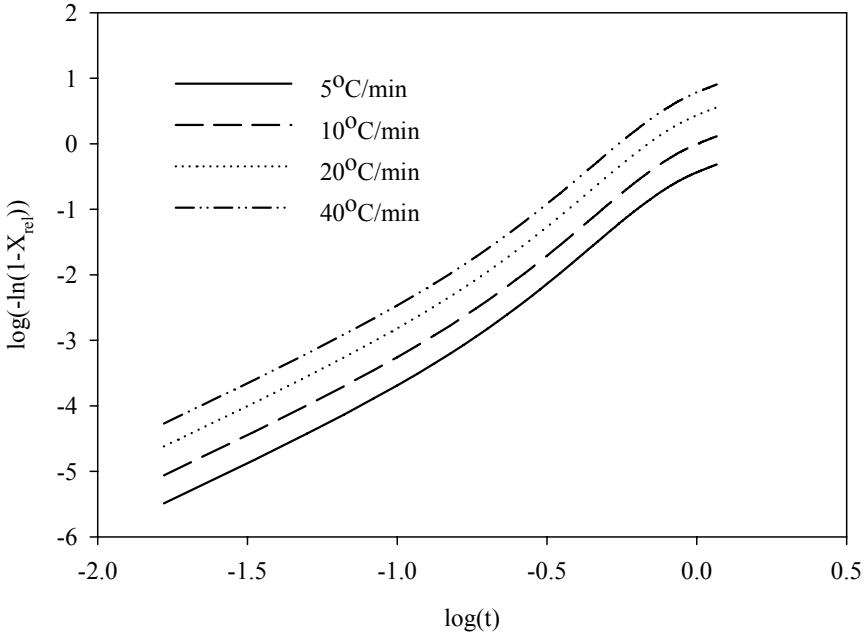

Figure 2.34. Non-isothermal Avrami plots of PHBV8/BN

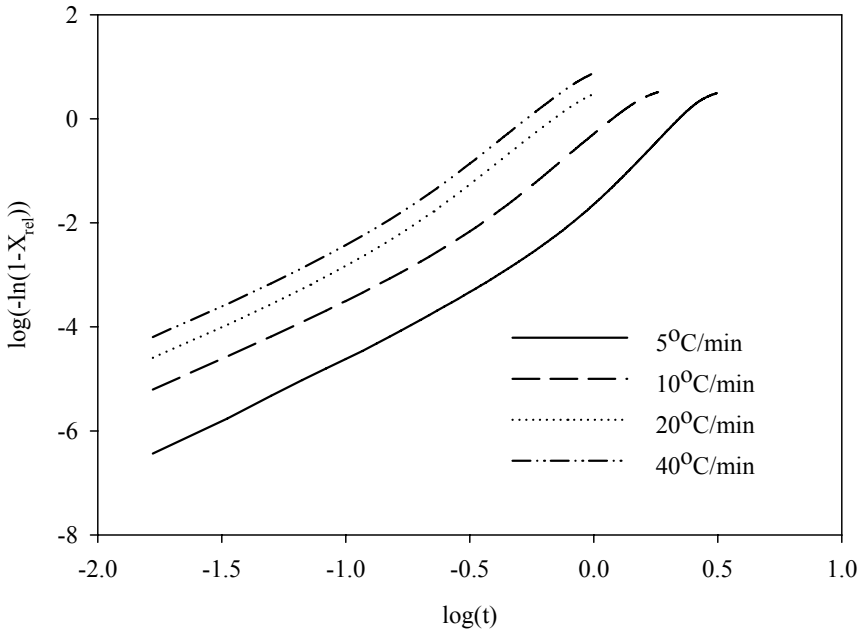

Figure 2.35. Non-isothermal Avrami plots of PHBV8/thymine

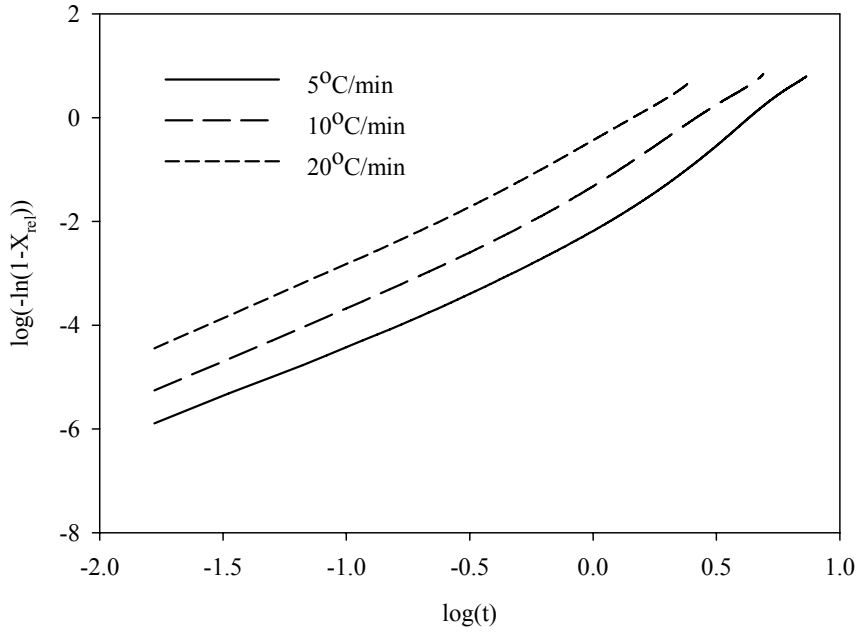

Figure 2.36. Non-isothermal Avrami plots of PHBV8/melamine

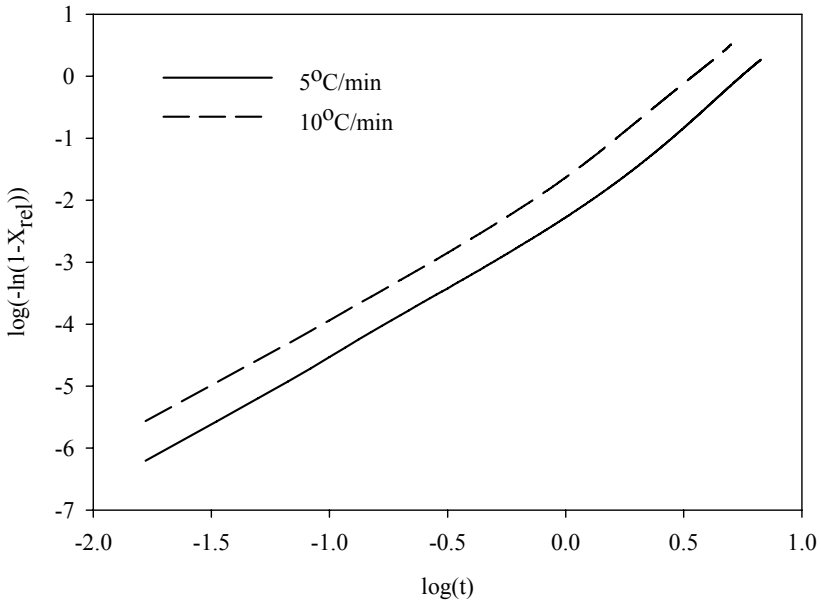

Figure 2.37. Non-isothermal Avrami plots of PHBV12

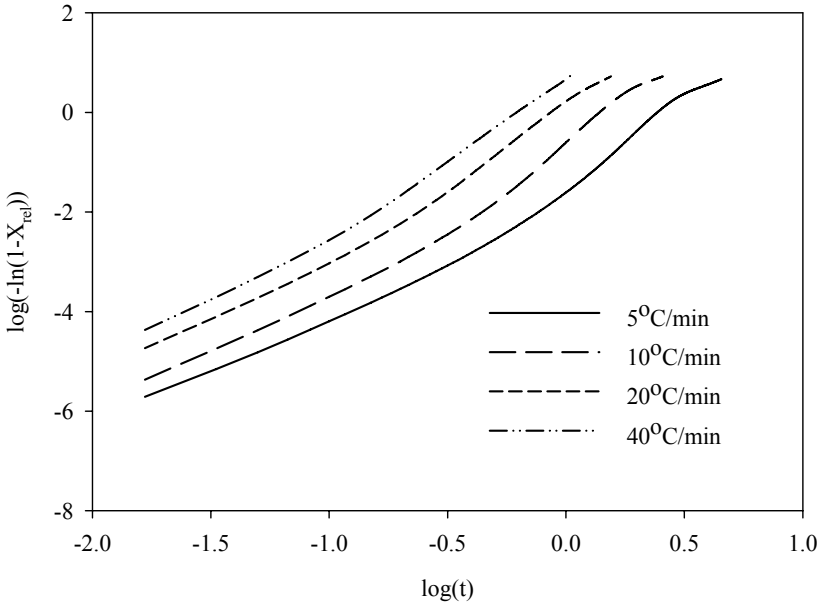

Figure 2.38. Non-isothermal Avrami plots of PHBV12/BN

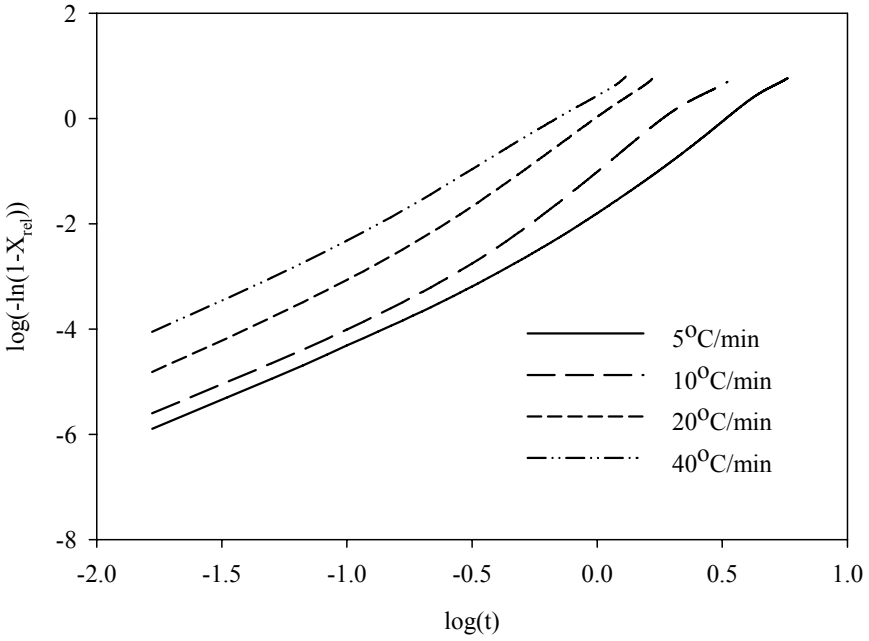

Figure 2.39. Non-isothermal Avrami plots of PHBV12/thymine

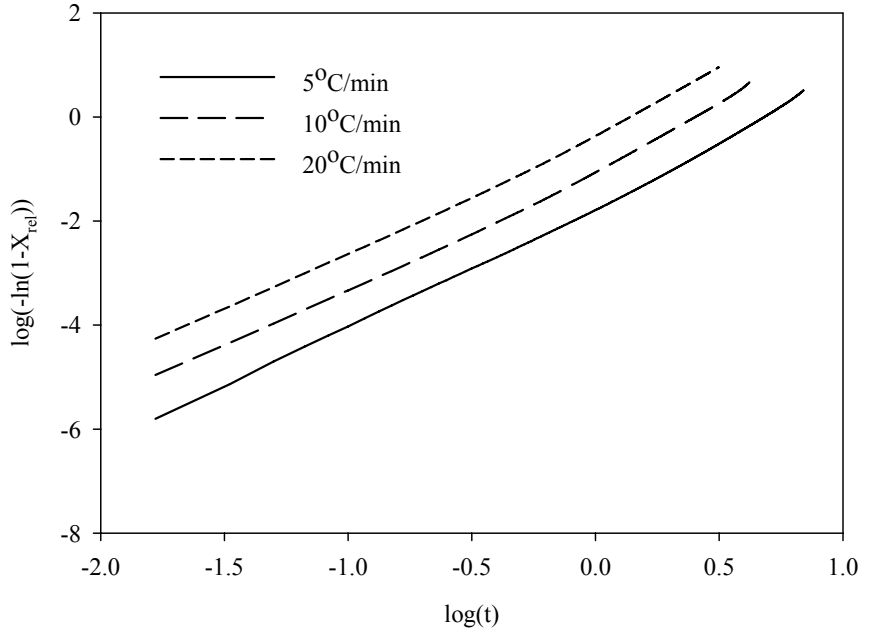

Figure 2.40. Non-isothermal Avrami plots of PHBV12/melamine

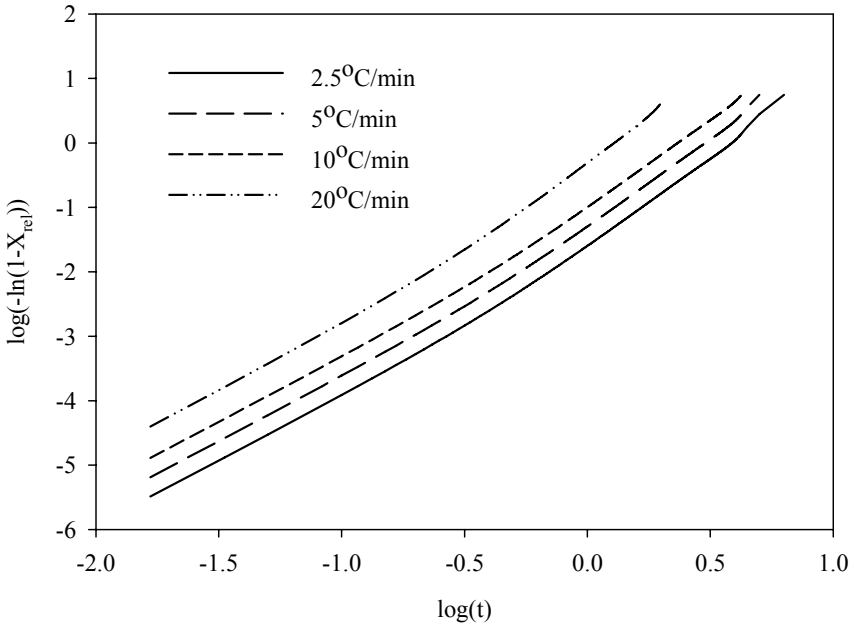

Figure 2.41. Non-isothermal Avrami plots of PHBV21/BN

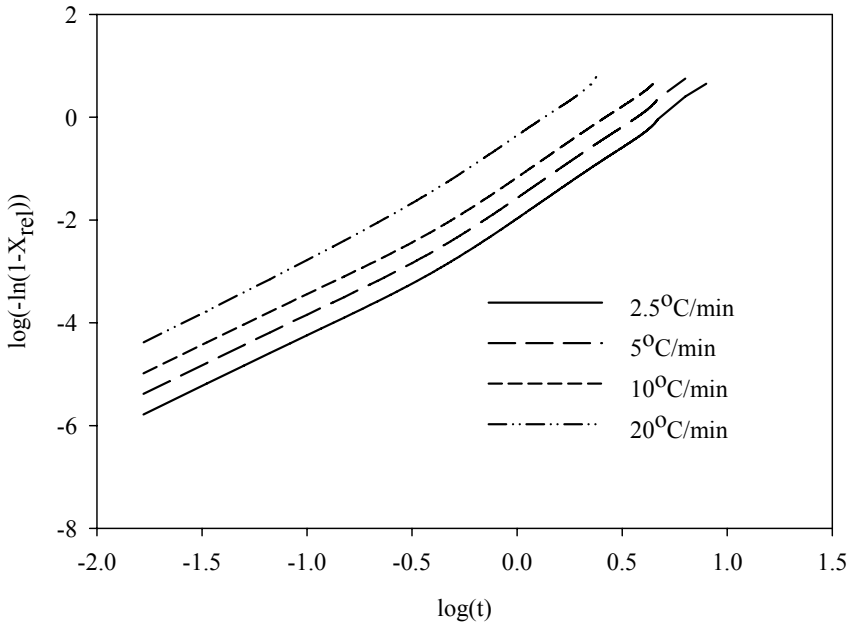

Figure 2.42. Non-isothermal Avrami plots of PHBV21/thymine

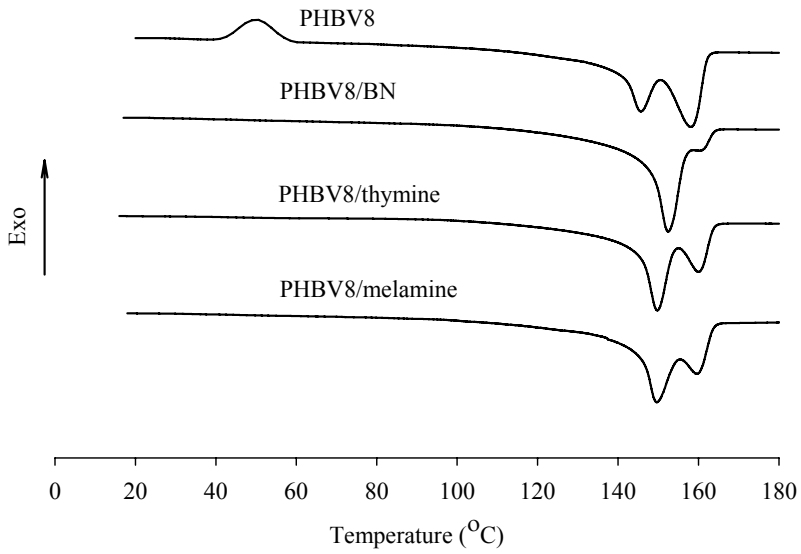

Figure 2.43. DSC thermograms of second heating after non-isothermal crystallization for PHBV8/NAs at the heating rate of 10°C/min

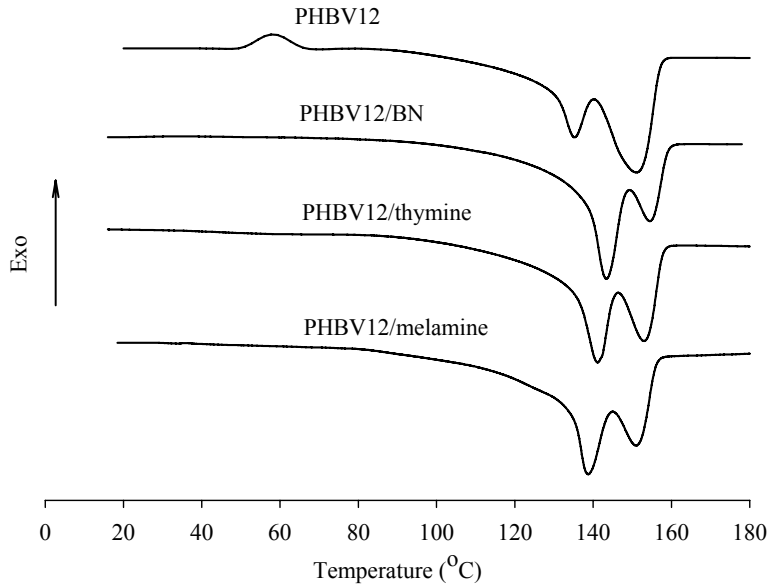

Figure 2.44. DSC thermograms of second heating after non-isothermal crystallization for PHBV12/NAs at the heating rate of 10°C/min

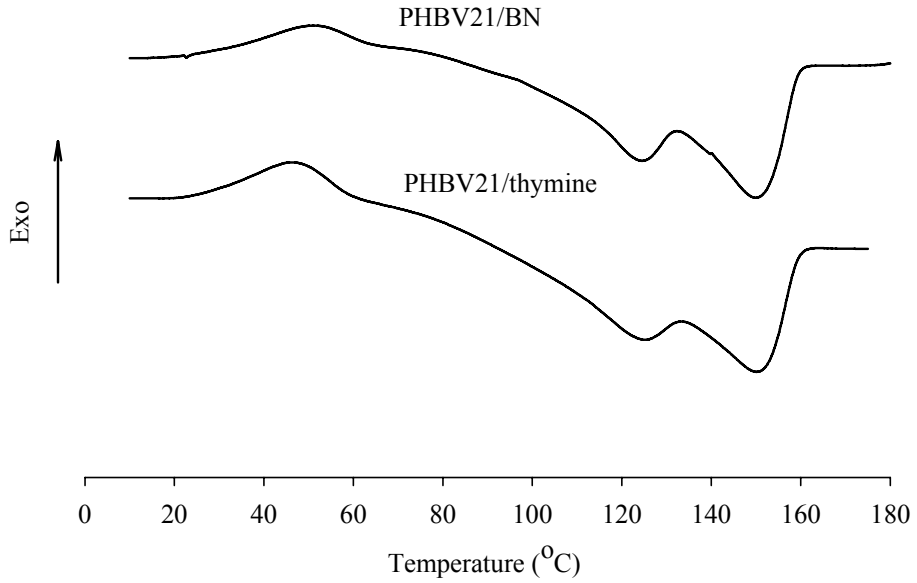

Figure 2.45. DSC thermograms of second heating after non-isothermal crystallization for PHBV21/NAs at the heating rate of 10°C/min

2.8 Tables

Table 2.1. Molecular weight and polydispersity of PHB and PHBVs

Material	3-HV (mol%)	M_w (10^3 Dalton)	M_n (10^3 Dalton)	PI
PHB	0	735	289	2.55
PHBV8	8	478	182	2.62
PHBV12	12	421	172	2.45
PHBV21	21	392	156	2.51

Table 2.2. Melt crystallization of PHB and PHBVs with nucleating agents at the cooling rate of 10ºC/min.

Nucleating agent	PHB		PHBV8		PHBV12		PHBV21	
	T_c[a](ºC)	ΔH_c(J/g)	T_c(ºC)	ΔH_c(J/g)	T_c(ºC)	ΔH_c(J/g)	T_c(ºC)	ΔH_c(J/g)
none	78.6	66.8	52.2	20.7	51.6	19.8	none[b]	none
BN	110.3	74.4	99.7	53.6	88.3	46.7	65.5	26.2
thymine	106.1	73.3	92.3	51.5	80.5	45.6	59.5	24.0
melamine	94.2	70.4	73.5	50.0	57.3	26.5	none	none
saccharin	96.9	68.0	59.3	36.3	50.8	27.3	none	none
abeitic acid	83.6	67.1	61.1	21.7	none	none	none	none
trithiocyanuric acid	86.2	53.9	63.4	16.1	none	none	none	none
NCC	86.9	60.6	57.8	17.5	none	none	none	none

Table 2.3. Isothermal crystallization data of PHBV8 with nucleating agents

Sample	T_{ic}[a](ºC)	ΔH_{ic}(J/g)	n	K(min^{-n})	$t_{0.5}$(min)
PHBV8	54	46.5	1.36	0.187	2.62
	76	43.3	1.38	0.0649	5.56
	78	40.7	1.68	0.0398	5.48
	80	39.5	1.91	0.0376	4.60
	82	33.6	2.14	0.0336	4.11
	84	34.5	2.21	0.0330	3.96
	94	32.3	2.32	0.0294	3.90
PHBV8/BN	94	52.0	2.40	0.285	1.45
	97	52.8	2.41	0.444	1.20
	100	50.2	2.41	1.13	0.82
	103	49.8	2.40	3.08	0.54
	106	49.3	2.40	5.53	0.42
PHBV8/thymine	88	47.7	2.35	0.249	1.55
	91	46.4	2.34	0.624	1.05
	94	46.1	2.35	1.73	0.68
	97	45.5	2.34	2.21	0.61
	100	45.2	2.34	5.57	0.41
PHBV8/melamine	68	42.2	2.32	0.137	2.01
	71	42.2	2.32	0.217	1.65
	74	41.2	2.32	0.344	1.35
	77	40.7	2.32	0.554	1.10
	80	40.3	2.31	0.650	1.03
	94	39.7	2.33	0.677	1.01

Table 2.4. Isothermal crystallization data of PHBV12 with nucleating agents

Sample	T_{ic}[a](ºC)	ΔH_c(J/g)	n	K(min^{-n})	$t_{0.5}$(min)
PHBV12	54	32.5	1.14	0.0421	11.67
	58	32.7	1.16	0.0404	11.66
	62	32.7	1.19	0.0378	11.51
	66	32.6	1.23	0.0345	11.45
	70	33.8	1.38	0.0276	10.34
	82	33.6	2.07	0.0154	6.29
PHBV12/BN	82	47.7	2.43	0.278	1.46
	85	42.5	2.43	0.441	1.21
	88	41.1	2.42	1.43	0.74
	91	40.6	2.43	2.14	0.63
	94	40.6	2.42	6.73	0.39
PHBV12/thymine	76	38.1	2.32	0.332	1.37
	79	36.8	2.33	0.532	1.12
	82	36.0	2.32	1.25	0.77
	85	35.4	2.33	1.54	0.71
	88	34.6	2.33	2.28	0.60
PHBV12/melamine	51	35.2	2.29	0.0358	3.65
	54	34.7	2.28	0.0430	3.38
	57	34.4	2.29	0.0517	3.10
	60	34.3	2.29	0.0623	2.87
	63	33.9	2.29	0.0658	2.79
	82	34.4	2.30	0.0979	2.34

Table 2.5. Isothermal crystallization data of PHBV21 with nucleating agents

Sample	T_{ic}[a](ºC)	ΔH_{ic}(J/g)	n	K(min^{-n})	$t_{0.5}$(min)
PHBV21/BN	59	20.5	2.36	0.226	1.61
	62	20.2	2.35	0.268	1.50
	65	19.8	2.36	0.421	1.24
	68	19.8	2.36	0.591	1.07
	71	19.9	2.33	0.861	0.91
PHBV21/thymine	53	19.1	2.25	0.329	1.39
	56	18.7	2.25	0.362	1.33
	59	18.2	2.26	0.456	1.20
	62	18.9	2.25	0.472	1.19
	65	19.1	2.24	0.773	0.95

Table 2.6. Non-isothermal crystallization data of PHBV8 with nucleating agents

Sample	Φ (°C/min)	T_{nc}[a](°C)	ΔH_{nc}(J/g)	n	Z_{nc}(min^{-n})	$t_{0.5}$(min)
PHBV8	5	64.5	45.7	2.04	0.366	9.77
	10	52.2	20.7	2.14	0.745	3.33
	20	none[b]	none	none	none	none
	40	none	none	none	none	none
PHBV8/BN	5	106.0	58.5	2.76	0.752	1.47
	10	99.7	53.3	2.77	0.945	1.07
	20	91.0	50.1	3.11	1.03	0.74
	40	76.0	47.2	3.11	1.03	0.60
PHBV8/thymine	5	96.67	56.7	2.59	0.389	4.37
	10	92.33	52.8	2.68	0.822	1.81
	20	85.67	49.8	3.11	1.03	0.75
	40	71.33	45.2	3.11	1.03	0.63
PHBV8/melamine	5	82.75	54.1	2.10	0.378	6.93
	10	73.50	47.6	2.18	0.766	3.08
	20	61.33	22.5	2.25	0.933	1.57
	40	none	none	none	none	none

Table 2.7. Non-isothermal crystallization data of PHBV12 with nucleating agents

Sample	Φ (°C/min)	T_{nc}[a](°C)	ΔH_{nc}(J/g)	n	$Z_{nc}(min^{-n})$	$t_{0.5}$(min)
PHBV12	5	57.2	44.3	2.21	0.345	9.43
	10	51.6	19.8	2.17	0.665	5.53
	20	none[b]	none	none	none	none
	40	none	none	none	none	none
PHBV12/BN	5	92.2	46.9	2.31	0.452	5.82
	10	88.3	45.9	2.62	0.767	2.39
	20	54.7	41.3	3.04	0.988	0.96
	40	66.0	40.1	3.04	1.02	0.74
PHBV12/thymine	5	84.1	45.1	2.29	0.388	6.71
	10	80.5	44.6	2.60	0.713	3.19
	20	78.3	40.5	2.89	0.973	1.07
	40	60.1	39.6	2.81	1.02	0.80
PHBV12/melamine	5	57.5	44.7	2.09	0.368	7.22
	10	54.5	42.6	2.17	0.683	3.93
	20	53.0	19.8	2.20	0.847	1.78
	40	none	none	none	none	none

Table 2.8. Non-isothermal crystallization data of PHBV21 with nucleating agents

Sample	Φ (°C/min)	T_{nc}[a](°C)	ΔH_{nc}(J/g)	n	$Z_{nc}(min^{-n})$	$t_{0.5}$(min)
PHBV21/BN	2.5	100.0	22.8	2.04	0.179	6.86
	5	89.1	22.5	2.06	0.443	6.01
	10	65.5	18.8	2.08	0.747	3.40
	20	63.0	16.5	2.09	0.923	1.80
PHBV21/thymine	2.5	98.2	22.0	2.06	0.118	11.22
	5	86.7	21.6	2.07	0.420	6.83
	10	59.5	19.7	1.98	0.713	4.58
	20	58.8	18.3	1.98	0.921	1.90

a: T_c was taken at the crystallization peak. (Table 2.1-2.7)

b: no crystallization observed. (Table 2.1)

CHAPTER 3 INVESTIGATION OF THERMAL AND PHYSICAL PROPERTIES OF BAMBOO PULP FIBER REINFORCED BIOPOLYMER COMPOSITES

3.1 Abstract

In this study, composites of bamboo pulp fiber (BPF) and PHBV8 (containing 8 mol% 3-hydroxyvalerate) were melted compounded using a Haake mixer. The standard tensile and flexural test specimens were prepared using an injection-molding machine. The crystallization and fiber-induced crystallization of PHBV8 and their effects on mechanical and other physical properties of the composites were investigated. Improvement of compatibility between fiber and polymer was studied using polymeric diphenylmethane diisocyanate (pMDI, Mondur 541, Bayer) or maleic anhydride (MA) grafted PHBV8 containing 0.3% MA (MA-PHBV). Fiber-induced crystallization was revealed by POM and DSC analyses. Because homogenous nucleation was substantial and competed with fiber-induced crystallization at low crystallization temperatures, orderly transcrystalline layer (TCL) was not confirmed by POM. Boron nitride (BN) as a nucleation agent appeared to minimize fiber-induced crystal growth, because the BN-nucleated spherulites outgrew the fiber-induced ones. Addition of BN also resulted in increases in tensile and flexural properties. Compared with the neat PHBV8, the glass transition temperature (T_g) of PHBV8 in composites increased slightly. Adding small amount of pMDI or MA-PHBV8 significantly increased mechanical properties of the composites. On the other hand, both pMDI and MA-PHBV8 showed certain decreasing effects on T_g and crystallinity of PHBV8. Scanning electron microscopy (SEM) revealed increased wetability between BPF and PHBV8 b pMDI or MA-PHBV8.

3.2 Introduction

In recent years, research has shown growing interest in using natural fibers as reinforcement for polymers including biopolymers (Herrmann *et al* 1998, Riedel and Nickel 1999, Wong *et al* 2002, Shanks *et al* 2004). Natural fiber reinforced biopolymer composites (biocomposites) are expected as alternates to glass fiber reinforced composites and natural fiber reinforced petrochemical composites. The promising benefits of biocomposites are twofold. First, natural fibers are from annual renewable resources,and biodegradable. They show low cost, low density, acceptable specific mechanical properties (Mohanty *et al* 2002). Second, the biopolymer matrix is also eco-friendly (Bhardwaj *et al* 2006). Biocomposites are emerging in many industries, such as automotive panels, decking and fencing (Kemir 2006).

PHAs have shown some interesting mechanical and physical properties. PHB and PHBVs are the main representatives in the PHA family. PHB is a highly crystalline polymer and has a melting point and strength and modulus comparable to that of isotatic polypropylene (iPP), but it is brittle and thermally instable during melt processing (Marchessault *et al* 1981, Barham *et al* 1984). PHBV is a random copolymer consisting of (R)-3-hydroxybutyrate (3-HB) and (R)-3-hydroxyvalerate (3-HV) units (Holmes *et al* 1988). Increasing the content of 3-HV comonomer results in decrease in melting point and increase in ductility, but reduces strength and stiffness. Recent studies have shown that adding natural fibers in the PHBV matrix can improve the thermal and structural properties as well as reduce the product cost (Reinsch and Kelly 1997, Luo and Netravali 1999, Mohanty *et al* 2000). PHB and PHBV biocomposites with wood fiber (Reinsch *et al* 1997, Fernandes *et al* 2004), flax (Wong *et al* 2002, Shanks *et al* 2004, VanDe Velde

and Kiekens 2002), recycled cellulose fiber (Bhardwaj *et al* 2006), pineapple fiber (Luo and Netravali 1999) and other natural fibers (Herrmann *et al* 1998, Riedel and Nickel 1999) have been reported. In general, PHA biocomposites demonstrate increased modulus and thermal properties such as glass transition temperature (T_g), heat distortion temperature (HDT) and thermal insulation. The reinforcing effects of natural fibers on the mechanical strengths of PHA biocompsoites, however, are dependent on several factors including interfacial adhesion, fiber dimension (diameter and aspect ratio), fiber content, dispersion in the matrix, fiber preparation method and fiber sources. Evidences showed tensile and flexural strength were increased by improving interfacial adhesion through fiber surface modification (Mohanty *et al* 2000), fiber surface treatment by plasticizer(s) (Wong *et al* 2002, Wibowo *et al* 2004, Fernandes *et al* 2004) and silane (Shanks *et al* 2004). Impact strength of PHA biocomposites was rarely studied in literature. The results of recycled cellulose fiber/PHBV composites (Bhardwaj *et al* 2006) indicated deterioration of impact strength by the fiber addition.

In recent years, bamboo fiber has attracted increasing attention as an alternative to wood fiber. Bamboo fiber composites with different resins have been reported, including epoxy resin (Saxena and Gowri 2003, Das *et al* 2006), poly(butylene succinate) (PBS) (Kori *et al* 2005), polyester (Saxena and Gowri 2003), polypropylene (Mi *et al* 1997, Chen *et al* 1998), and PLA (Lee and Wang 2006). Like other natural fiber/polymer composite systems, the interfacial adhesion between bamboo fiber and the polymer was critical for high mechanical properties.

For fiber reinforced semicrystalline polymer composites, the fiber-induced crystallization is frequently noted. This crystallization is originated from the

heterogeneous nucleation of the matrix polymer at the fiber surface. In its extreme case when the nucleation density on fiber surface is so high that crystal growth along the fiber axis is inhibited by neighboring crystals, but manifest as tightly aligned spherulites growing outward from the fiber, called transcrystalline layer (TCL). Transcrystalization was observed in PHBV/flax fiber (Wong *et al* 2002), PHB/wood fiber (Reinsch and Kelley 1997), PP/bamboo fiber (Mi *et al* 1997), respectively. However, it was not founded in bamboo fiber reinforced PBS composites (Kori *et al* 2005). The exact role of the transcrystallization in the mechanical properties is still not quite clear, and it appears to differ for different fiber/polymer systems (Dean *et al* 1999). Furthermore, the characterization of trnascrystallization has relied mainly on optical microscopy, which is effective only for the model systems such as isolated fiber in the thin plastic film under well controlled thermal conditions. Such an observation of transcrystallization may deviate significantly from the crystalline reality in composites.

In this study, BPF reinforced PHBV8 composites were prepared and investigated for the structure-composition-property relationships. Since the fiber-induced crystallization complicates the crystalline structure of a polymer composite and the crystalline structure and crystallinity strongly influence its properties, BN as a nucleating agent was added in an attempt to suppress the fiber-induced crystallization and achieves more homogeneous crystalline structures. The effects of nucleation agent (BN) on the crystallization, mechanical and dynamic mechanical properties were studied. Polymeric diphenylmethane diisocyanate as a coupling agent and maleic anhydride (MA) grafted PHBV8 (MA-PHBV) as a compatibilizer were also studied for the improvements of the interfacial bonding and mechanical properties.

3.3 Experimental

3.3.1 Materials

PHBV8 was provided by Metabolix Inc (Cambridge, MA) and was in a fine powder form. The weight average molecular weight is 482K Da with a polydispersity index of 3.3 as measured by gel permeation chromatography. BN in fine power (~2μm) was obtained from Advanced Ceramics Corporation (Cleveland, OH) and used as received. BPF was obtained from the Suzhou University, China. BPF appeared similar to the softwood pulp and was puffy. Prior to mixing, BPF was cut into pieces of approximate a half-inch long using a paper cutter. The polymeric diphenylmethane diisocyanate (pMDI) was provided by Bayer (Mondur 541). MA-PHBV8 was prepared in our laboratory by reactive extrusion of MA and PHBV8 using a twin-screw extruder, following the general method in literatures (Carlson *et al* 1999, John *et al* 1998). The reacted polymer was pelletized into fine pellets and the residual MA was removed by extraction with acetone. The extraction of MA was conducted by refluxing ca. 300 g of the crude MA-PHBV8 with 800 mL of acetone in a flask for 24 hours. The degree of MA grafting was measured by titration using phenolphthalein as indicator (Chen *et al* 2003). The MA content in thus extracted product was found to be 0.30 wt%. To evaluate the effectiveness of this extraction method, a small amount of the extracted product was dissolved in chloroform and then precipitated in acetone for further purification. Comparing the MA contents in those two samples, it turned out the difference in MA content was smaller than 0.01%. Therefore, the above extracted MA-PHBV8 was used as a compatibilizer without further purification.

3.3.2 Sample preparation and testing

The mixing of the PHBV8 with BPF and others was performed in a HAAKE mixer (HAAKE PolyLab 3000P). BPF and PHBV8 were pre-dried at 80°C for 8 hrs before mixing. PHBV8, BN and pMDI (or MA-PHBV8) was first manually mixed by tumbling in a sealed plastic bag. The chopped BPF could not be mixed this way because it is very puffy. Subsequently the mixture was fed into the mixer and followed by the chopped BPF as soon as the polymer is melted. The mixing temperature was controlled by three independent heating plates which all were set at 170ºC. The roller speed was maintained at 50-rpm and the total mixing time was 5 minutes for all samples. After mixing was done, the blend was removed and scratched into small pieces when it was still hot. Thus obtained chunks were then ground into pellets using a granulator (Nelmor) with a screen size of 1/4 inches. For those samples containing nucleating agent, 1wt% BN on the basis of PHBV8 weight was added. Similarly, pMDI or MA-PHBV8 was added on the basis of the total weight of PHBV8 and BPF. The loading levels were 1wt%, 2wt% and 3wt% for pMDI, and were 2wt%, 3.5wt% and 5wt% for MA-PHBV8, respectively.

Standard tensile (ASTM D638, Type I) and flexural (ASTM D790) test samples were prepared using an injection-molding machine (Sumitomo SE 50D). The barrel of the injection mold machine has three heating zones. From feeding throat to nozzle each zone was set at 165, 170 and 170 ^{o}C, respectively. The nozzle temperature was set at 165^{o}C, and the mold temperature was 50 ^{o}C Prior to injection molding, the pellets of the composites were dried in an over at 80ºC for 8 hrs. Tensile test was performed on a 8.9-kN, screw-driven universal testing machine (Instron 4466) equipped with a 10-kN electronic load cell and mechanical grips. The testing was conducted at a crosshead speed

of 5-mm/min with deformations measured using a 25-mm extensometer (MTS 634.12E-24) and data acquired by computer. Flexural test was performed on the same machine and conducted at a crosshead speed of 1.46mm/min with data acquired by computer. All samples were conditioned for 48 hrs prior to the testing. All tests were carried out according to the ASTM standard and repeated four times for each sample to get an average value.

Notched Izod impact was performed according to the ASTM D256 method C on a plastic impact tester (Tinius Olsen). The straight bars same as those used for flexural test samples were cut into halves and the halves far from the gate (far end) were used for the impact testing. The test samples were made a sharp v-type notch on the edge according the ASTM standard using a cutter with a tip radius of 0.25 mm.

Fracture surfaces from the tensile and impact tests were examined using the scanning electron microscopy (SEM) (Hitachi S-570). All specimens were sputter coated with gold prior to examination. Morphological structures of the BPF surface and cross-section were also studied using SEM.

The nucleation and spherulite growth of the polymer in the PHBV8/BPF and PHBV8/BPF/BN composites were observed using a polarized optical microscope (Olympus BX51) (POM) equipped with a hot stage (Linklam TMS 94). Each sample was heated to 185^{o}C at 25^{o}C/min, then kept isothermally for 4 minutes and cooled to 100^{o}C at 40^{o}C/min.

To get the information on the final lengths of the BPF in the injection molded composites, a piece of molded plaque was added to chloroform and the polymer was dissolved and removed. The resulting fibers were measured using an optical microscope.

Total 50 fibers were randomly selected. The average fiber length in the composite was ca. 6.2 mm. The average diameter of the fibers in the composite was measured from the SEM micrographs of the fiber. The average fiber diameter was ca. 18.5μm. Therefore the average aspect ratio was approximately 324.

Thermal properties of the composites were studied using DMA and DSC. The samples used for DMA analysis were prepared from flexural test bar. It was shaped into a strip of 4 x 2 x 45-mm using a mini-milling machine (Sherline Model 2000). The specimens were vibrated in dual-cantilever mode at a frequency of 1 Hz. Prior to analysis; the linear viscoelastic region was determined using a strain sweep. All subsequent tests were conducted from -25 to 100^{o}C at 2^{o}C/min with a strain of 0.05%. DSC analysis was also conducted on the injection-molded specimens. The samples were crimp sealed in 40-μL aluminum crucibles. All samples were first scanned from 25 to 180^{o}C at the heating rate of 10^{o}C/min, isothermally kept for 3 minutes, and then cooled from 180 to 0^{o}C at the cooling rate of 10^{o}C/min. Asecond heat scan was followed from 0 to 180 ^{o}C at 10 ^{o}C/min. Melt crystallization on the fiber and in the PHBV8 matrix were studied using a polarized optical microscope (Olympus BX51) (POM) equipped with a hot stage (Linklam TMS 94).

Non-isothermal crystallization kinetics was performed on PHBV8/BPF/BN composites with 2% pMDI and 3.5% MA-PHBV8, respectively. The sample was heated to 185^{o}C at 25^{o}C/min, and kept isothermally for 3 minutes to erase previous thermal history. It was then cooled at 10ºC/min to -25^{o}C. Finally, a second heat scan was performed at 10^{o}C/min. For all DSC tests, the enthalpy changes of melt crystallization, melting temperature and crystallization kinetics parameters were calculated.

3.4 Results and discussion

3.4.1 Effects of BPF on the nucleation and crystallization of PHBV8

Table 3.1 gives the summary of some thermal properties of PHBV8 and PHBV8/BPF (80/20 w/w) composites. Melt crystallization temperature (T_c) of PHBV8 increased from 52.3°C of the pure polymer to 75.2°C in presence of BPF. Similarly, the enthalpy of crystallization (ΔH_c) increased from 20.7 to 53.3 J/g with the addition of BPF. Since the high T_c and large ΔH_c can be taken as indicators for fast crystallization and high crystallization ability, these results suggest that BPF is acting as an NA in the PHBV8/BPF composite. Apparently, different crystallization mechanism was incurred in the composite system in contrast to the pure PHBV8. Figure 3.1 shows the photomicrograph of spherulite growth of PHBV8 in the presence of BPF under a polarized optical microscope. The sample for the POM analysis was taken from the injection molded specimen of the composites. Nucleation at BPF surfaces and individual spherulites grown from the fiber surfaces were clearly observed. However, nucleation density at the fiber surface was not high enough so that the transcrystalline growth was not observed. Homogeneous nucleation also occurred throughout the matrix and produced spherulites with the regular shape. It is a common phenomenon that the fiber surface can provide nucleation sites for semicrystalline polymers in many composites. Wong *et al* (2002) observed extensive heterogeneous nucleation of PHB on flax fibers, and Reinsch and Kelley (1997) also reported PHBV nucleation on wood fibers. Mi *et al* (1997) studied bamboo fiber-induced nucleation and crystal growth of isotactic polypropylene. All these studies reported the formation of transcrystalline layer (TCL). Nevertheless, Kori *et al* claimed in their study of PBS/bamboo fiber composites that there

was no fiber-induced crystallization observed. It is worthy to be mentioned that all these remarks were based on the observations of crystal growth at well-controlled conditions under the polarized optical microscope. The observations on the model systems in the POM experiment may have some discrepancies from the realistic situations. However, using two-dimensional wide-angle X-ray scattering measurements on unidirectional fiber-reinforced isotactic polypropylene, Dean *et al* (1999) confirmed the formation of transcrystallization in the composites. There is not a definite conclusion so far that how the TCL affects the mechanical properties in the composites, which differs from system to system. (Dean *et al.* 1999)

The glass transition temperatures (T_gs) in Table 3.1 were measured from the peak temperatures of the α-transition (tanδ curves) in the DMA experiment. The slight increase in T_g suggests that a certain degree of restriction of the polymer chain movement might be incurred by BPF. It appeared that the heat of fusion (ΔH_m) of PHBV8 showed a slight difference in presence of BPF. However, Reinsch and Kelley (1997) argued that the difference in ΔH_m might be the result of variation incurred by the uncertain fiber content in that particular sample under testing. The changes in melting point (T_m) are interesting. In the first heat scan, the T_{m1} of PHBV8 in the composites was much lower than that of the neat PHBV8 (with or without BN). In the second heat scan, however, there was little difference between them. This was probably attributed to the difference of the PHBV8crystalline structures between the injection-molded composites (1^{st} scan) and the slow cooled composites (2^{nd} scan). Since the mold temperature was set at 50°C, the melt of the composite likely experienced kind of fast cooling that led to an inhomogeneous crystalline structure, particularly when the fiber-induced crystallization

was involved. On cooling from the melt at 10°C, which was well controlled and much slower cooling processing relative to the injection molding, a more homogeneous crystalline structure was resulted. It is also noted in Table 3.1 that the ΔH_m of the neat PHBV8 was much large than its ΔH_c, indicating the slow crystallization of neat PHBV8 in normal process. Because of its low T_g, however, it underwent post-process cold crystallization and eventually high crystallinity (1^{st} heat scan) was still obtained.

3.4.2 Effects of nucleating agent on nucleation and crystallization of PHBV8

The interfacial adhesion strongly influences the mechanical properties of fiber reinforced composites. When fiber-induced crystallization happens, however, the situation become complicated. The influence of fiber-induced crystallization and in its extreme scenario the transcrystallization on mechanical properties of a composite is still not very clear, and the effects appear to differ for different fiber/polymer systems (Lustiger 1992). On the other hand, although BPF significantly increased the T_c of PHBV8 in the composite, its T_c value at 75.8°C still suggested a large supercooling was required for fast crystallization. Furthermore, the coexistence of heterogeneous (fiber-induced) and homogeneous nucleation results in complicated crystalline structures. This may also present a problem for the final articles to have a constant quality. In this study, boron nitride (BN) was added as a nucleating agent and its effects on thermal properties and mechanical properties of the composites were investigated. Nucleating agent was added to the composites in an attempt to suppress the fiber-induced nucleation/crystal growth and to achieve more homogeneous crystalline structures. Figure 3.2 shows that addition of BN promoted the nucleation in the matrix and largely minimized the fiber

induced nucleation. The T_c of PHBV8/BPF composites further increased from 75.8 to 104.5°C with the addition of BN. In addition, the T_{m1} of the composites also slightly increased with the addition of BN (Table 3.1).

3.4.3 Effects of BPF and nucleating agent on mechanical and dynamic mechanical properties

3.4.3.1 Dynamic mechanical properties

Figures 3.3 and 3.4 give the dynamic mechanical properties of PHBV8 and PHBV8/BPF composites. The dynamic mechanical properties of BPF composite clearly demonstrated the reinforcing effects of the BPF. The storage modulus (E′) of the BPF composite was superior to that of neat PHBV8 across the whole temperature range from glassy to rubbery states. Particularly, E′ of the composite was substantially higher than that of the neat PHBV8 in the α-transition region and rubbery state. In contrast, addition of BN slightly decreased the modulus of both the neat PHBV8 and the BPF composites. The decrease in E′ with the addition of BN might be attributed to the smaller and homogeneous crystals resulted. The obvious change of damping (tanδ) at α-transition was just the opposite to modulus, meaning the higher the storage modulus the lower the energy dissipation. This result indicates the addition of BN increased the damping effect during α-transition because of the smaller storage modulus.

3.4.3.2 Tensile and flexural mechanical properties

Reinforcing BPF resulted in an overall improvement of the mechanical properties of PHBV8 (Figures 3.5 - 3.8). Addition of nucleation agent (BN) improved the tensile

strengths. It also resulted in an increase in strain at break and a small decrease in modulus (Figure 3.5). The improved perfection of the crystalline structure by the addition of BN might be responsible for all these changes in mechanical properties. These results were consistent with that from dynamic mechanical properties. Both tensile and flexural strengths increased with fiber up to 20 wt%, then tended to decrease with further increase in fiber concentration (Figure 3.6). Tensile elastic modulus increased with fiber content up to 40 wt%, while the flexural modulus started to decrease above 30 wt% fibers (Figure 3.7). Tensile strain showed little change and started to decrease above 20% fibers, flexural strain increased with fiber concentration up to 30 wt% (Figure 3.8). It is worth mentioning that in many other studies of natural fiber composite systems, except modulus, the strength and strain usually decreased with fiber content and were lower than that of the neat polymers. The results presented in this study suggest that BPF reinforcement is superior to many other fibers. The fineness and large aspect ratio of BPF were probably the major reasons. Because of the discontinuous nature of the short fiber reinforcement, the tensile stress experienced by the fibers must derive from shear stresses transmitted by the polymer matrix. Since interfacial shear stress is zero in the center and a maximum at the ends, tensile stress is not uniformly distributed along the fiber. It is presumed to be zero at the ends and increases inward and eventually reaches a maximum or a steady value in the center. There is a critical fiber length over which tensile stress builds up to the maximum. The extents of strength and modulus enhancements depend on the mean stress taken by the fibers. Furthermore, short fibers are usually not unidirectional but rather randomly orientated in the matrix.

For aligned short fiber composites, the Halpin-Tsai equation is usually used to predict the theoretical modulus. The equation for the longitudinal (E_L) and transverse (E_T) moduli can be written as:

$$E_L = E_m \frac{1 + \xi \eta_L v_f}{1 - \eta_L v_f} \tag{11}$$

$$E_T = E_m \frac{1 + 2\eta_T v_f}{1 - \eta_T v_f} \tag{12}$$

$$\eta_L = \frac{(E_f / E_m) - 1}{(E_f / E_m) + \xi} \tag{13}$$

$$\eta_T = \frac{(E_f / E_m) - 1}{(E_f / E_m) + 2} \tag{14}$$

$$\xi = 2(l / d) \tag{15}$$

Where E_f and E_m are tensile moduli of the fiber and matrix, and ν_f and ν_m are the fiber and matrix volume fractions, respectively. ξ is a measure of the geometry of the fiber. For a composite with randomly oriented fibers, the Tsai-Pagano equation can be used to predict the elastic modulus:

$$E_{random} = \frac{3}{8} E_L + \frac{5}{8} E_T \tag{16}$$

In the study of Amada *et al* (1997), bamboo fiber was characterized to have a tensile strength of 600 MPa, modulus of 46 GPa and density of 1.16 g/cm^3. In this study, PHBV8 demonstrated a tensile strength of 23.5 MPa, modulus of 1.45 GPa and density of 1.25 g/cm^3. These data were applied to above equations for the theoretical prediction.

Figure 3.9 gives the comparison of the theoretical and experimental tensile elastic moduli. When fiber volume fraction was high (>10), theoretical prediction gradually deviated from the experimental results. There could be many factors contributed to the deviation. One major reason might be the aggregation of the fibers at higher concentration. Lack of strong interfacial bonding might also contribute to the deviation.

The mechanical properties of short fiber reinforced composites can also be molded by the modified "rule of mixture". The modified "rule of mixture" considering the relationship between modulus and fiber length and orientation is given by the Cox-Krenchel equation:

$$E_c = \alpha_0\alpha_1 E_f \nu_f + E_m \nu_m \qquad (17)$$

Where α_0 and α_1 are orientation and length efficiency factors, E_f and E_m are tensile modulus of the fiber and matrix, and ν_f and ν_m are the fiber and matrix volume fraction.

Applying the above physical properties of bamboo fiber and PHBV8 to equation 17 yields a value of 0.25 for the $\alpha_0\alpha_1$. The average aspect ratio of BPF in this study was ca. 324, which was 3 times higher than the aspect ratio of 100 generally required for maximum enhancement of modulus (Sheldon 1996). Because the test samples were injection-molded, a certain degree of fiber orientation along the melt flow direction was also expected. Considering that the value of $\alpha_0\alpha_1$ is 1 in the case of ideal unidirectional fiber reinforcement and 0 in the case of no reinforcement, the value of 0.25 for $\alpha_0\alpha_1$ is relatively low. However, it should be pointed out that equation 17 is still built on the same assumptions for the "normal rule of mixture" for continuous fiber composites: namely same Poisson's ratio for both phases and no debonding. This model may present

a large difference from reality. The large deviation from expectation may be also attributed to some other factors, such as insufficient interfacial adhesion, large fiber length distribution, and debonding. It was possible the inadequate interfacial adhesion had a significant effect for the low efficiency, as it will be found in the following sections. Further more, the changes in polymer crystalline structure were not considered in the equation.

3.4.3.3 Impact strength

Impact strength exemplifies the special toughness of polymer engineering materials under high strain rates. Like other methods for the measurement of toughness, impact testing also detects the energy consumed on the creation of fracture. Fiber length is found to be an important parameter in the toughening of polymer with discontinuous fibers, and the best effect is developed at about the critical length (Sheldon 1982). The toughening effect the fibers produce with resin is attributed to the extra energy needed for pullout, debonding or redistribution of stress, involving also the creation of new surfaces. In a particular situation, the mode of fracture may depend upon many factors including fiber and matrix strength, load transfer efficiency, resistance to crack propagation, bonding strength, volume fraction, fiber distribution and geometry. Figure 3.10 gives results of the notched Izod impact tests. With 10 % BPF, the impact strength of the composite was almost 3 times that of the neat pHBV8. The impact strength increased monotonously with BPF content from 10 to 40 wt%. The results again suggest the BPF reinforced PHBV8 composites were superior to many other natural polymer composite systems (Bhardwaj *et al* 2006, Tobias 1993, Nielsen 1976) with respect to impact strength. The impact strength in other systems was usually lower than that of the neat polymers and

decreased with increasing fiber content (Wibowo *et al* 2004, Oksman and Clemons 1998). According to Shelton (1982), in both long and short fiber reinforced composites except where the polymer itself is inherently tough, the impact resistance increases with concentration, although eventually at high concentrations, the strength must fall again. Nucleating agent also resulted in a minor increase in impact strength in both tests.

Figures 3.11 and 3.12 show the SEM micrographs of the fracture surfaces in tensile and impact tests. These micrographs show that BPF had a good dispersion in the PHBV8 matrix. Extensive pullout of the BPF was noted in both tests. Similar to the non-reinforced PHBV8, the polymer at the fracture surfaces appeared smooth and lack of plastic deformation, indicating a brittle fracture. These results suggest that the improved impact strength was mainly attributed to the extra energy consumption on pullout and new surfaces created. The extensive fiber pullout also indicated the interfacial adhesion was not high.

3.4.4 Effect of coupling agent and compatibilizer on properties of the PHBV8/BPF composites

3.4.4.1 Crystallization

Table 3.2 gives the DSC results of melting and crystallization of PHBV8 in the composites. . All these composites contained 1% BN on the basis of polymer weight. The decreasing effect of pMDI on crystallization ability of PHBV8 was probably attributed to the polymer chain extension and coupling reaction between fiber and polymer. A similar effect of chain extension on crystallization was noted in the compounding of PLA with MDI (Li and Yang 2006). The extended molecules exerted

certain hindrance to the chain segment diffusion into the lattice. Maleated PHB itself shows reduced crystallization ability. Chen *et al* (2002) found the crystallization of maleated PHB deteriorated greatly and attributed it to the steric hindrance from the grafting MA group. The MA group may further intensify the molecular interactions which restrict the diffusion of PHB segment during crystallization process. Different from pMDI, MA-PHBV8 reacting with the hydroxyl ends of the PHBV8 could result in molecular branching. The molecular linearity was disrupted by the branching, consequently, decreased the crystallization ability. Besides the restriction of chain segment movement by chain extension and branching, the reduction of the number of chain ends owing to the reactions also accounted for the T_g increase. In fact, because MA-PHBV8 contained only 0.3 wt% MA, it showed slight influence on the crystallization ability of PHBV8. On the other hand, pMDI contained much high percentage of the functional group; thereby it resulted in a large decrease in crystallization ability.

The kinetics of non-isothermal crystallization of the composites was investigated. The peak temperature of melt crystallization (T_{nc}), enthalpy of isothermal crystallization (ΔH_{ic}) and Avrami parameters, n, K and $t_{0.5}$, are listed in Tables 3.3. Avrami plots of composites with and without MDI or MA-PHBV8 are shown in Figures 3.13-3.15. The non-isothermal crystallization cooling rates were selected to be 5^{o}C/min, 10^{o}C/min, 20^{o}C/min and 40^{o}C/min, respectively. The DSC thermograms from the second heating at 10^{o}C/min after non-isothermal crystallization are given in Figure 3.16. For each composite, Avrami plots gave almost parallel lines at different cooling rates, indicating same nucleation and crystal growth mechanism in non-isothermal crystallization process

under different cooling rates. However, Table 3.3 showed that addition of MDI or MA-PHBV8 in the composites decreased the n value from 3 to 2. This result suggests that the crystallization of PHBV8 in the composite changed from the athermal (simultaneous) nucleation spherical growth on contact to growth on diffusion. The change of rate determination mode from contact to diffusion was likely caused by the chain extension or branching of PHBV8. Compared to the control, addition of MDI or MA-PHBV8 in the composites also decreased Z_c value at the same cooling rate, indicating the decrease in crystallization rate. Again, chain extension or branching played a role in this change. From the DSC thermograms of the second heating after the non-isothermal crystallization (Figure 3.16), the first peak (T_{m1}) of the melting was decreased by MDI or MA-PHBV8. As discussed in isothermal crystallization process, the lower the T_{m1} was, the less perfection the crystals possessed. All these results indicated that addition of MDI or MA-PHBV8 hindered crystallization process of the matrix polymer.

3.4.4.2 Dynamic mechanical properties of composites

pMDI and MA-PHBV8 are added into the composite as coupling agent and reactive compatibilizer, respectiveely. They were expected to strengthen the interfacial adhesion between BPF and the PHBV8 matrix; and the change in molecular level should manifest its effect on viscoelastic properties. Figures 3.17 – 3.20 show the DMA thermograms of composites with and without pMDI or MA-PHBV8. It is noted that the storage modulus (E′) was clearly increased by pMDI or MA-PHBV8, particularly in the glassy state. It also appeared that MA-PHBV8 demonstrated higher efficiency on increasing E′. Both pMDI and MA-PHBV8 had an increasing effect on the α-transition temperature of

PHBV8 (Figures 3.18 and 3.20). Nevertheless, they showed different effects on the intensity of the damping at the α-transition. While damping peak decreased with increase in pMDI concentration, it increased with the increase in MA-PHBV8 concentration. The difference was resulted from the different responses of the extended chains and branched chains to energy dissipation at the α-transition.

3.4.4.3 Mechanical properties of composites

Figure 3.21 - 3.24 show the effects of pMDI and MA-PHBV8 on tensile and flexural mechanical properties of the composites. For the composite with 1% MDI, 2% MDI and 3% MDI, the tensile strength increased 4.0%, 20.6% and 28.8% respectively. Similarly the flexural strength increased 2.6%, 9.6% and 13.1% respectively. For the composite with 2% MA-PHBV8, 3.5% MA-PHBV8 and 5% MA-PHBV8, the tensile strength increased 5.6%, 24.4% and 32.2% respectively. The flexural strength increased 4.0%, 11.0% and 14.4% respectively. Accordingly, the strain at break in both testing decreased with the reagent concentration. In contrast, impact strength decreased continuously with increase in the pMDI and MA-PHBV8 concentration (Figures 3.25 & 3.26). This result indicated that the improved interfacial adhesion increased the tensile and flexural strengths at the expense of impact strength. Since impact strength is virtually a measurement of toughness at high strain rate, as discussed above it depends on the energy dissipation during the impact process. The increased bonding between fiber and matrix effectively transfers the applied load to the fiber through the matrix, resulting high tensile (or flexural) strength and modulus. On the other hand, it decreases the possible fiber pullout or slippage between fiber and matrix, hence reduces the energy consumption on

creation of more surfaces or on frictions. The morphological changes of fracture surfaces by the addition of pMDI and MA-PHBV8 support this argument.

For the composites containing 2 % pMDI, Figures 3.27 and 3.28 show that almost all bamboo fibers were broken at the fracture surfaces during the tensile and impact tests. For the composites containing 3.5% MA-PHBV8, broken bamboo fibers were also noted on both tensile and impact fracture surfaces (Figures 3.29 & 3.30). In contrast, there were no broken fibers at the fracture surfaces noted in the control sample. This result demonstrated that both pMDI and MA-PHBV8 increased the interfacial adhesion between BPF and PHBV8. Moreover BPF showed a better dispersion in the matrix than the control composite because of the improved wetability by pMDI or MA-PHBV8.

3.5 Conclusions

BPF induced nucleation and increased the crystallization temperature of PHBV8. It also slightly increased the glass transition temperature of PHBV8. Nucleation at and crystal growths from fiber surfaces were observed by POM, but orderly transcrystalline layers were not found. However, if the observation under the well-controlled condition can represent realistic crystalline state was unknown. The storage modulus of the composite was significantly higher than that of the neat polymer, particularly in the rubbery state. The intensity of the damping peak of the polymer was also greatly reduced by the BPF addition. Reinforcing BPF demonstrated significant effects on mechanical properties. Tensile and flexural moduli and strengths of the composites were significantly higher than that of neat polymer and increased with BPF concentration. Tensile strain is slightly decreased but flexural strain is increased with BPF. Different from many other

natural fiber composites, impact strength of the composite was superior to the neat polymer and increased with BPF concentration.

Since BPF had little effect on the final crystallinity of PHBV8 in the composite, it is not clear what the role of the fiber induced crystallization in the properties of the final products. Adding BN as nucleating agent promoted the homogenous nucleation and minimized the fiber induced nucleation. The melt crystallization temperature was significantly increased with BN, but the crystallinity was not clearly changed. Adding BN increased both tensile strength and strain of the composite, but decreased elastic modulus of the composite. Apparently, the homogeneous crystalline structure by using BN played significant role in these changes.

SEM micrographs of fracture surface from tensile and impact tests showed extensive fiber pullout, suggesting that inadequate interfacial adhesion between BPF and PHBV8. Adding pMDI or MA-PHBV8 in the composite improved the wetability of the fiber by the matrix. SEM micrographs showed invreased amount of broken fiber at the fracture surfaces by adding either pMDI or MA-PHBV8. As a result pMDI or MA-PHBV8 greatly increased tensile and flexural strength and modulus of the composite. On the other hand, impact strength decreased with pMDI or MA-PHBV8. Similarly pMDI or MA-PHBV8 increased storage modulus in dynamic mechanical properties, and slightly shifted the α-transition temperature higher. Nevertheless, they showed different effects on the intensity of the damping peak at the α-transition. While damping peak decreased with increasing pMDI concentration, it increased with increasing MA-PHBV8 concentration.

3.6 References

- Amada, S.; Lchikawa, Y.; Munekata, T.; Nagase, Y.; Shimizu, H. Fiber texture and mechanical graded structure of bamboo, Composites Part B, 1997, 28B, 13 - 20.
- Barham, P. J.; Keller, A.; Otun, E. L.; Holmes, P. A. Crystallization and morphology of a bacterial thermoplastic: poly-3-hydroxybutyrate, *J. Mater. Sci.* 1984, 19, 2781-2794.
- Bhardwaj, R.; Mohanty, A.; Drzal, L. T.; Pourboghrat, F.; Misra, M. Renewable resource-based green composites from recycled cellulose fiber and poly(3-hydroxybutyrate-*co*-3-hydroxyvalerate) bioplastic, *Biomacromolecules* 2006, 287, 647-655.
- Carlson, D.; Nie, L.; Narayan, R.; Dubois, P. Maleation Of Polylactide (PLA) by Reactive Extrusion, *J. Appl. Polym. Sci.* 1999, 72, 477-485.
- Chen, C.; Fei, B.; Peng, S.; Zhuang, Y.; Dong, L.; Feng, Z. Nonisothermal crystallization and melting behavior of poly(3-hydroxybutyrate) and maleated poly(3-hydroxybutyrate), Euro. Polym. J. 2002, 38, 1663 – 1670.
- Chen, C.; Peng, S.; Fei, B.; Zhuang, Y.; Dong, L.; Feng, Z.; Chen, S.; Xia, H. Synthesis and characterization of maleated poly(3-hydroybutyrate), *J. Appl. Polym. Sci.* 2003, 88, 659-668.
- Chen, X.; Guo, Q.; Mi, Y. Bamboo Fiber-Reinforced Polypropylene Composites: A Study of the Mechanical Properties, *J. Appl. Polym. Sci.* 1998, 69, 1891-1899.

- Das, M.; Pal, A.; Chakraborty, D. Effects of mercerization of bamboo strips on mechanical properties of unidirectional bamboo-Novolac composites, *J. Appl. Polym. Sci.* 2006, 100, 238 – 244.
- Dean, D.; Marchione, A.A.; Rebenfeld, L.; Register, R. Flexural properties of fiber-reinforced polypropylene composites with and without a transcrystalline layer, *Polym. Adv. Technol.* 1999, 10, 655 - 668.
- Fernandes, E.G.; Pietrini, M.; Chiellini, E. Biobased polymeric composites comprising wood flour as filler, Biomacromolecules 2004, 5, 1200 – 1205.
- Gatenholm, P.; Kubat, J.; Mathiason, A. Biodegradable natural composites: I. Processing and properties, *J. Appl. Polym. Sci.* 1992, 45, 1667-1677.
- Herrmann, A.; Nickel, J.; Riedel, U. Construction materials based upon biologically renewable resource- from components to finished parts, *Polym. Degrad. Stabil.* 1998, 59, 251-261.
- Holmes, P. A.; Basset, D. C. Syntheses of hydrophobically modified cationic hydrogels by copolymerization of alkyl substituted diallylamine monomers and their use as bile acid sequestrants, *Elsevier Applied Science: London* 1988, 2, 1.
- John, J., Tang, J., Bhattacharya, M. Grafting of Oxazoline Functional Group to Polycaprolactone, *J. Appl. Polym. Sci.* 1998, 67, 1947-1955.
- Kemir, H.; Atikler, U.; Balkose, D.; Tihminlioglu, F. The effect of fiber surface treatments on the tensile and water sorption properties of polypropylene-luffa fiber composites, *Composites: Part A* 2006, 37, 447-456.

- Kori, Y.; Kitagawa, K.; Hamada, H. Crystallization behavior and viscoelasticity of bamboo-fiber composites, *J. Appl. Polym. Sci.* 2005, 98, 603 – 612.
- Li, B. H.; Yang, M. C. Improvement of thermal and mechanical properties of poly(l-lactic acid) with 4,4-methylene diphenyl diisocyanate, Polym. Adv. Technol. 2006, 17, 439 – 443.
- Luo, S.; Netravalli, A. N. Interfacial and mechanical properties of environment-friendly "green" composites made from pineapple fibers and poly(hydroxybutyrate-*co*-valerate) resin, *J. Mater. Sci.* 1999, 34, 3709-3719.
- Marchessault, R. H.; Coulombe, S. PHB lamellar single Crystals: Origin of the Splintered Texture *Can. J. Chem.* 1981, 59, 38.
- Mi, Y.; Chen, X.; Guo, Q. Bamboo fiber-reinforced polypropylene composites: Crystallization and interfacial morphology, *J. Appl. Polym. Sci.* 1997, 64, 1267 – 1273.
- Mohanty, A. K.; Khan, M. A.; Hinrichsen, G. Surface modification of jute and its influence on performance of biodegradable jute-fabric/Biopol composites, *Compos. Sci. Technol.* 2000, 60, 1115-1124.
- Mohanty, A.K.; Misra, M.; Drzal, L.T. Sustainable Bio-Composites from renewable resources: Opportunities and challenges in the green materials world, *J. Polym. Environ.* 2002, 10, 19-26.
- Nielsen, E. L. In mechanical properties of polymer and composites; Marcel Dekker: New York, 1976, 2, 483-484.
- Oksman, K.; Clemons, C. Mechanical properties and morphology of impact modified polypropylene-wood flour composites, *J. Appl. Polym. Sci.* 1998, 67, 1503 – 1513.

- Reinsch, V.; Kelley, S. Crystallization of poly(hydroxybutyrate-co-hydroxyvalerate) in wood fiber-reinforced composites, *J. Appl. Polym. Sci.* 1997, 64, 1785-1796.
- Riedel, U.; Nickel, J. Natural fibre-reinforced biopolymers as construction materials new discoveries, *Die Angewandte Makromolekulare Chemie* 1999, 272, 34-40.
- Saxena, M.; Gowri, S. Studies on Bamboo polymer composites with polyester amide polyol as interfacial agent, *Polym. Comp.* 2003, 24, 428 – 436.
- Shanks, R. A.; Hodzic, A.; Wong, S. Thermoplastic biopolyester natural fiber composites, *J. Appl. Polym. Sci.* 2004, 91, 2114-2121.
- Sheldon, R. P. Composite Polymer Materials, Applied Science Publisher, 1982; D. Hull and T.W. Clyne, An introduction to Composite Materials, Cambridge University Press, 1996.
- Takagi. H.; Ichihara, Y. Effect of fiber length on mechanical properties of "green" composites using a starch-based resin and short bamboo fibers, *JSME International Journal Series A* 2004, 47, 551-555.
- Tobias, B. C. Proceedings of the international conference on advanced composite materials; Minerals, Metals & Materials Society, 1993, 623.
- Van De Velde, K.; Kiekens, P. Biopolymers: overview of several properties and consequences on their applications, *Polymer Testing.* 2002, 21, 433-442.
- Wibowo, A.C.; Mohanty, A.K.; Misra, M.; Drzal, L.T. Chopped industrial hemp reinforced cellulosic plastic biocomposites: Thermomechanical and morphological properties, Ind. Eng. Chem. Res. 2004, 43, 4883 – 4888.

- Wong, S.; Shanks, R.; Hodzic, A. Properties of poly(3-hydroxybutyric acid) composites with flax fibres modified by plasticiser absorption, *Macromol. Mater. Eng.* 2002, 287, 647-655.

3.7 Figures

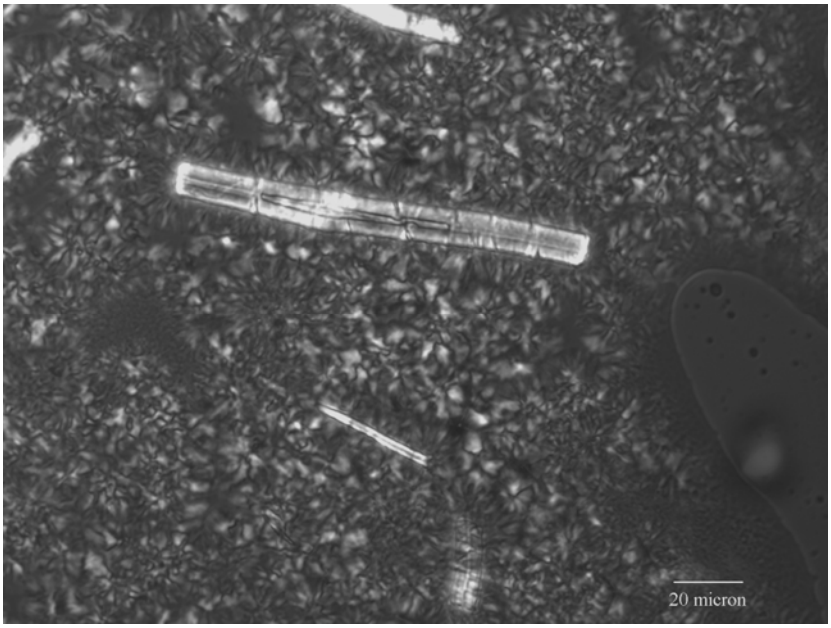

Figure 3.1. POM micrograph of PHBV8/BPF (80/20 w/w) composite without agents, isothermal at 100^{o}C

Figure 3.2. POM micrograph of PHBV8/BPF (80/20 w/w) composite containing 1wt% BN on the basis of PHBV8, isothermal at 100^{o}C

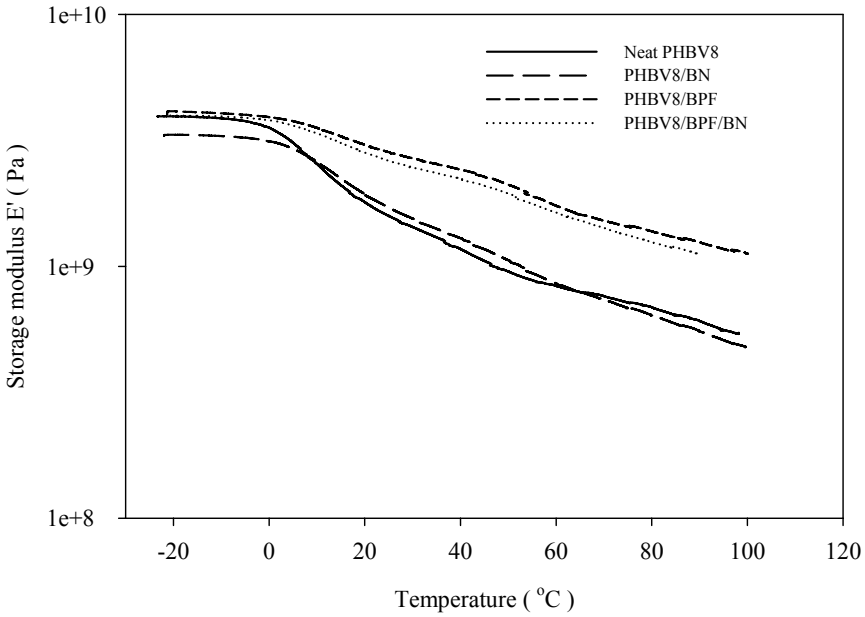

Figure 3.3. Storage modulus of PHBV8 and its PHBV8/BPF (80/20 w/w) composites. BN was added 1 wt% on the basis of PHBV8 weight.

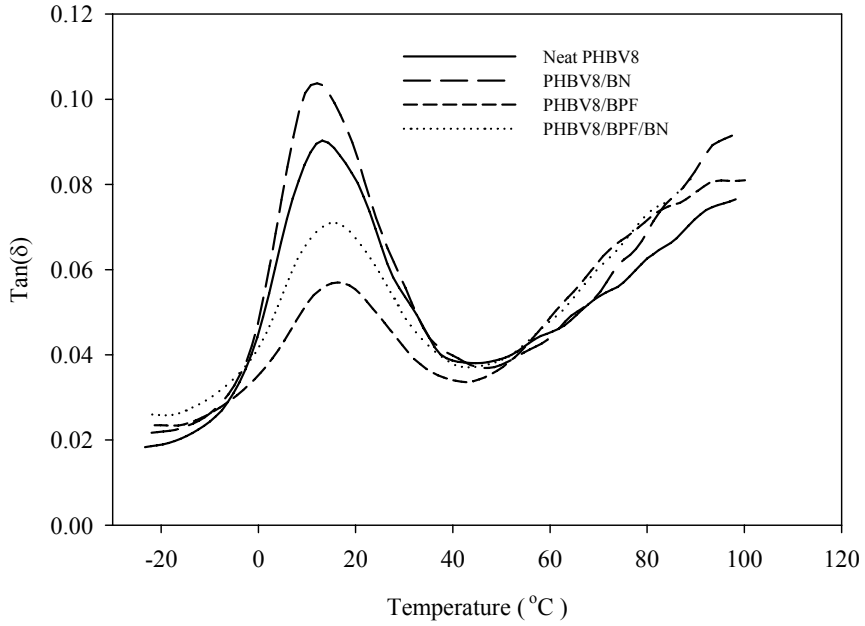

Figure 3.4. Tan(δ) of PHBV8 and its PHBV8/BPF (80/20 w/w) composites. BN was added 1 wt% on the basis of PHBV8 weight.

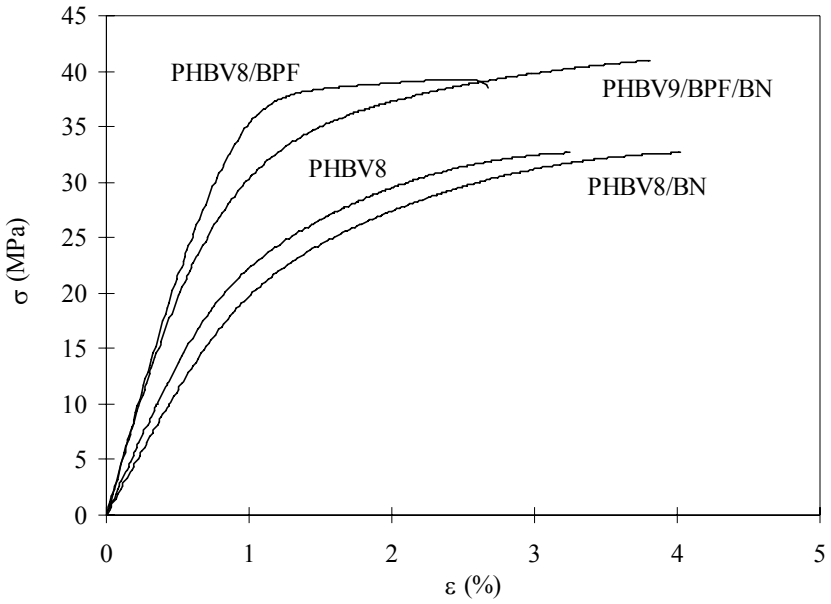

Figure 3.5. Tensile stress-strain curves of PHBV8 and its PHBV8/BPF (80/20 w/w) composites. BN was added 1 wt% on the basis of PHBV8 weight.

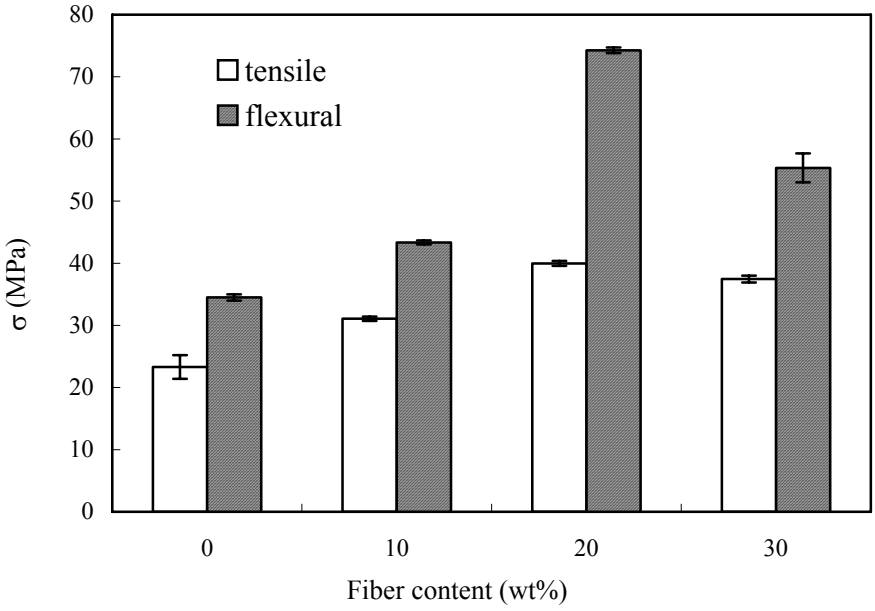

Figure 3.6. Tensile/flexural strength of PHBV8 and its PHBV8/BPFcomposites. BN was added 1 wt% on the basis of PHBV8 weight.

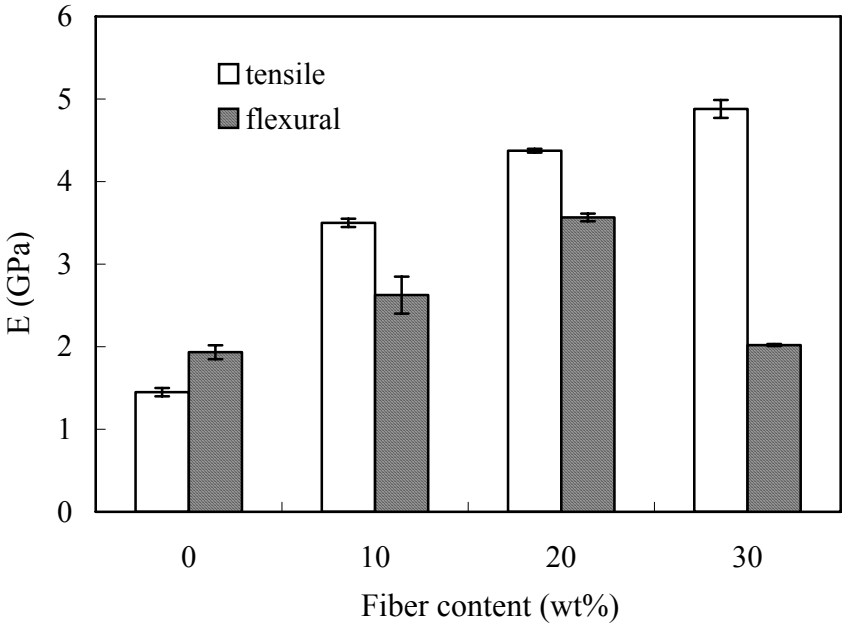

Figure 3.7. Tensile/flexural modulus of PHBV8 and its PHBV8/BPF composites. BN was added 1 wt% on the basis of PHBV8 weight.

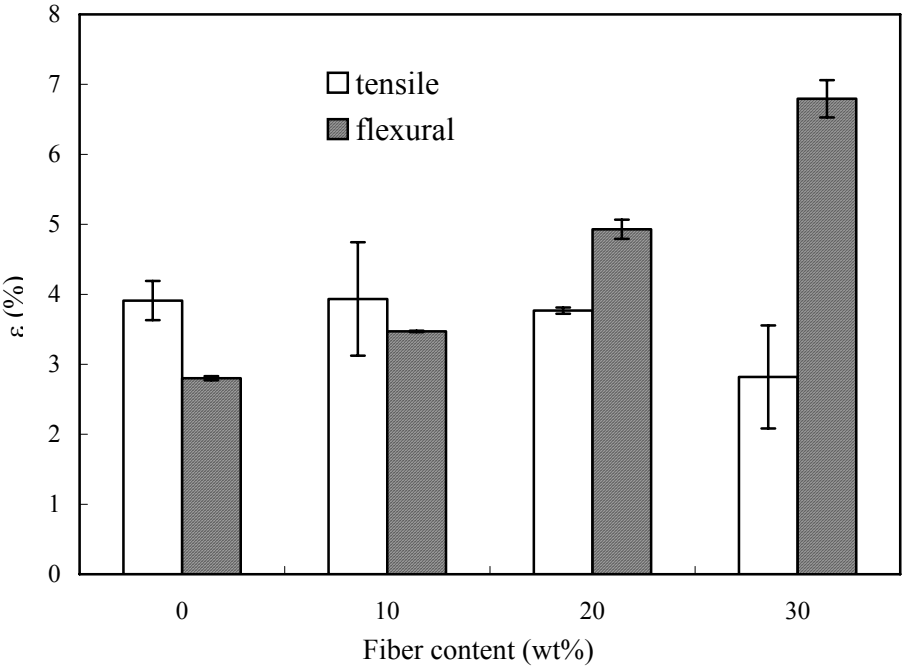

Figure 3.8. Tensile/flexural elongation of PHBV8 and its PHBV8/BPF composites. BN was added 1 wt% on the basis of PHBV8 weight.

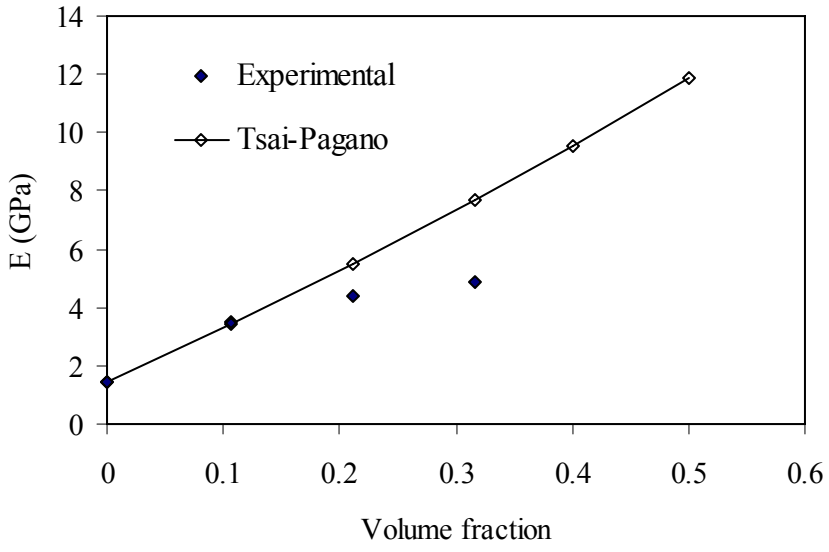

Figure 3.9. Comparison of experimental and theoretical tensile modulus of PHBV8/BPF composites as a function of fiber volume content.

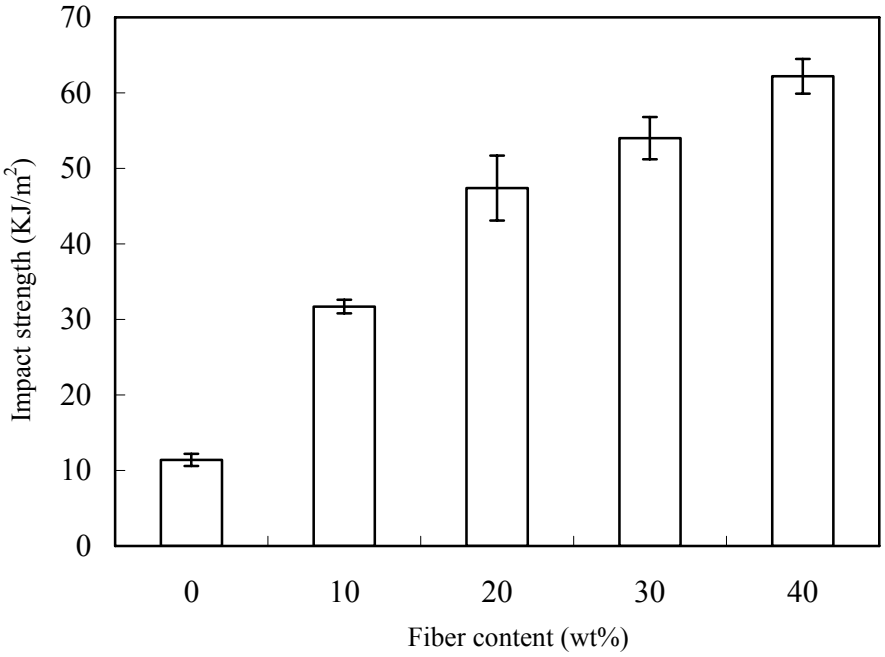

Figure 3.10. Impact strength of PHBV8 and its PHBV8/BPF/BN composites. BN was added 1 wt% on the basis of PHBV8 weight.

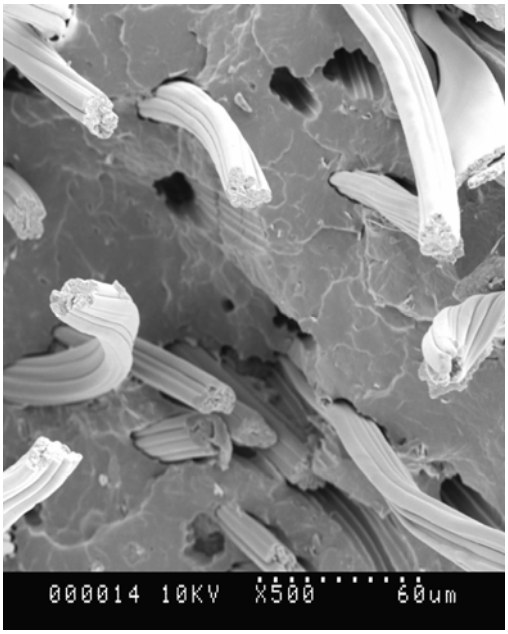

Figure 3.11. SEM micrograph of tensile fracture surface of PHBV8/BPF (80/20 w/w) composite with 1wt% BN added on the basis of PHBV8.

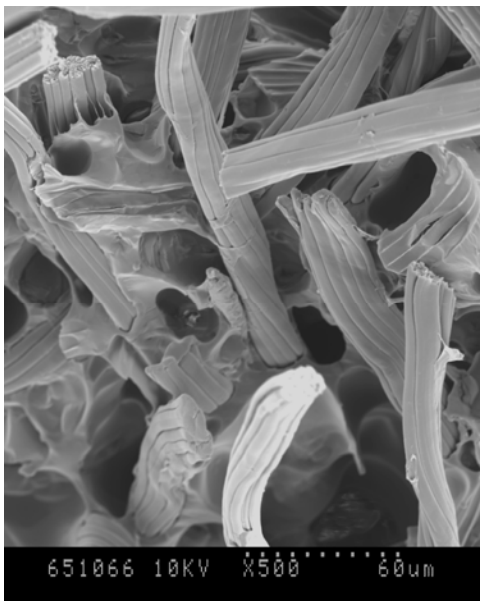

Figure 3.12. SEM micrograph of impact facture surface of PHBV8/BPF (80/20 w/w) composite with 1wt% BN added on the basis of PHBV8.

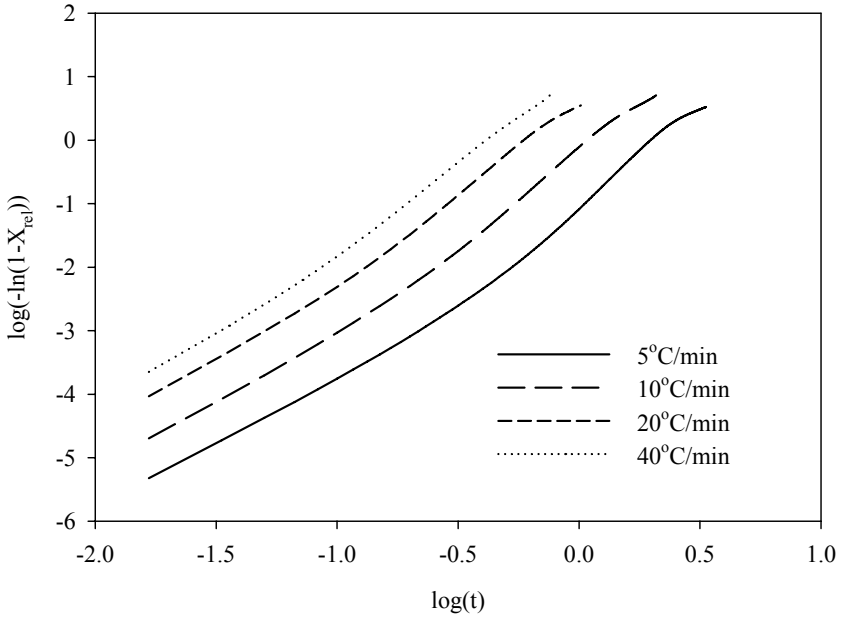

Figure 3.13. Non-isothermal Avrami plots of PHBV8/BPF (80/20 w/w) composite with 1wt% BN added on the basis of PHBV8.

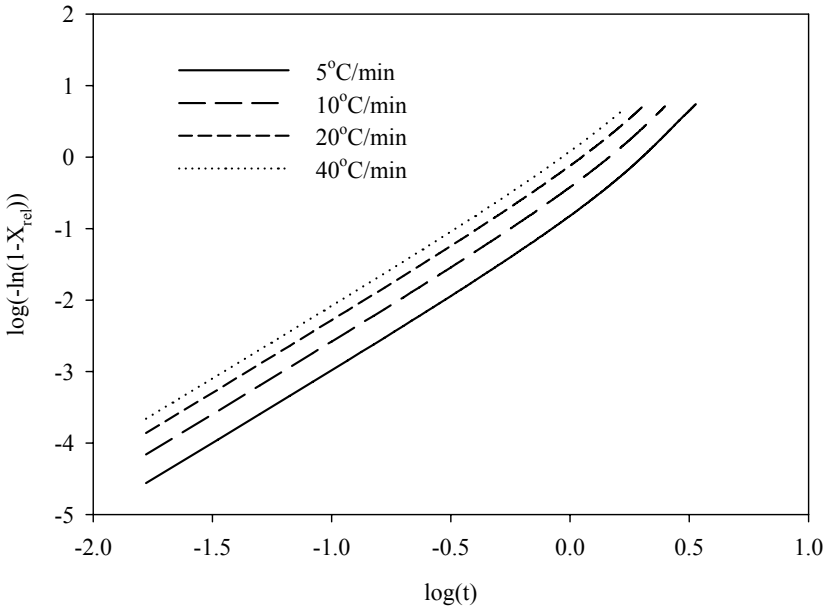

Figure 3.14. Non-isothermal Avrami plots of PHBV8/BPF (80/20 w/w) composite with 1wt% BN of PHBV8 and 2wt% pMDI added on the basis of composites.

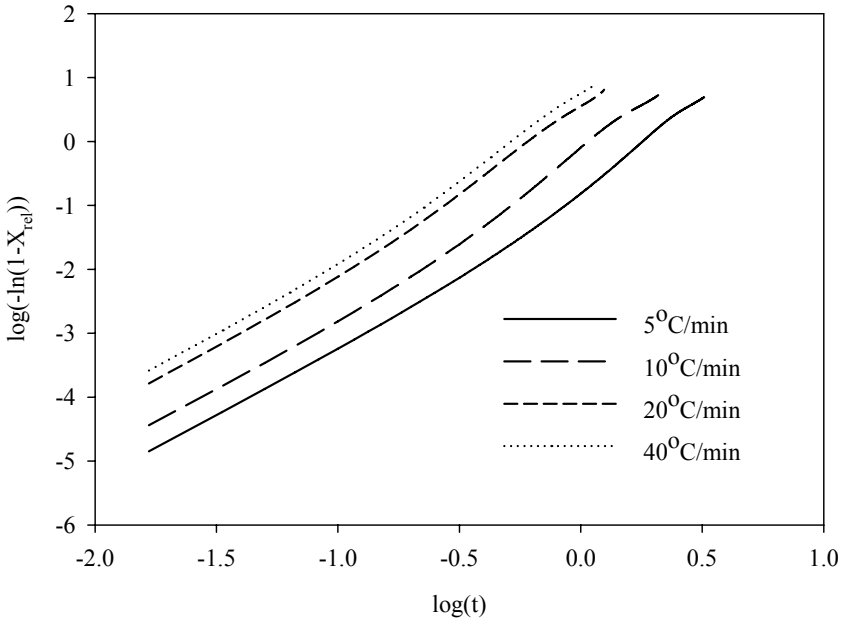

Figure 3.15. Non-isothermal Avrami plots of PHBV8/BPF (80/20 w/w) composite with 1wt% BN of PHBV8 and 3.5wt% MA-PHBV8 added on the basis of composites.

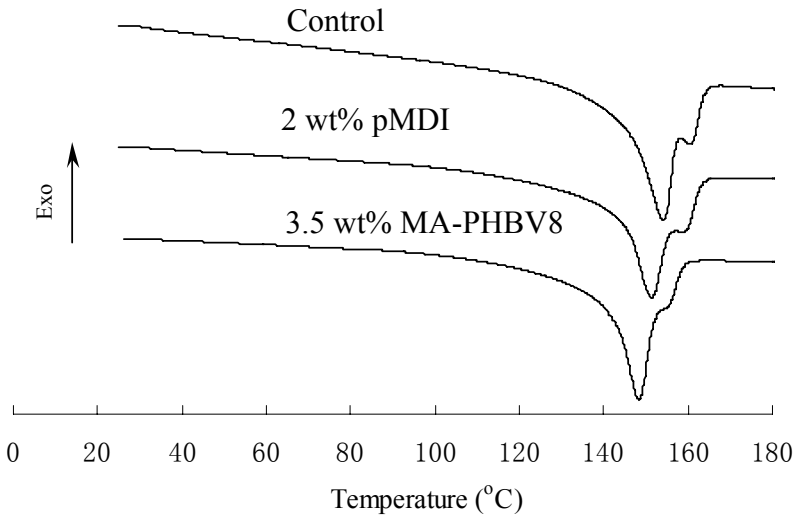

Figure 3.16. DSC thermogram of second heating of PHBV8/BPF (80/20 w/w) composite with 1wt% BN of PHBV8 and agent was added on the basis of composites.

Heating rate = 10°C/min

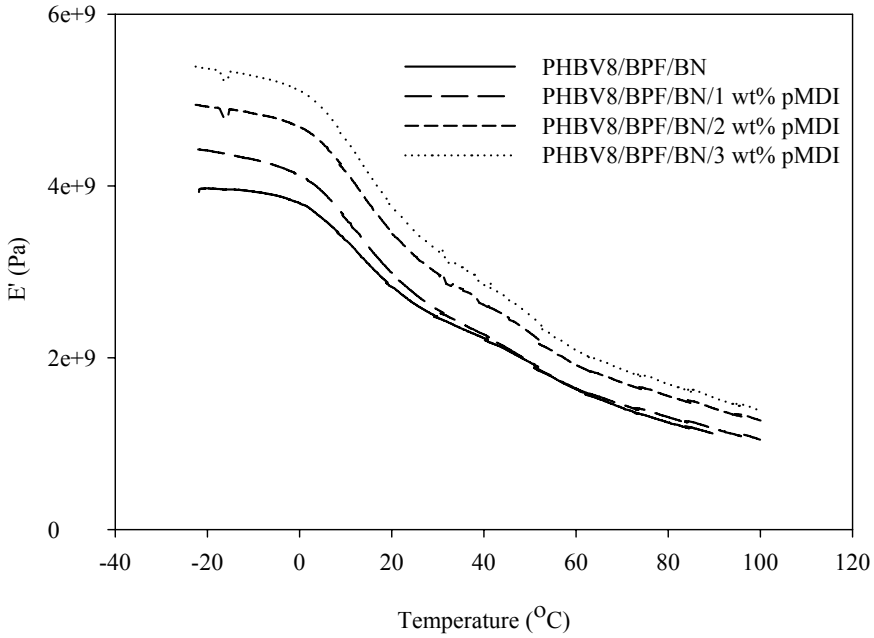

Figure 3.17. Storage modulus of PHBV8/BPF (80/20 w/w) composite with 1wt% BN of PHBV8 and pMDI was added on the basis of composites.

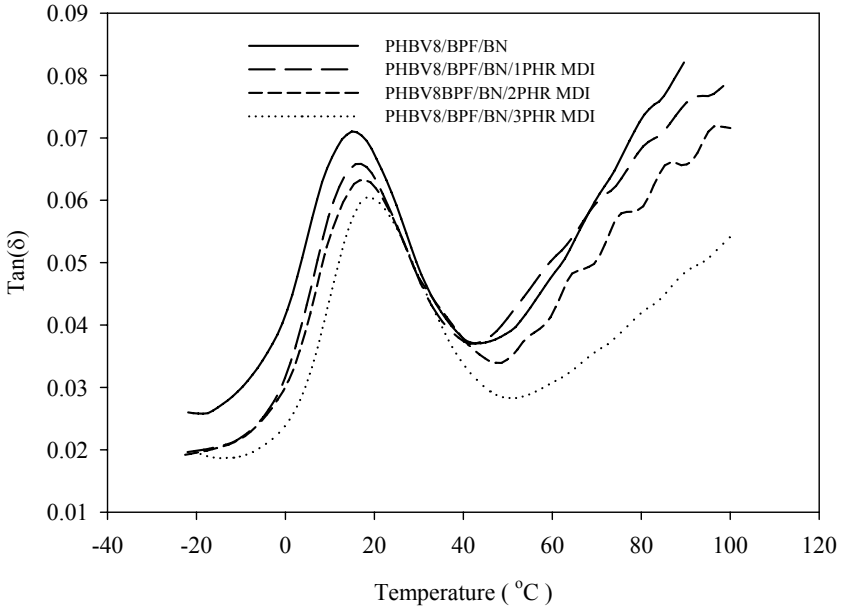

Figure 3.18. Tan(δ) of PHBV8/BPF (80/20 w/w) composite with 1wt% BN of PHBV8 and pMDI was added on the basis of composites.

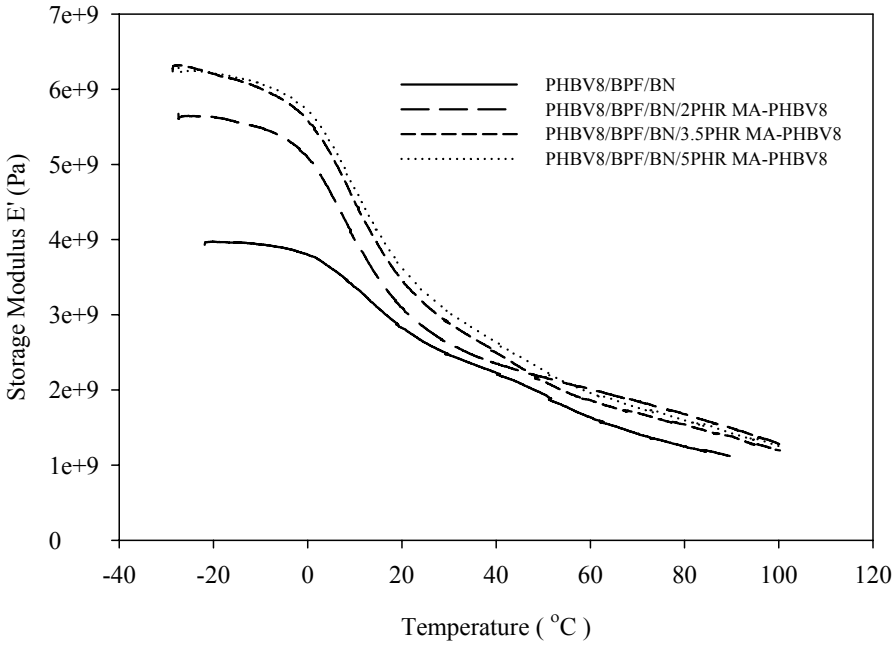

Figure 3.19. Storage modulus of PHBV8/BPF (80/20 w/w) composite with 1wt% BN of PHBV8 and MA-PHBV8 was added on the basis of composites.

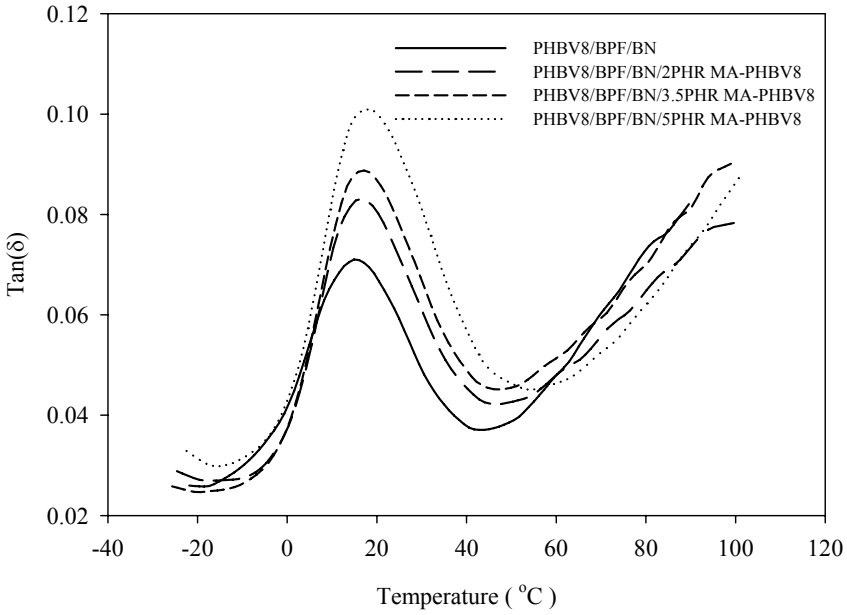

Figure 3.20. Tan(δ) of PHBV8/BPF (80/20 w/w) composite with 1wt% BN of PHBV8 and MA-PHBV8 was added on the basis of composites.

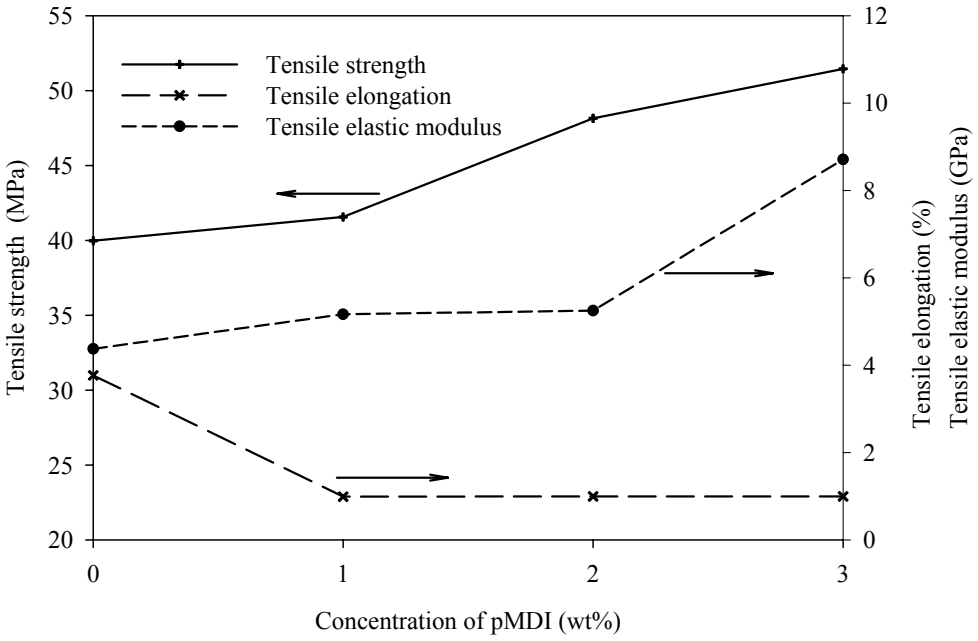

Figure 3.21. Tensile test results of PHBV8/BPF (80/20 w/w) composite with 1wt% BN of PHBV8 and pMDI was added on the basis of composites.

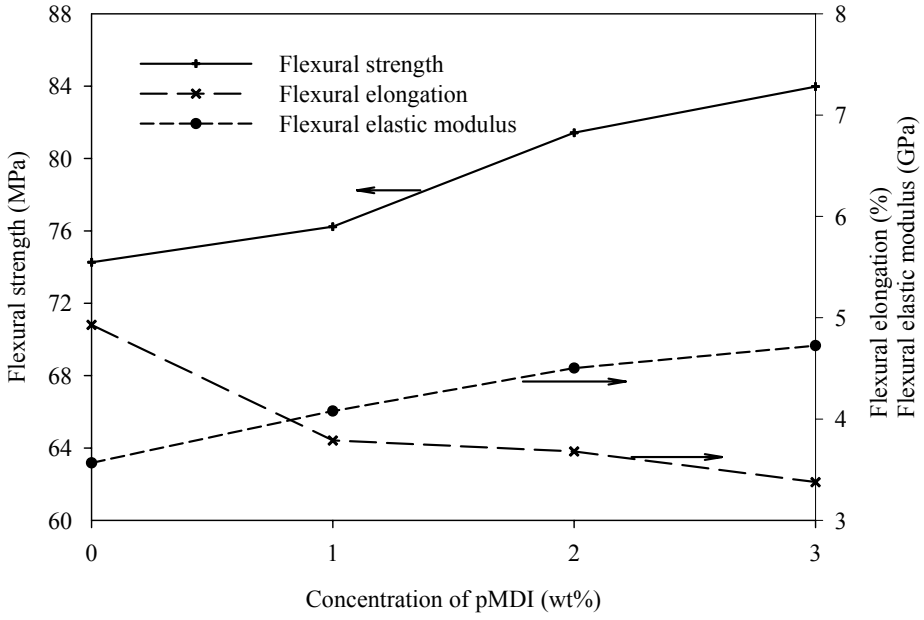

Figure 3.22. Flexural test results of PHBV8/BPF (80/20 w/w) composite with 1wt% BN of PHBV8 and pMDI was added on the basis of composites.

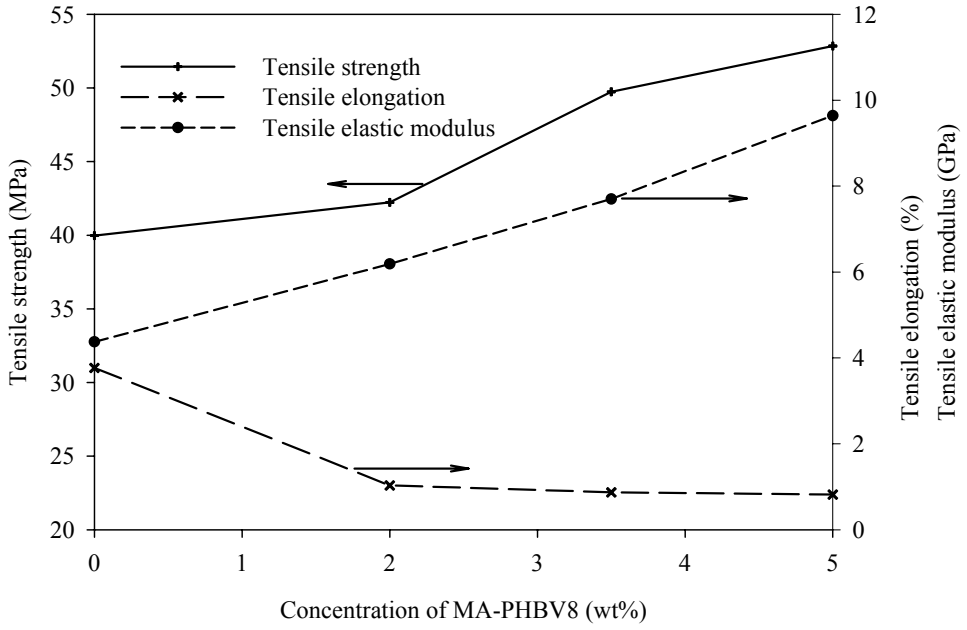

Figure 3.23. Tensile test results of PHBV8/BPF (80/20 w/w) composite with 1wt% BN of PHBV8 and MA-PHBV8 was added on the basis of composites.

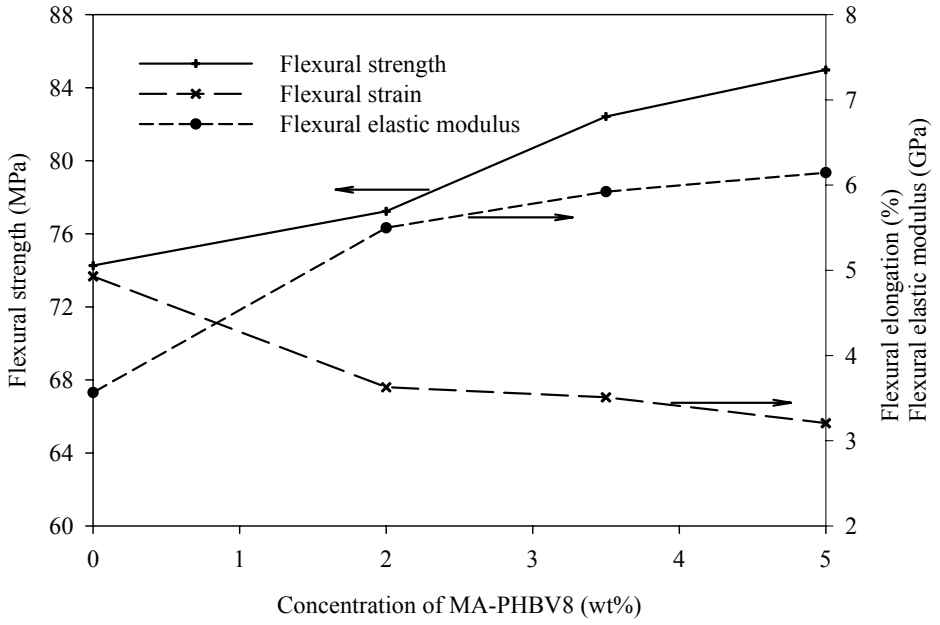

Figure 3.24. Flexural test results of PHBV8/BPF (80/20 w/w) composite with 1wt% BN of PHBV8 and MA-PHBV8 was added on the basis of composites.

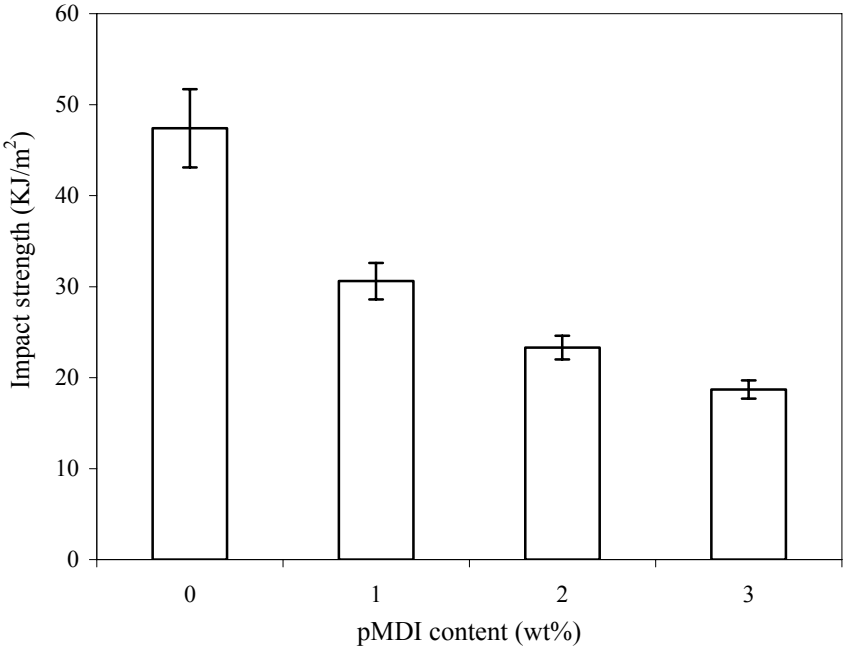

Figure 3.25. Impact strength of PHBV8/BPF (80/20 w/w) composite with 1wt% BN of PHBV8 and pMDI was added on the basis of composites.

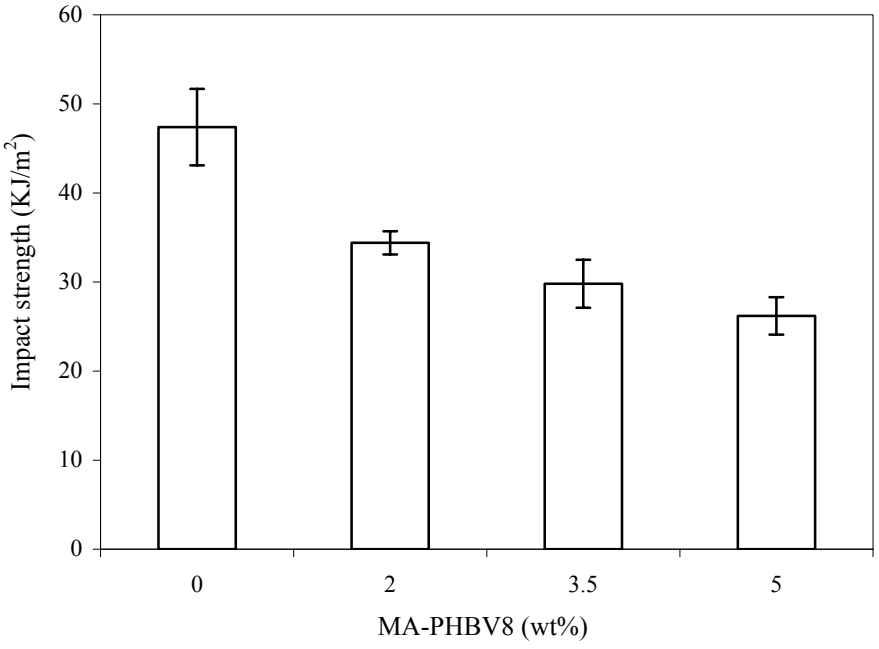

Figure 3.26. Impact strength of PHBV8/BPF (80/20 w/w) composite with 1wt% BN of PHBV8 and MA-PHBV8 was added on the basis of composites.

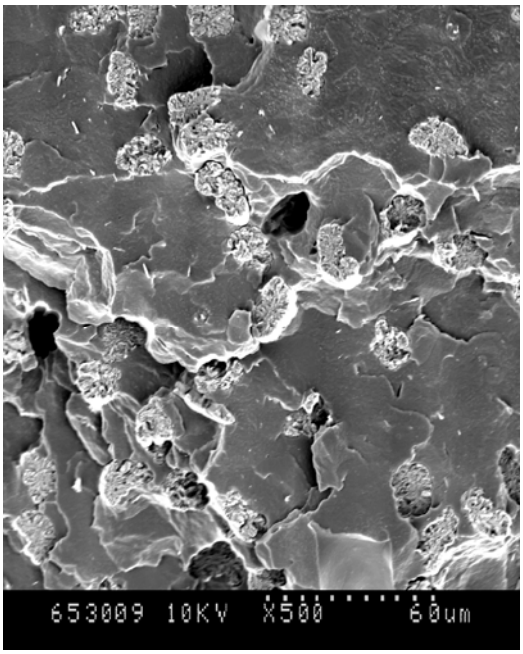

Figure 3.27. SEM micrograph of tensile fracture surface of PHBV8/BPF (80/20 w/w) composite with 1wt% BN of PHBV8 and 2 wt% pMDI of composites.

Figure 3.28. SEM micrograph of impact fracture surface of PHBV8/BPF (80/20 w/w) composite with 1wt% BN of PHBV8 and 2 wt% pMDI of composites.

Figure 3.29. SEM micrograph of tensile fracture surface of PHBV8/BPF (80/20 w/w) composite with 1wt% BN of PHBV8 and 3.5 wt% MA-PHBV8 of composites.

Figure 3.30. SEM micrograph of impact fracture surface of PHBV8/BPF (80/20 w/w) composite with 1wt% BN of PHBV8 and 3.5 wt% MA-PHBV8 of composites.

3.8 Tables

Table 3.1. Thermal Properties ofPHBV8 and PHBV8/BPF Composites

Composite	T_g(ºC)	Melt crystallization[b]		Melting					
				1st scan			2nd scan		
		T_c(ºC)	ΔH_c (J/g)	T_m(ºC)		ΔH_m (J/g)	T_m(ºC)		ΔH_m (J/g)
				1	2		1	2	
PHBV8	8.6	52.3	20.7	150.7	159.8	54.9	152.8	161	54
PHBV8/BN[a]	8.6	105.7	54.4	153.2	160.8	55.1	154	--	55.9
PHBV8/BPF	10.2	75.2	53.3	140	155.9	52.2	145.3	157.5	50.8
PHBV8/BPF/BN	10.2	104.5	57.1	143.8	156.7	52.8	153.2	159.8	58.5

a. Containing 1wt% BN based on the weight of PHBV8 in the PHBV8/BPF(80/20 w/w composite.

b. Measured from the nonisothermal melt crystallization at cooling rate of 10°C.

Table 3.2. Effects of pMDI and MA-PHBV8 on thermal property of composites

	(wt%)	T_g (ºC)	Melt crystallization[c]		Melting					
					1st scan			2nd scan		
			T_c (ºC)	ΔH_c (J/g)	T_m (ºC)		ΔH_m (J/g)	T_m(ºC)		ΔH_m (J/g)
					1	2		1	2	
	0	10.2	104.5	57.1	143	157.3	53.1	153	159.3	56.5
MDI[b]	1	11.7	98.2	55.3	143.2	157.5	54	153.8	161.8	58.8
	2	12.6	95.5	47.4	144.7	157.7	47.9	152	161.3	48.8
	3	13.7	89.3	50.1	141	155.8	48.8	148.7	158.3	51.2
MA-PHBV8[b]	2	11.9	98.3	55.8	143.5	155.5	51.1	150.7	158.3	57.4
	3.5	13.2	98.2	52.9		157	50.5	151	159.3	56.1
	5	13.9	99.3	56.3	142.7	155	52.6	153.2	160.3	57.5

a. Containing 1% BN based on the weight of PHBV8.

b. Based on the total weight of PHV8/BPF (80/20 w/w) composite.

c. Measured from the non-isothermal melt crystallization at cooling rate of 10°C/min.

Table 3.3. Non-isothermal crystallization kinetics data for composites with agents

Sample	Φ (°C/min)	T_{nc}[a](°C)	H_{nc} (J/g)	n	Z_c(min^-n)	$t_{0.5}$ (min)
No agent[b]	5	106.8	56.6	2.92	0.7842	1.34
	10	102.7	57.3	2.99	0.9518	1.04
	20	92.7	52	3.12	1.9518	0.60
	40	77.0	51.6	3.12	2.9518	0.39
2 wt% MDI[c]	5	94.2	53.7	2.08	0.6577	2.30
	10	86	44.6	2.08	0.8893	1.47
	20	75.7	45.8	2.08	0.9763	1.06
	40	44.3	40.4	2.08	0.9995	0.85
3.5 wt% MA-PHBV8[c]	5	102.4	56.1	2.07	0.6215	2.65
	10	96.5	54	2.07	0.8732	1.61
	20	89.7	49	2.07	0.9637	1.20
	40	53.7	48.1	2.08	0.9988	0.86

a. Measured from the peak value of the non-isothermal crystallization

b. The neat composite is PHBV8/BPF composite with 1% BN based on the weight of PHBV8

c. Based on the total weight of PHBV8/BPF (80/20 w/w) composite

CHAPTER 4 CONCLUSIONS AND FUTURE WORK

4.1 Conclusions

The market for fiber reinforced polymer composites is rapidly growing with their increasing applications in various industries, such as decking and construction products. Biopolymers, as alternatives to petrochemical polymers, will become more and more important in the sustainable developments of polymer and plastic industries. To date, materials based on petrochemical polymers have been extensively investigated and developed, while the knowledge and application development on biopolymers, such as PHAs, are still very limited. Therefore, the intent of this research was to contribute to the advance in biopolymer science and engineering. Particularly, this research aimed at several aspects of PHAs and PHA-based materials, including crystallization of PHB and PHBVs using different nucleation agents, effects of crystalline structures on mechanical and dynamic mechanical properties, reinforcement using bamboo fibers and effects of coupling agent and compatibilizer on the composite properties.

Crystalline structure and crysllinity is very important to the mechanical properties of the final products. Crystallization of PHBV is characteristic of low nucleation density and slow growth rate. In this study, some potential agents which have been reported to nucleate PHBVs in literature were first screened. Two new candidates were identified, thymine and melamine, which have not been used as nucleating agents for PHB and PHBVs elsewhere. It turned out that boron nitride, thymine and melamine nucleated PHBVs faster than others. Therefore, study of crystallization kinetics of PHBVs was further conducted using these three nucleating agents. Both boron nitride and thymine effectively increased the crystallizaiton rates of PHBV8, PHBV12 and PHBV21, and

yielded very similar nucleating kinetic parameters. Melamine also accelerated the crystallization of PHBV8 and PHBV12, but was less effective than BN and thymine. Furthermore, melamine could not nucleate PHBV21. POM revealed that the addition of NAs increased the nucleation density and appeared to yield simultaneous nucleation of the PHBVs. Isothermal crystallization indicated that the crystallization of neat PHBVs was more nucleation-determined and slower, while the crystallization of PHBVs containing NAs was more growth-determined and much faster. Both isothermal and non-isothermal kinetics studies suggests the PHBVs with nucleating agents yielded crystalline structures with similar perfection, as shown in the higher melting temperatures than neat PHBVs.

Bamboo pulp fiber (BPF) induced the nucleation and increased the crystallization temperature of PHBV8. It also slightly increased the glass transition temperature of PHBV8. Heterogeneous nucleation and homogeneous nucleation were both present in the composites. However, the final crystallinity was not obviously affected by BPF. Polarized optical microscopy revealed the nucleation on fiber surfaces and consequent crystal growth, but not the transcrystalline layers. Adding BN (nucleating agent) significantly increased the nucleation in the matrix and minimized the fiber-induced nucleation. Adding BN resulted in a more homogeneous crystalline structure and required a smaller degree of supercooling for fast crystallization. BPF greatly increased the storage modulus from glassy to rubbery states, and reduced the damping intensity in the α-transition region. Addition of BN slightly decreased the modulus of the composite but increased the damping effect.

BPF showed its great reinforcing effects on mechanical properties of the composites. Both tensile and flexural moduli and strengths of the composites increased with BPF concentration, and were higher than the neat polymer. Tensile strain slightly decreased but flexural strain increased with BPF. Addition of BN increased both strength and strain of the composite, but decreased elastic modulus of the composite. Different from many other natural fiber/polymer composites, the impact strength of PHBV8/BPF composite was multiple times higher than the neat polymer and increased with fiber content. This result suggested the BPF reinforced PHBV8 composites were superior to many other natural polymer composite systems.

SEM micrographs of the fracture surfaces in tensile and impact specimens showed extensive fiber pullout when no coupling agent or compatibilizer was used, indicating insufficient interfacial adhesion between BPF and PHBV8. In order to improve the interfacial bonding, pMDI or MA-PHBV8 were added into the composites. As a result both the tensile and flexural strength and modulus increased substantially. In contrast, impact strength decreased with pMDI or MA-PHBV8. The impact strength of the composite with pMDI decreased more than that of the composite with MA-PHBV8. The decrease of impact strength with improved interfacial bonding was consistent with the observation by Sheldon (1982). It also indicated a certain degree of orientation of the fibers along the melt follow direction. SEM analysis of the fracture surfaces revealed that both pMDI and MA-PHBV8 improved the interfacial adhesion between BPF and PHBV8, as seen in the broken fibers at the fracture surfaces. For composites containing pMDI, most fibers were broken at the tensile or impact fracture surfaces, and this was not observed in the composites without pMDI. For composites containing MA-PHBV8,

broken fibers were also noted but to a less content. Similarly pMDI and MA-PHBV8 increased storage modulus of the composites. Nevertheless they showed different effects on the intensity of the damping peak at the α-transition. While damping peak decreased with increasing pMDI concentration, it increased with increasing MA-PHBV8 concentration. Addition of pMDI or MA-PHBV8 slightly decreased the glass transition temperature of PHBV8. On the other hand, addition of pMDI or MA-PHBV8 led to the reduction of crystallization ability og PHBV8 in the composites.

This research provides an initial examination into the crystallization properties of PHB and PHBVs; the properties of PHBV8-based bamboo pulp fiber reinforced composites. However, since the amount of work on the materials and composites is limited, there is a great deal of research that needs to be accomplished before a full understanding of material properties can occur.

4.2 Future work

This thesis research has investigated into only a few important issues of PHA polymers and biocomposites. Significant progress has been made and some interesting results have been achieved. The findings from this study will provide a framework for the future development of cost effective and high performance PHA biocomposites. There are many challenging tasks ahead. Some of the findings are still preliminary and further investigations will be needed. Although BN and thymine showed higher efficacy than melamine to nucleate and accelerate the crystallization of PHB and PHBV, the nucleation mechanisms of these NAs are still not clear. It will be interesting to find out what make the difference between thymine and melamine on nucleating PHBVs. The crystalline structure of PHAs in the biocomposites and its effects on properties need further

investigation. There is also need for the investigation of the effects of fiber length on composite properties. Besides bamboo pulp fiber, it is also necessary to know the reinforcing effects of the ordinary bamboo fiber. There are no lubricants added in the PHBV/BPF composites for this study. Since al commercial fiber reinforced polymer composite will invariably contain some amount of lubricants, it will be important for future work to examine the effects of these materials on thermal and physical properties.